UNIVERSITY OF SOUTHAMPTON

FACULTY OF PHYSICAL AND APPLIED SCIENCES

Optoelectronics Research Centre

Controlling light with photonic metamaterials

Jianfa Zhang

Thesis for the degree of Doctor of Philosophy

March 2013

UNIVERSITY OF SOUTHAMPTON

ABSTRACT

FACULTY OF PHYSICAL AND APPLIED SCIENCE

OPTOELECTRONICS RESEARCH CENTRE

Doctor of Philosophy

CONTROLLING LIGHT WITH PHOTONIC METAMATERIALS

by Jianfa Zhang

This thesis reports on my research efforts towards controlling light with photonic metamaterials for desired functionalities:

I have demonstrated a new family of continuously metallic metamaterials-'intaglio' and 'bas-relief' metamaterials. They are formed of indented or raised sub-wavelength patterns with depth/height of the order 100 nm and offer a robust and fexible paradigm for engineering the spectral response of metals in the vis-NIR domains. Controlling the colour of metals by intaglio/bas-relief metamaterials has been realized. I have also demonstrated the concept of 'dielectric loaded' metamaterials where nanostructured dielectrics on unstructured metal surfaces work as optical frequency selective surfaces.

I have demonstrated for the first time controlling light with light without nonlinearity using a plasmonic metamaterial. I have experimentally shown that the interference of two coherent beams can eliminate the plasmonic Joule losses of light energy in the metamaterial with thickness less than one tenth of the wavelength of light or, in contrast, can lead to almost total absorbtion of light. The phenomenon provides functionality that can be implemented freely across a broad visible to infrared range by varying the structural design.

I have demonstrated for the first time that a strong light-driven force can be generated when a plasmonic metamaterial is illuminated in close proximity to a dielectric or metal surface. This near-field force can exceed radiation pressure to provide an optically controlled adhesion mechanism mimicking the gecko toe. I have first demonstrated resonant optical forces which are tens of times stronger than radiation pressure within planar dielectric metamaterials and introduced the concept of optomechanical metamaterials. An optomechanical metamaterial consisting of an array of dielectric meta-molecules supported on free-standing elastic beams has been designed. It presents a giant nonlinear optical response driven by resonant optomechanical forces and exhibits optical bistability and nonlinear asymmetric transmission at intensity levels of only a few hundred $\mu W/\mu m^2$. Furthermore, I have experimentally demonstrated optical magnetic resonances in all-dielectric metamaterials.

I have demonstrated for the first time a non-volatile bi-directional all-optical switching in a phase-change metamaterial. By functionalising a photonic metamaterial with the phase-change chalcogenide glass, phase transitions across a 2000 μm^2 area are initiated uniformly by single laser pulse. Reversible switching both in the near- and mid-infrared spectral ranges with a shift of optical resonance position up to 500 nm has been achieved at optical excitation levels of 0.25 $mW/\mu m^2$, leading to a reflection contrast ratio exceeding 4:1 and transmission contrast around 3.5:1.

Contents

List of Figures

DECLARATION OF AUTHORSHIP

I, Jianfa Zhang, declare that the thesis entitled "Controlling light with photonic metamaterials" and the work presented in the thesis are both my own, and have been generated by me as the result of my own original research. I confirm that:

- this work was done wholly or mainly while in candidature for a research degree at this University;
- where any part of this thesis has previously been submitted for a degree or any other qualification at this University or any other institution, this has been clearly stated;
- where I have consulted the published work of others, this is always clearly attributed;
- where I have quoted from the work of others, the source is always given. With the exception of such quotations, this thesis is entirely my own work;
- I have acknowledged all main sources of help;
- where the thesis is based on work done by myself jointly with others, I have made clear exactly what was done by others and what I have contributed myself;
- parts of this work have been published as the journal papers and conference contributions listed in Appendix D.

Signed: _____

Date: _____

Acknowledgements

I am very grateful to my supervisors, Prof. Nikolay Zheludev and Dr. Kevin MacDonald. Prof. Zheludev is both a great scientist and mentor, providing inspiration and guidance for my research, while encouraging me to pursue my own ideas. And I have always admired Prof. Zheludev's creativity, insights and vision, from which I benefit a lot. Dr. MacDonald is a fantastic co-supervisor. He cannot be more helpful in every aspect of my research from setting up experiments to writing journal papers. And there are so many things that I will never forget, such as how patiently he helped me prepare my oral presentation in NANOMETA 2011, which is my first international conference.

I would like to thank all my collaborators, without whom some of my work would not have been possible. Especially Jun-Yu Ou for patiently assisting with fabrication of metamaterial samples by focused ion beam, Dr. Yifang Cheng for fabricating the Al bas-relief metamaterial sample, Nikitas Papasimakis for helping me build and optimize my first COMSOL models. I have enjoyed and benefited a lot from my collaboration with Behrad Gholipour in the phase change metamaterial experiments. I would also like to thank Ruiqi Chen and Dr. Martin Charlton for their help of all-dielectric metamaterial sample fabrication by e-beam lithography.

I would like to thank all other members of the Nanophotonics & Metamaterials group not only for their help in my research, but also for the great time together. Especially, I enjoyed the great friendship with Mengxin Ren and I would like to thank him for his useful advice on my optical experiments. I would like to thank Eric Plum for many fruitful discussions, Zsolt Smson for helping me gain familiarity with various instruments for sample characterization, Takashi Uchino for his kind help and useful advice on dielectric-loaded metamaterial sample fabrication.

I would like to thank all ORC support staffs and ORC/ECS cleanroom technicians.

Especially, Neil Sessions and Dr. Owain Clark for training me to use the clean room machines.

I would also like to express my gratitude towards Prof. Weimin Ye, Prof. Jiarong Ji, Prof. Xiaodong Yuan, Prof. Yazhou Zhang and Prof. Din Ping Tsai for their encouragement.

I am deeply indebted to my family. Confucius said, "While one's parents are alive, one should not travel to distant places. If it is necessary to travel, there should be a definite direction." My pursuit of knowledge and dream has motivated me to work hard, study abroad and finally get where I am now. But nothing can I achieve without the endless support of my family, particularly my parents. Words cannot express my gratitude to them for their love.

Finally, I would like to acknowledge China Scholarship Council and National University of Defense Technology for partly funding my PhD study through China State-Sponsored "Postgraduate Study Abroad Program".

Chapter 1

Introduction

Photonics technology plays a significant role in creating the world as we know it today. From everyday life to the most advanced science, photonics technology is everywhere around us with applications in telecommunications, information procession, sensing, manufacturing, lighting and photovoltaics, metrology, health and so on. Photonics technology is also widely regarded as a key enabling technology for the 21st century and it offers the potential for even greater societal impact over the next few decades [1, 2]. Controlling light is in the key of photonics technology. The ability of molding the flow of light, from light focusing with objectives in optical microscopes to light trapping with nanostructures in solar cells and optical switching on a chip, is critical for every single applications of optics and photonics. In the past decades, various optical materials, structures and devices have been developed to manipulate light and its interactions with matter, among which artificial materials with properties that do not exist in naturally occurring media, know as 'Metamaterials', have attracted great attentions [3].

Metamaterials are artificial media structured on a size scale smaller than the wavelength of external stimuli. Whereas conventional materials derive their electromagnetic characteristics from the properties of atoms and molecules, metamaterials enable us to design our own 'meta-atoms' and thus access new functionalities (Fig. 1.1(a)). First designed and demonstrated at microwave frequencies (Fig. 1.1(b)) [5], metamaterials have since been scaled to work at nearly all frequencies of the electromagnetic spectrum from THz to infrared and visible range [6–8]. Many novel functionalities, such as perfect lensing (Fig. 1.2(a)) [9, 10], negative refraction (Fig. 1.2(b)) [11, 12], invisible cloaking

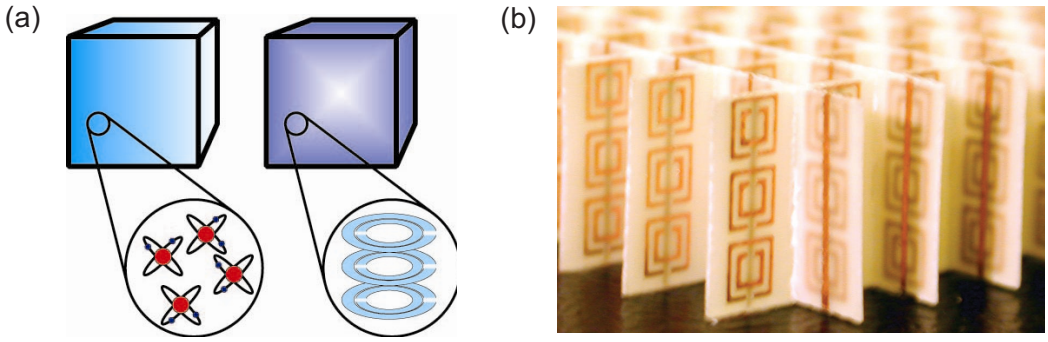

Figure 1.1: Metamaterials: Beyond nature. (a) Concept of metamaterials:in convential (natural) materials, the electromagnetic (EM) properties of materials derive from the constituent atoms; in metamaterials, their EM properties are decided by the subwavelength meta-molecules such as metallic split rings which may contain many atoms [4]. (b) One of the first fabricated metamaterials showing negative index of refraction at microwave frequency [5]. Figure reproduced with permission from: (a), ref. [4], ©2007 OSA; (b), ref. [5], ©2001 AAAS.

(Fig. 1.2(c)) [13,14], subwavelength THz (Fig. 1.2(d)) [15] and optical (Fig. 1.2(f)) [16, 17] modulators as well as broadband circular polarizers (Fig. 1.2(e)) [18], have been demonstrated using metamaterials. Along with the parallel advances in the capabilities and availability of micro and nano-fabrication technologies, photonic metamaterials provide us unprecedented ability of controlling light and have the potential to revolutionize many optical components and devices [19].

This thesis shows several numerical and experimental efforts towards controlling light with photonic metamaterials for desired functionalities. One of the most widely used type of devices for manipulating electromagnetic waves are frequency selective surfaces (FSSs), which have been employed at microwave and radio frequencies for more than half a century. In Chapter 3, the concept of 'bas-relief' and 'intaglio' metamaterials is introduced. This new family of plasmonic metamaterials are formed of raised or indented sub-wavelength patterns on a continuously metallic surface. The interaction of light with these continuously metallic structures is studied both theoretically and experimentally and it is shown that, via the excitation of localized plasmonic modes, a variety of phenomena from electromagnetic field enhancement to modification of intensity and phase of reflected light could be realized. Intaglio and bas-relief metamaterials bring frequency-selective surface functionality into the optical domain and provide a flexible paradigm for engineering the spectral response of metals. The versatility of design is further explored and it is experimentally demonstrated that structural control

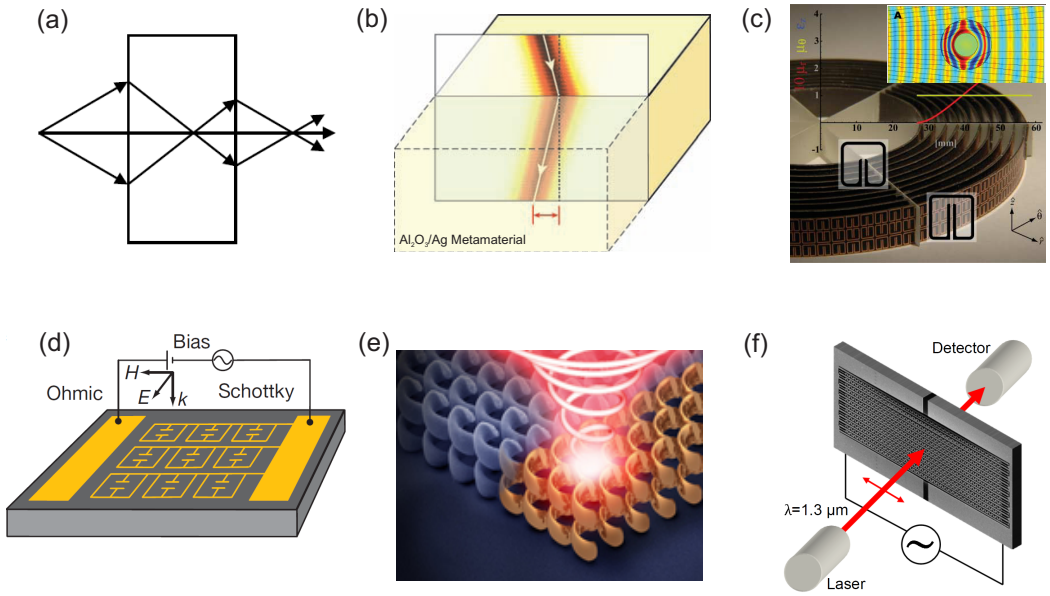

Figure 1.2: Controlling light: From metamaterials to metadevices. (a-c) Exotic electromagnetic properties proposed and realized in metamaterials such as perfect lens (a) [9], negative refraction (b) [12] and invisible cloaking (c) [20]; (d-f) Examples of novel devices for controlling electromagnetic waves enabled by metamaterial concepts such as terahertz metamaterial modulators (d) [15], photonic metamaterials based broadband circular polarizers (e) [18] as well as reconfigurable optical metamaterial modulators (f) [17]. Figure reproduced with permission from: (a), ref. [9], ©2000 APS; (b), ref. [12], ©2008 AAAS; (c), ref. [20], ©2006 AAAS; (d), ref. [15], ©2006 NPG; (e), ref. [18], ©2009 AAAS.

over the visible colour of pure metal surfaces can be dramatically controlled via intaglio and bas-relief metamaterials. Finally, as an extension to the bas-relief metamaterial family, the concept of 'dielectric loaded' metamaterial is introduced, which comprises sub-wavelength patterns of thin-film dielectrics on planar metal surfaces and provides an alternative way of manipulating the optical properties of metal surfaces.

According to the fundamental Huygens superposition principle, light beams traveling in a linear medium will pass though one another without mutual disturbance. Indeed, the field of photonics is based on the premise that controlling light signals with light requires intense laser fields to facilitate beam interactions in nonlinear media. However, coherent interactions, which have been successfully engaged in applications ranging from phased array antennas to the manipulation of light distributions, provide us a leeway of controlling light with light without nonlinearity. In Chapter 4, by employing a plasmonic metamaterial film, coherent control of light-matter interactions within the metamaterial is shown. It is demonstrated that two coherent beams of light of arbitrarily low intensity can interact on the metamaterial layer of nanoscale thickness

in such a way that one beam modulates the intensity of the other. Furthermore, it is shown that the interference of beams can eliminate the plasmonic Joule losses of light energy in the metamaterial or, in contrast, can lead to almost total absorption of light. Applications of this phenomenon will be discussed.

Chapter 5 studies the opto-mechanical forces in metamaterials. Optical forces are extremely important in mesoscopic systems: they are exploited in all forms of optical tweezing, manipulation and binding, and in optomechanical photonic devices. The convergence of nanophotonics and nanomechanics via optical forces presents considerable potential for nanomechanical photonic functionalities. Metamaterials provide an unique platform for manipulating electromagnetic fields and thereby optical forces, on the nanoscale. Firstly, study is conducted on a plasmonic systems, which is known to be able to realize gigantic field enhancement, subwavelength light localization, and strongly enhanced interactions between nano-objects. Numerical simulations show that a strong light-driven force may be generated when a plasmonic metamaterial is illuminated in close proximity to a dielectric or metal surface. This near-field force is attractive near the resonance and provides an optically controlled adhesion mechanism mimicking the gecko toe. Then optical forces in all-dielectric metamaterials are studied. Dielectric metamaterials don't suffer from inherent losses caused by metals and strong resonant optical forces on the resonator elements of dielectric metamaterials are observed. A planar dielectric metamaterial consisting of silicon bricks supported by moveable mechanical beams is investigated and the concept of 'Optomechanical Metamaterials' is introduced. The mutual interactions of optical and mechanical responses of the optomechanical metamaterial present a giant nonlinearity at relatively low optical intensity levels. Finally, planar dielectric metamaterials exhibiting sharp magnetic resonances in the VIS-NIR range are experimentally demonstrated, which makes an important step towards dielectric optomechanical metamaterials.

Chapter 6 presents the work on non-volatile, bi-directional, all-optical switching in phase-change metamaterials. Switchable metamaterials are both appealing and challenging. Metamaterials with tunable properties will significantly enhance their functionalities by operating at dynamic situations and broader frequencies spectra. The ability to tune and switch the properties of materials, something very rarely offered by nature, are also of great significance for applications in optical switches and modulators.

The most effective way of making switchable metamaterials is incorporating materials with tunable electrical or optical properties with metamaterials. Phase-change materials are prime agents for switching: Chalcogenide glasses have been used in rewritable optical disk technology for several decades, providing fast and reproducible changes in optical properties in response to excitation. Phase-change metamaterials based on chalcogenide glasses thus provide non-volatile, highly stable, robust and fast switching capability and this first demonstration of all-optical switching in such type of metamaterials may be an important step towards bringing metamaterials from lab to practical applications.

Chapter 2

Background

2.1 Introduction to surface plasmons

Plasmonics and metamaterials are two closely related fields. Metamaterials generally consist of metallic resonators such as split rings to achieve desired electric and magnetic responses [21]. At the optical frequency ranges, the properties of such metallic structures are associated with excitation of surface plasmons [22]. As such, surface plasmons play a significant role in the electromagnetic properties of photonic metamaterials and it is important to know the surface plasmons in order to understand the optical responses of photonic metamaterials.

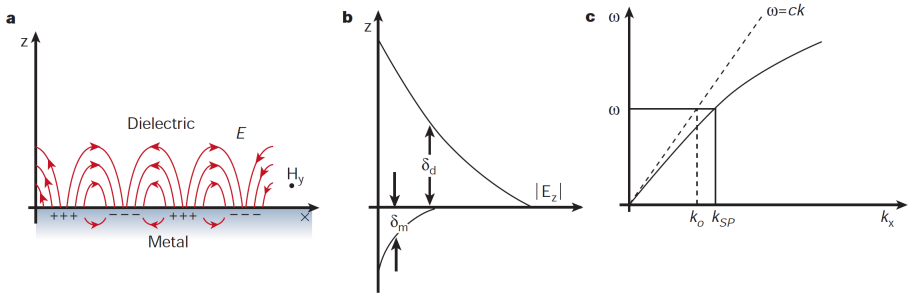

Figure 2.1: Surface plasmons at the interface between a metal and a dielectric material. (a) Surface plasmons show a combined electromagnetic wave and surface charge character. The generation of surface charge requires an electric field normal to the surface; (b) The field component perpendicular to the surface is enhanced near the surface and decays exponentially with distance away from it; (c) The dispersion curve for a surface plasmon mode. Surface plasmon mode always lies beyond the light line and has greater momentum than a free space photon of the same frequency. Figure reproduced with permission from: ref. [23], ©2003 NPG.

Surface plasmons are collective electron excitations at the interface of two materials

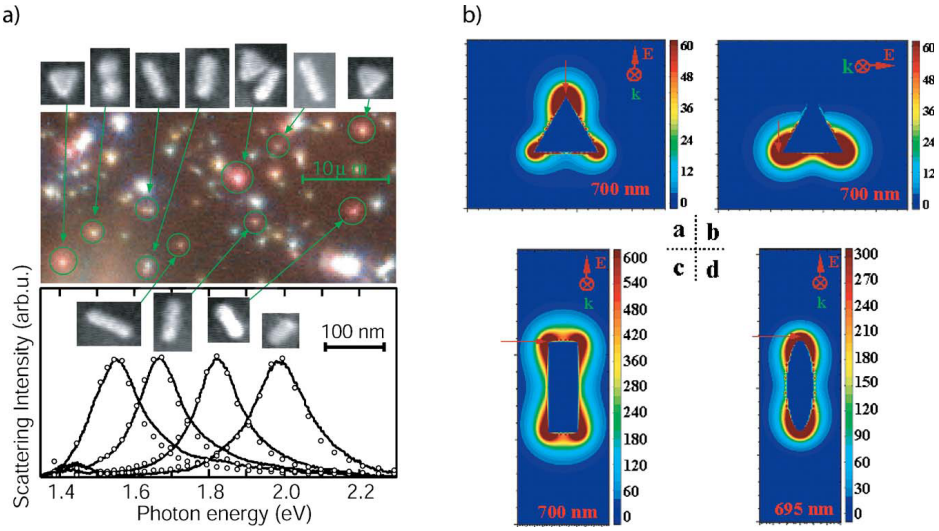

Figure 2.2: Localized surface plasmon. (a) Dark-field microcopy image (top) and light scattering spectra (bottom) of Au nanocrystals of different shapes [24]; The measured spectra (black curves) show good agreement with predictions from a simple analytical extension of quasistatic Mie theory (open circles). (b) Electric near-field profile of the lowest-order modes of Ag nanoprisms calculated using the discrete dipole approximation formalism [25]. Figure reproduced with permission from: ref. [26], ©2005 AIP.

where the real part of the dielectric function changes sign across the interface, typically a metal/dielectric boundary (Fig. 2.1). Surface plasmons can be excited by electromagnetic radiation and the resulting excitations are called surface plasmon polaritons. The properties of surface plasmon polaritons are described by Maxwell's equations. A smooth semi-infinite metal/dielectric boundary can support propagating surface plasmon polaritons and the dispersion of these modes is given by the expression [27]:

$$k_{spp}(\omega) = \frac{\omega}{c}\sqrt{\frac{\varepsilon_m(\omega)\varepsilon_d}{\varepsilon_m(\omega)+\varepsilon_d}}$$

where k_{spp} is the SPP wavevector, ω is the electromagnetic frequency, c is the speed of light in vacuum, and $\varepsilon_m(\omega)$ and ε_d are the complex dielectric coefficients of the metal and dielectric media, respectively. Surface plasmon polaritons can also propagate along other metal/dielctric interfaces, such as a thin metal film, a gap filled with dielectric between two metal surfaces, a groove on a metal surfaces and a metal wedge. Surface plasmons are responsible for a host of phenomena unique to metals, e.g., surface enhanced Raman scattering [28] and extroordinary transmission of light through subwavelength holes in metal films [29]. A perfect conductor, whose dielectric function is quite different from that of a metal at optical frequency ranges, can also

be induced to support surface modes by drilling an array of holes in the surface. Such surface electromagnetic waves are called spoof surface plasmons [30].

While collective electron excitations can propagate along a smooth surface, they are sometimes confined to metallic nanoparticles and metallic nanostructures, called localized surface plasmons (LSPs) (Fig. 2.2) [31]. Excitation of LSPs by light at an wavelength where the resonance occurs results in strong light scattering, along with an intense absorption band and enhancement of local electromagnetic fields. Localized plasmon resonances can greatly enhance light-matter interactions and are widely studied for applications such as light concentration and manipulation [32], solar energy harvesting [33], sensing [34] as well as ultra-fast all-optical signal processing [35].

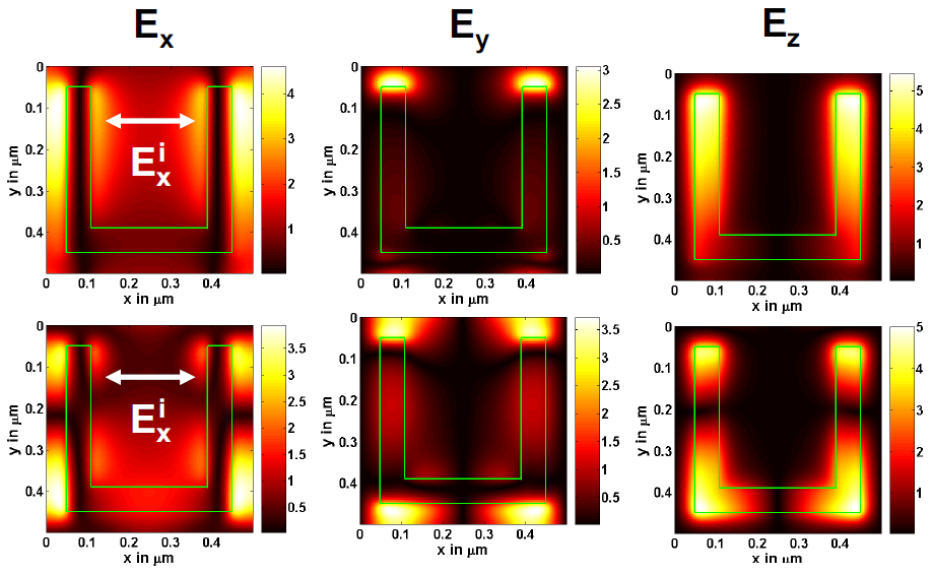

Figure 2.3: Plasmonic resonance model for photonic metamaterials. The figures show magnitude of the electric field distribution for the first two plasmon modes. The illuminating electric field is chosen to be polarized parallel to the gap (x-polarized). The fields are normalized to the illuminating electric field. Figure reproduced with permission from: ref. [36], ©2006 OSA.

Localized surface plasmon resonances can also be utilized to explain the optical properties of plasmonic metamaterials. Giessen *et al.* did comprehensive study of 'U'-shaped split-ring-resonators and found that all resonances can be understood as plasmonic resonances of increasing order of the entire structure (see Fig. 2.3) [36], which was verified by experiment [37]. In such a model, for an electrical field polarized parallel to the gap the so-called LC-resonance [7] corresponds to the fundamental plasmonic mode while higher order of modes are responsible for resonances at higher frequencies

that can not be explained by the LC-circuit model.

2.2 Planar plasmonic metamaterials and trapped-mode resonances

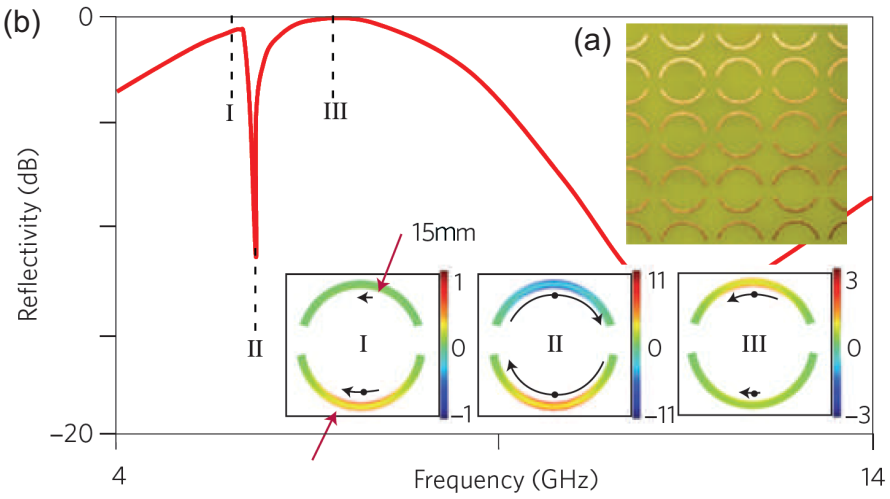

Figure 2.4: Trapped-mode resonances in metamaterials. In a microwave metamaterial an array of wire asymmetric split rings (a), trapped mode resonance (II) is formed by excitation of anti-phase currents in two wires with slightly different lengths in metamaterial unit cell. The spectrum (b) displays Fano line shape due to the interference between high-Q magnetic dipole mode (II) and low-Q electric dipole modes (I and III). Black arrows indicate instantaneous directions of the current flow. The spectrum and current distributions are obtained by three dimensional numerical simulations. Figure reproduced with permission from: ref. [38], ©2010 NPG.

Planar plasmonic metamaterials consisting of periodical unit cells made of asymmetric split rings cut through thin metallic film are widely employed in this thesis. This type of planar metamaterials support Fano resonances arising from symmetry-breaking and they belong to a group of plasmonic structures showing Fano resonances [38]. This type of modes are weakly coupled to free space and thus allow in principle to achieve high quality resonances and are called 'trapped modes' or 'closed modes' [39]. Trapped-mode resonances in metamaterials were observed for the first time in asymmetrically split-ring arrays at microwave frequencies (Fig. 2.4) [40]. When excited by an electromagnetic wave, the two uneven arcs of the split-ring structure support in-phase current oscillations (I and III), except in a narrow frequency range in which an anti-phase current is established (II). The antisymmetric excitations form an array of

magnetic dipoles oscillating perpendicular to the plane of the metamaterial. This collective subradiant mode couples only weakly to free space through interaction with a much broader super-radiant dipole mode of in-phase currents, creating a classical Fano complex.

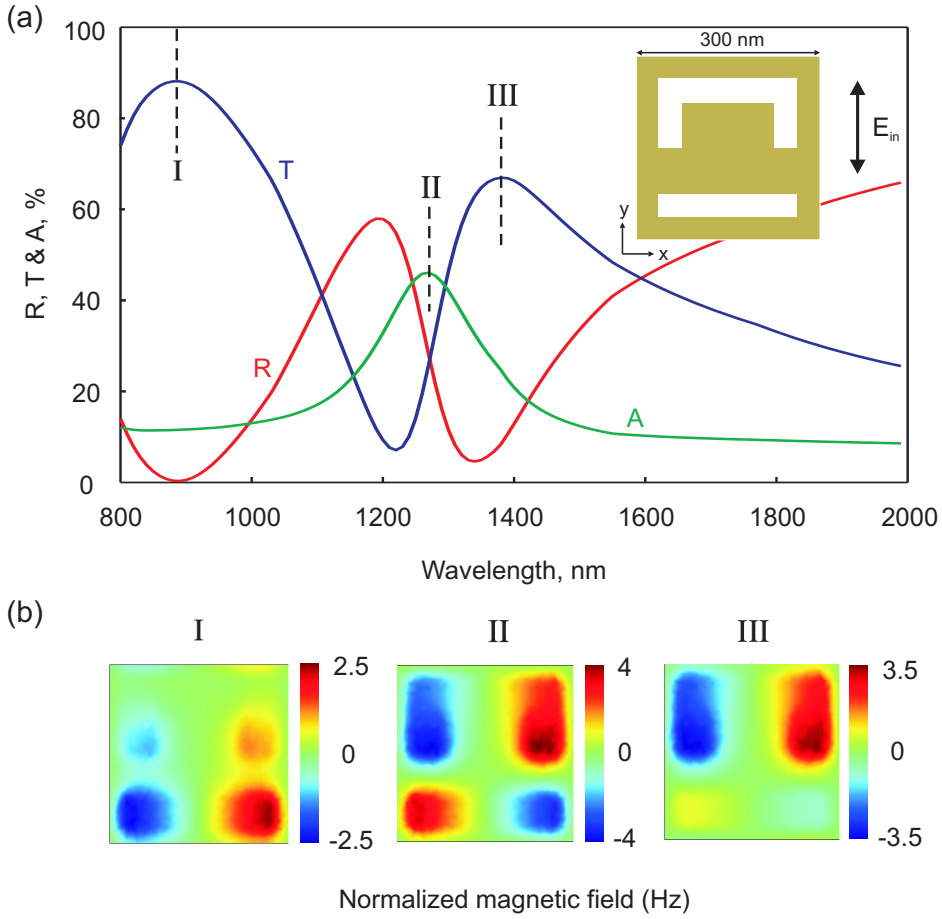

Figure 2.5: A plasmonic metamaterial displaying a trapped mode resonance in the near infrared. (a) Simulated reflection, transmission and absorption spectra for y-polarized plane wave radiation at normal incidence. A trapped mode resonance was observed at around 1270 nm due to symmetry breaking. (b) Magnetic field distributions (normalized to incident magnetic field, in z direction) taken at 5 nm above the metal surface for the high-Q trapped mode resonance (II) and another two low-Q modes (I and III).

Trapped-mode resonances can also be realized in planar plasmonic metamaterials in optical frequency ranges. Fig. 2.5a shows the simulated optical spectra of a photonic metamaterial formed by cutting an array of asymmetric split rings through a 50 nm thick gold film. This metamaterial is a complementary structure of a photonic metamaterial consisting of an array of asymmetric split rings and can be understood by taking

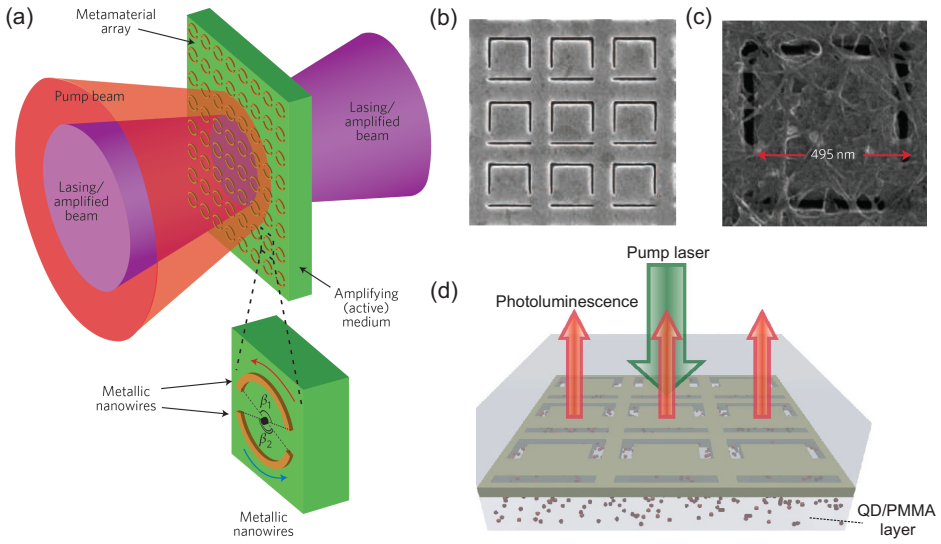

Figure 2.6: Applications of plasmonic metamaterials supporting trapped mode resonances. (a) Conceptual design of the lasing spaser [41], a lasing device fuelled by plasmonic oscillations at the trapped mode resonance. (b) A photonic metamaterial, in the form of an array of asymmetric slits in a gold film manufactured by focused ion beam. This structure is complementary to the structure shown in Fig. 2.4 and it is simplified for fabrication. (c) A unit cell of such a photonic metamaterial functionalized with a 'nanoscale feature' of single-walled carbon nanotubes and imaged with a helium-ion microscope shows enhanced ultrafast nonlinear response owing to plasmonexciton coupling [42]. (d) Schematic of a plasmonic metamaterial functionalized with quantum dots. The trapped mode resonance can significantly enhance the luminescence of quantum dots in the vicinity [43]. Figure reproduced with permission from: (a), ref. [41], ©2008 NPG; (c), ref. [42], ©2010 APS; (d), ref. [43], ©2010 APS.

advantage of Babinet's principle [44]. It exhibits a complementary spectral response, which shows a trapped mode resonance at around 1270 nm due to symmetry breaking for incident radiation with electric field parallel to its axis of symmetry (y-direction). For a positive structure of asymmetric split rings, the electric field in the direction perpendicular to the metamaterial plane shows the distribution of oscillating charges and is generally employed to analyze the properties of plasmonic resonances [36]. According to Babinet's principle, here the magnetic field in z- direction must be used for the complementary structure. The field distributions show that the trapped mode resonance is formed by antisymmetric excitation in the two rings with slightly different lengths (Fig. 2.5b). Importantly, the optical responses (e.g. resonance wavelength, Q factor *etc.*) of planar plasmonic metamaterials can be engineered with great freedom through design [45].

Planar photonic metamaterials displaying trapped mode resonances have been suc-

cessfully employed for a range of applications (Fig. 2.6). Fig. 2.6(b) shows an electron microscope image of a planar plasmonic metmaterials. The transmission band of this type of metamaterials is accompanied by a steep normal dispersion, enabling low group velocities, electro magnetically induced transparency (EIT)-like and slow-light behaviour in both passive and gain-assisted metamaterials [46]. And it will greatly enhance linear and nonlinear effects in light-matter interactions. One of the striking ideas based on this type of metamaterials is the 'Lasing spaser', which combines metamaterial and spaser ideas to create a narrow-divergence, coherent source of electromagnetic radiation (Fig. 2.6(a)). The lasing spaser is fuelled by collective, dark plasmonic oscillations which draw energy from the substrate with gain medium and leak into free space through a highly radiating mode [41]. Other demonstrated applications include enhancement of nonlinear effects in carbon nanotubes (Fig. 2.6(c)) [42], graphene [47], gold [48] as well as enhancement of quantum dot luminescence (Fig. 2.6(d)) [43].

Chapter 3

Intaglio and bas-relief metamaterials

3.1 Introduction

Metamaterials, for any spectral domain from microwaves [5] to THz [6], IR [7] and visible [49], are conventionally made up of discrete resonant elements. Those elements are usually metallic split rings surrounded by dielectric, or patterns of slots cut through metallic thin films, which are used to achieve desired magnetic and electric responses. Either way, they present a discontinuous profile of metal and dielectric to incident radiation and the electromagnetic properties of metamaterials are significantly shown by the transmitted radiation [50]. This chapter presents another type of metamaterials that are continuously metallic and are formed of a raised or indented subwavelength pattern in an optically thick plasmonic metal film. Borrowing terminology from the art world, these are called 'bas-relief' and 'intaglio' metamaterials [51].

The general idea of modifying the electromagnetic properties of a metal surface by texturing is not entirely new. We could go back nearly half a century to concepts of microwave or radio frequency selective surfaces (FSSs), where metals behave as perfect conductors. FSSs are a well-established paradigm for filtering electromagnetic waves [54], and are recognized as the foundation of the modern field of metamaterials [3]. They commonly comprise either cascaded partially transmitting boundaries (akin to distributed Bragg reflectors in optics) or, like their metamaterial counterparts,

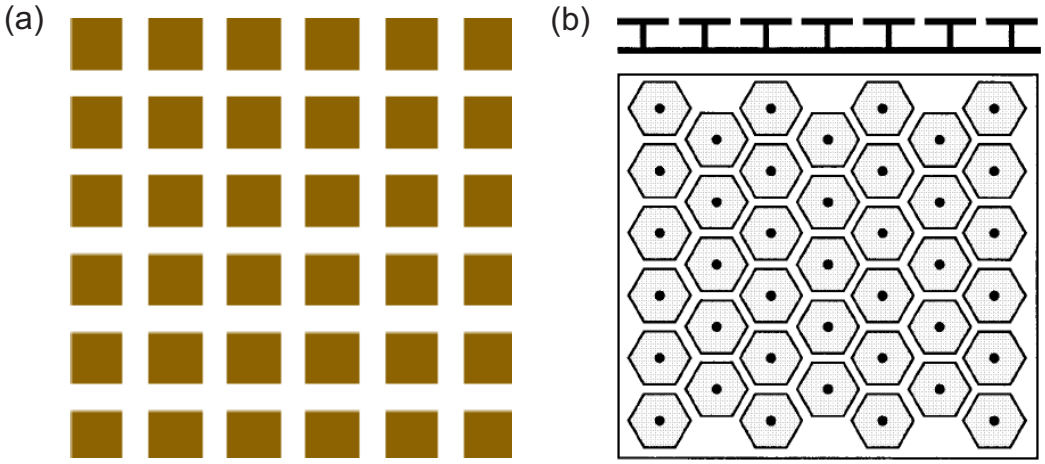

Figure 3.1: Frequency selective surfaces. (a) A mesh filter consisting of a grid of metal squares forms a simple frequency selective surface for microwave and radio frequency electromagnetic applications [52]. (b) Cross section and top view of a 'mushroom' high-impedance surface, fabricated as a printed circuit board. The structure consists of a lattice of metal plates, connected to a solid metal sheet by vertical conducting vias [53]. Figure reproduced with permission from: (b), ref. [53], ©1999 IEEE;

resonant periodic arrays of conducting elements in a dielectric matrix or apertures in a conducting screen [52] (Fig. 3.1). In such systems, functionality relies on manipulation of the balance between reflected and transmitted waves. More sophisticated structures such as 'mushrooms' have also been investigated for high impedance surfaces (HIS) [53], artificial magnetic conductors (AMC) [55] and other applications. However, some of these designs are not easily scalable into the photonic domain. And the electromagnetic properties of metals in the photonic domain behave quite differently from those in microwave or radio frequency ranges due to the excitation of surface plamons [22]. Bas-relief and intaglio metamaterials to be discussed in this chapter derive their properties from the plasmonic resonances of metamolecules arrayed on the metal surface and form a family of real photonic metamaterials. They provide freedom to engineer the geometry and dimensions of meta-molecules at the subwavelength scale to achieve desired properties and offer great potential for a range of photonic functionalities [56].

3.2 Intaglio and bas-relief metamaterials: Frequency selective surfaces in the optical range

In the visible and infrared range, Joule losses in metals become very significant and plasmonic resonances play a crucial role in determining the optical properties of metallic nanostructures. The interaction between surface plasmons at a metal-dielectric interface and an external electromagnetic field can produce surface electromagnetic modes called surface plasmon polaritons (SPPs).The dispersion of these modes, for a flat metal-dielectric interface, is given by the expression [27]:

$$k_{spp}(\omega) = \frac{\omega}{c}\sqrt{\frac{\varepsilon_m(\omega)\varepsilon_d}{\varepsilon_m(\omega)+\varepsilon_d}}$$

where k_{spp} is the SPP wavevector, ω is the electromagnetic frequency, c is the speed of light in vacuum, and $\varepsilon_m(\omega)$ and ε_d are the complex dielectric coefficients of the metal and dielectric media, respectively. More complicated metallic geometries (slots, ridges, particles, ...) support a wide variety of either propagating or spatially localized surface plasmon modes [31, 57–59]. Momentum conservation conditions must be satisfied for the coupling of light into propagating SPPs and the optical properties of structures supporting such modes are therefore strongly dependent on the incident angle of impinging radiation. In contrast, localized surface plasmon resonances are relatively insensitive to the angle of incidence [22].

In the surface intaglio/relief metamaterials discussed here, the subwavelength structure and periodicity of 'meta-molecule' unit cells excludes the generation of propagating SPPs; the nanostructure efficiently couples and traps incident light at resonant frequencies determined by meta-molecule size and geometry, leading to strong absorption and local field enhancement.

In what follows, numerical results are obtained from fully three-dimensional finite element Maxwell solver simulations (in Comsol MultiPhysics, see Appendix A for details of modeling). By modeling single meta-molecules with periodic boundary conditions, calculations assume planar metamaterial arrays of infinite extent; The analyses utilize established experimental values of the complex dielectric parameters for gold (see Appendix B) [60], exclude losses in dielectric media and assumes normally incident, monochromatic coherent illumination. In all cases, metal films are optically thick (i.e.

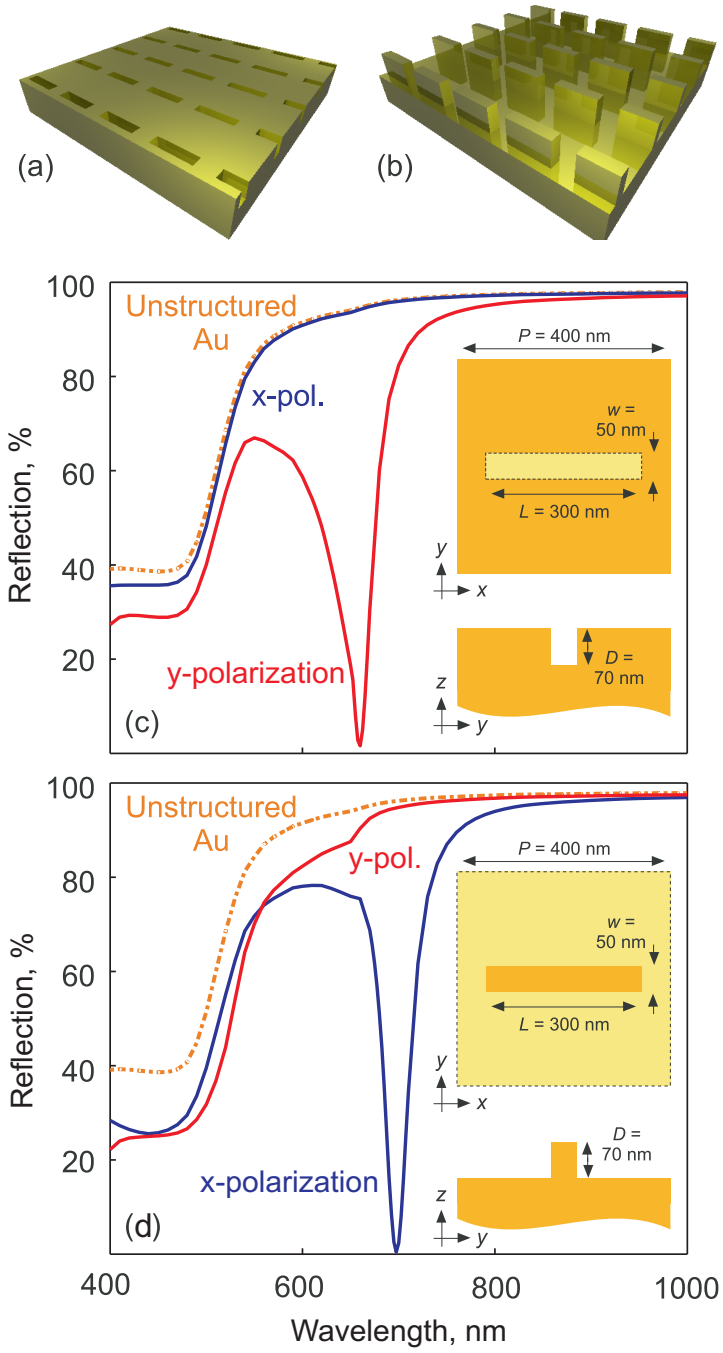

Figure 3.2: Simulated spectra for intaglio and bas-relief metamaterials. (a) Artistic renderings of intaglio slot metamaterials. (b) Complementary bas-relief bar metamaterials. (c) and (d) show corresponding numerically simulated reflection spectra, respectively, for incident light polarizations parallel and perpendicular to the slot/bar features. Dimensional details of the meta-molecule unit cells are shown inset to (c) and (d); Both plots also show the reflection spectrum of an unstructured gold surface for comparison.

transmission is negligible) and modifications of reflection spectra can therefore be taken to correspond directly with changes in absorption. Here the reflection spectra include

a sum over all polarization states. However, in all the cases below no polarization rotation will happen during reflection and the reflected light has the same polarization state as the incident light.

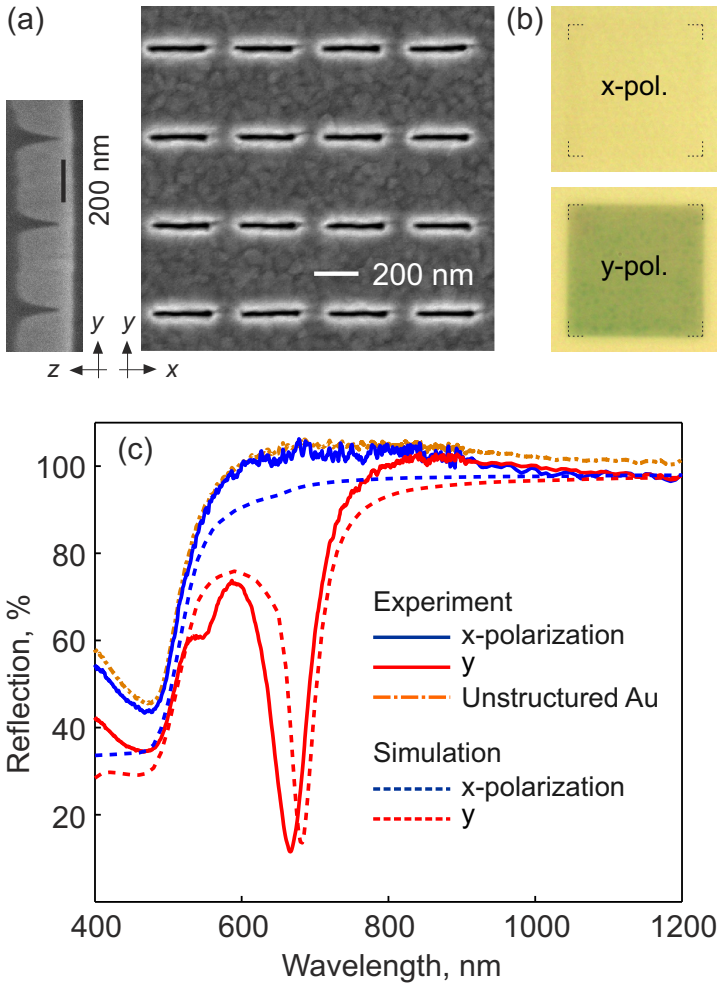

Figure 3.3: Experimental a spectra for intaglio slot metamaterial. (a) Scanning electron microscope images of a gold intaglio slot metamaterial in plane [right] and cross-sectional [left] views. (b) Optical microscope images of the sample under illumination with x- and y-polarized light [as defined in part (a)]. The patterned area marked by the dashed corners measures 30 μm $\times$ 30 μm; the surface outside this boundary is unstructured gold. (c) Experimentally measured and corresponding numerically simulated reflection spectra for the metamaterial structure shown in part (a) for x and y polarizations of incident light. The reflection spectrum of the unstructured gold sample surface is also shown for comparison.

Fig. 3.2 shows simulated reflection spectra for complementary gold intaglio and bas-relief metamaterials with simple unit cell structures comprising a single linear (intaglio) slot or (bas-relief) bar, for incident light polarizations parallel (x) and perpendicular (y) to the long axis of the feature. For the intaglio case (Fig. 3.2a and c), there is

strong resonant absorption of y-polarized light (perpendicular to the slots), giving a reflection minimum at around 660 nm, while x-polarized light is reflected almost as if no pattern were present (its reflection spectrum is virtually identical to that of an unstructured gold surface). These behaviours are reversed by the corresponding bas-relief metamaterial (Fig. 3.2b and d): In this case there is resonant absorption of light polarized in the x direction (along the bars) while the y-polarization reflection spectrum is broadly unperturbed by the pattern. Thus the different optical responses of intaglio metamaterials and bas-relief metamaterials here are similar to those of complementary transmissive metamaterials and nanoapertures that can be understood by taking advantage of Babinet's principle [44].

As explained, these modifications of reflection spectra are attributed to the excitation of localized plasmons, which for highly anisotropic meta-molecules are strongly dependent on the polarization of incident light. The raised bars function as metallic nano-antennas backed by a metallic wall and the charge density oscillates preferentially along these features when driven by an external light field. As such, the bas-relief metamaterial couples efficiently with the light polarized along the long (x) axis of the bars. For intaglio patterns, the slot serves as a metal-dielectric-metal (MDM) 'waveguide' supporting a gap plasmon mode that is resonantly excited by light polarized perpendicular to the slot (i.e. in the y direction).

Fig. 3.3 illustrates an experimental implementation of the anisotropic intaglio slot metamaterial considered above. The pattern was fabricated by focused ion beam milling (FEI Helios NanoLab 600) in a 250 nm thick gold film deposited on an optically polished fused silica substrate by thermal evaporation(Au samples shown in this chapter were prepared with the assistance of Jun-Yu [Bruce] Ou using the ORC focused ion beam milling facility); Normal incidence reflection spectra were measured using a microspectrophotometer (CRAIC QDI2010) with a broadband linear polarizer to control the polarization of incident light (reflected/transmitted light always keeps the same polarization as incident light in our setup). As prescribed by the simulations above: under x-polarized light the metamaterial sample has a reflection spectrum that is almost identical to that of unstructured gold and as such is visually indistinguishable from the flat metal; while under y-polarized light it presents a strong absorption resonance, centred in this case at $\sim$670 nm, which markedly changes the colour of the

metal.

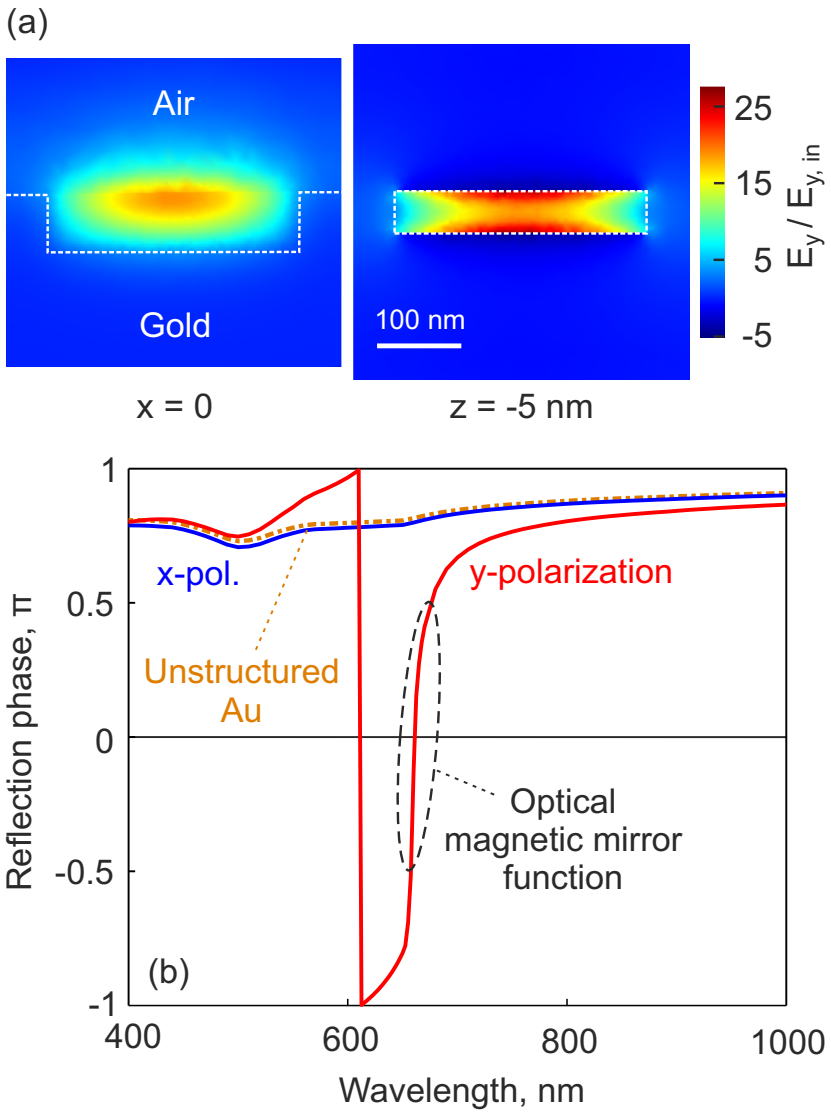

Figure 3.4: Electric field distribution and reflection phase near the resonance of a intaglio slot metamaterial. (a) Maps of electric field intensity, relative to that of the incident y-polarized field, for a unit cell of the intaglio slot metamaterial presented in Fig. 3.2c at its 660 nm resonance [in the y=0 mirror symmetry plane of the cell and in a z-plane 5 nm below the gold surface]. (b) Computationally evaluated dispersion of the phase change in electric field on reflection from the aforementioned intaglio slot metamaterial for both x and y polarizations of normally incident light. The phase change for light reflected from an unstructured gold surface is also shown for reference.

Fig. 3.4a shows electromagnetic field maps of the above intaglio slot metamaterial under illumination at the 660 nm resonance with y-polarized light at normal incidence. Light is trapped in the form of a gap plasmon mode and the magnitude of the electric field is enhanced by a factor of up to ∼27, with a maximum located at the top (open

face) of the slot. It is established that resonances occur in such cavities when the cavity length is equal to an odd multiple of a quarter plasmon wavelength due to boundary conditions requiring an electric field node at the closed base (mirror) and an antinode at the open top [61–63]. Here the effective depth of the slot is one quarter of the gap plasmon wavelength and as a consequence of this resonance the metamaterial acts as a HIS [53]. The phase of the reflected light (Fig. 3.4b) provides further insight into the effect of the plasmonic resonance on surface impedance: For the y-polarization, which couples strongly to the gap plasmon mode, the reflected phase varies dramatically around the resonance wavelength. Indeed, it crosses zero, implying a reflected electric field with the same phase as the incident field (as opposed to one shifted by $\sim \pi$ relative to the incident field, as is the case for reflection from an unstructured metal and in this instance for x-polarized light). In this range the continuously metallic metamaterial functions as a HIS, or 'optical magnetic mirror' [64] for the y-polarization.

Optical magnetic mirrors impose extremely unusual electromagnetic boundary conditions: rather than reversing the electric field of a light wave upon reflection, they reverse the magnetic field - an exotic behaviour with a number of potentially useful applications. While the emission of an electric dipole is quenched when it is located in close proximity to a normal electric conductor (due to the presence of its mirror-image dipole), the radiation of a dipole near a magnetic mirror is enhanced, presenting interesting opportunities, for example, in molecular spectroscopy.

In the interaction between an incident plane wave and an intaglio metamaterial, the unit cells of the latter act as open resonator described by a resonant frequency and 'quality factor' Q. The reflection coefficient R is close to unity off resonance and is characterized by sharp resonant dips on-resonance. The resonant reflection coefficient is given by the expression [65]:

$$R = \frac{(-Q_{leak}^{-1}+Q_{diss}^{-1})^2}{(Q_{leak}^{-1}+Q_{diss}^{-1})^2}$$

where Q_{leak} and Q_{diss} are Q-factors responsible for, respectively, the leakage and dissipation of the plasmonic resonators. If the leakage and dissipation Q-factors are equal, the reflection spectrum exhibits a pronounced resonant dip, with R=0. This is the so-called 'critical coupling' effect. Where the sub-wavelength structure and periodic arrangement of meta-molecule unit cells precludes any kind of diffraction or

polarization conversion, surface relief metamaterials can be engineered to absorb light completely if designed in such a way that the radiative decay rate of the resonance is equal to the dissipative rate. Fig. 3.2 illustrates how the simplest intaglio and bas-relief metamaterials can achieve near-total absorption at plasmonic resonances.

'Perfect absorption' has many potential applications, from preventing crosstalk between optical interconnects to controlling thermal emission [66]. Metamaterial perfect absorbers have been proposed and achieved in various frequency domains [67–70], and almost invariably comprise meta-resonators separated from a metallic mirror backplane by a thin dielectric layer. Wide-angle, near-perfect VIS/NIR absorption by structured metal surfaces has also been demonstrated through the excitation of localized plasmons in spherical cavities and gratings [71,72]. Results here (Fig. 3.2 and 3.5) illustrate that perfect absorption may be achieved through both indented and raised sub-wavelength patterns with depths/heights of just a few tens of nanometers on continuously metallic surfaces. Both isotropic and anisotropic absorption for linearly polarized light can be achieved through pattern geometry variation and circular dichroism may be realized by relief metamaterials with planar chiral meta-molecules.

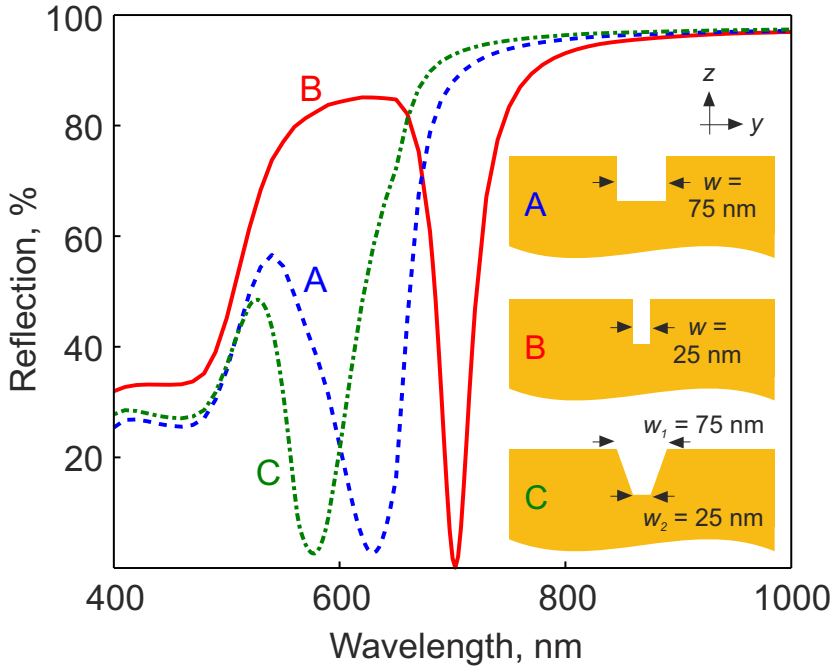

Figure 3.5: Impact of geometric parameters on the spectral response of continuously metallic surface relief metamaterials: Numerically evaluated reflection spectra for gold intaglio slot metamaterials of identical periodicity, slot length and slot depth [P=400, L=300, D=70 nm] but varying slot cross-section as illustrated inset.

The optical properties of surface relief metamaterials are dictated by geometric parameters including the in-plane size, out of plane height/depth, anisotropy, cross-sectional shape and periodic arrangement of features.

As illustrated above, the (an)isotropy of unit cells determines the polarization dependence of optical properties. The cross-sectional shape of slots/bars has a strong impact on the spectral position and width of absorption resonances. Consider for example, the intaglio slot pattern: the condition for resonance is: $Dk_z(\omega)+\Delta\phi \sim m\pi+\frac{\pi}{2}$ where D is the depth of slot, $\Delta\phi$ is the phase shift on (plasmon) reflection at the base of the slot, $k_z(\omega)$ is the component of the gap SPP wavevector in the vertical (z) direction. The dependence of resonance frequency on slot depth is clear. $k_z(\omega)$ obviously depends on the dispersion of the gap plasmon mode(s) and numerous studies have previously addressed the significance of slot shape here [59, 61, 73, 74].

If the cross-section of the slot is a rectangle, $k_z(\omega)$ is constant and its value can be determined from the dispersion of the MDM structure. These support symmetric and asymmetric modes, as defined by their electric field distributions in the (y) direction perpendicular to the slot. The coupling efficiency between incident radiation and localized plasmons is proportional with the spatial and temporal overlap of modes. In the present case, the air gap between the walls of the intaglio metamaterial slot is typically only a few tens of nanometres wide and the incident field is almost constant across the gap, so only the symmetric mode can be efficiently excited. As the slot becomes narrower (for fixed depth) the confinement of the mode increases and its propagation constant increases, leading to a red-shift in the absorption resonance (see Fig. 3.5).

If the slot is not rectangular, the situation is more complex: For example, Fig. 3.5 shows the reflection spectrum for an intaglio metamaterial comprising slots with a profile tapering from w_1=75 nm at the top to w_2=25 nm at the base. Its resonance lies at a wavelength shorter than that of any rectangular slot of the same depth with a width between w_1 and w_2. Of course, the meta-molecule feature(s) need not be linear or singly-resonant, as the experimental examples in Fig. 3.6 show: circular rings deliver an isotropic, polarization-independent absorption resonance; a second ring inside the first adds a second (shorter wavelength) absorption resonance, creating a low reflectivity band extending from around 700 to 850 nm.

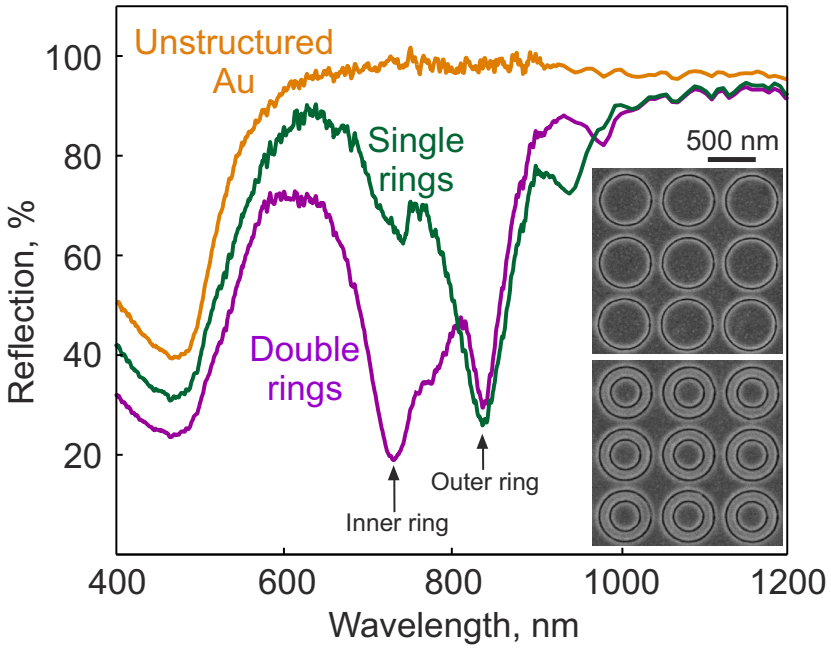

Figure 3.6: Impact of meta-molecule pattern geometry on the spectral response of continuously metallic surface relief metamaterials: Experimentally measured, polarization-independent reflection spectra for single- and concentric-ring gold intaglio metamaterials, sections of which are shown in the inset scanning electron microscope images. The reflection spectrum of the unstructured gold sample surface is also shown for comparison.

Fig. 3.7a shows reflection spectra for a family of intaglio metamaterials with identical slot sizes but different periodicities. As the optical response of surface relief metamaterials is attributed to localized surface plasmon resonances, and the sub-wavelength arrangement unit cells excludes diffraction effects, changes in the periodic spacing of features impact primarily on the coupling between neighboring unit cells. As is shown, the resonant wavelength is only very slightly affected by changes in structural periodicity due to near field coupling between individual nanogrooves, but the resonance width decreases as the spacing increases - a behaviour consistent with prior studies of conventional (discrete split ring resonator array as opposed to continuously metallic) metamaterials [75, 76].

Also in keeping with conventional metamaterial forms, the optical properties of surface relief metamaterials depend critically on those of the adjacent dielectric medium. The presence of a 'cladding' layer with a refractive index n greater than unity brings about a substantial red shift in absorption resonance frequencies (Fig. 3.7b) and points both to techniques for controlling, indeed actively switching/tuning, the re-

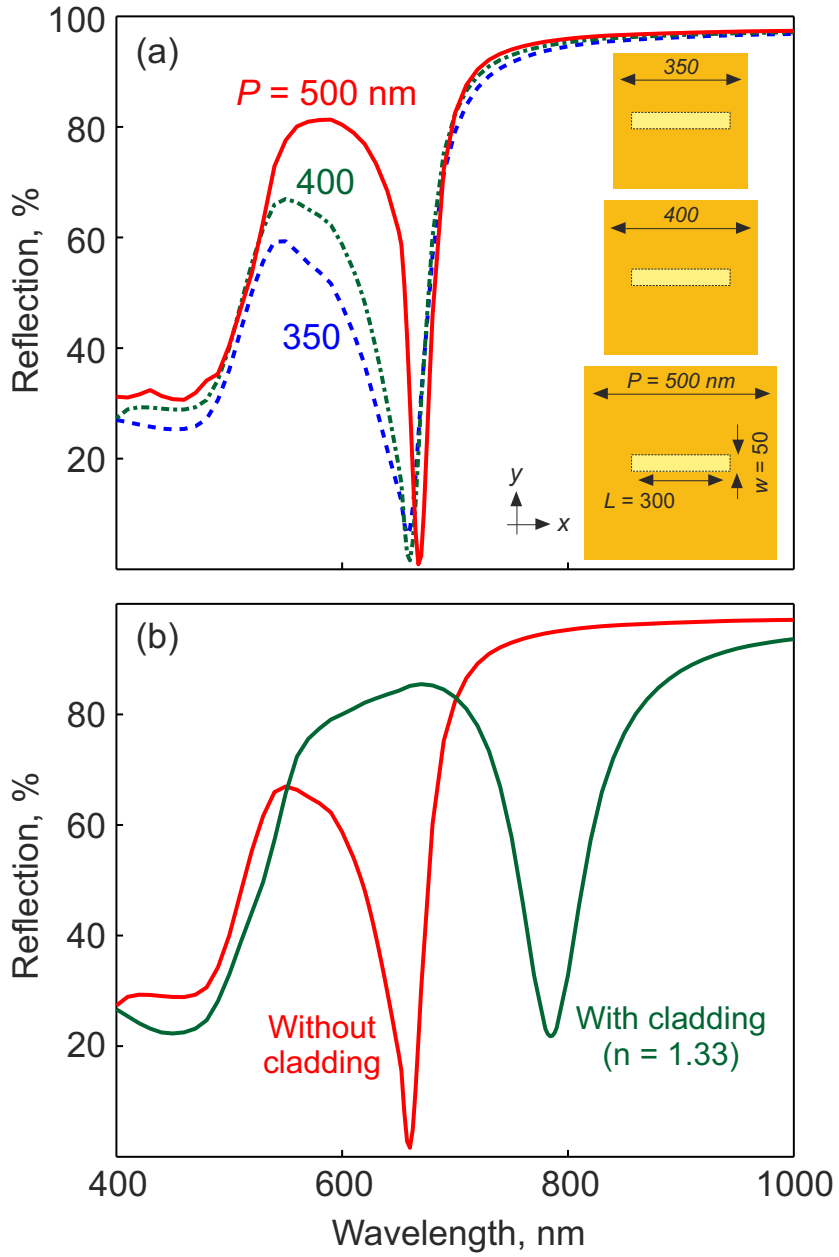

Figure 3.7: Impact of unit cell periodicity and dielectric environment on the spectral response of continuously metallic surface relief metamaterials. (a) Numerically evaluated reflection spectra for gold intaglio metamaterials with identical slot dimensions [L=300, w=50, D=70 nm] but varying meta-molecule cell size as illustrated inset. (b) y-polarization spectra for the metamaterial structure presented in Fig. 3.2c with and without a 100 nm thick cladding layer of refractive index n=1.33.

sponse of intaglio/bas-relief structures using optically/electrically/thermally responsive functional media [16, 42, 77–79].

3.3 Controlling the colour of metals

Intaglio and bas-relief metamaterials form a class of FSSs operating in the visible/near-infrared spectral domain, where the plasmonic response of metals facilitates the modification of reflection spectra through the formation of arrays of nanoscale elements inscribed into or raised above the surface to a depth/height of the order 100 nm. These intaglio and bas-relief metamaterials can radically change a metal's reflection spectrum and, in the visible range, its perceived colour (Fig. 3.8) without recourse to chemical modification (e.g. anodization) or application of secondary coatings (paints, dielectric multilayers, etc.). Moreover, the colours produced can, by design, be polarization-dependent or -independent and are largely insensitive to viewing angle.

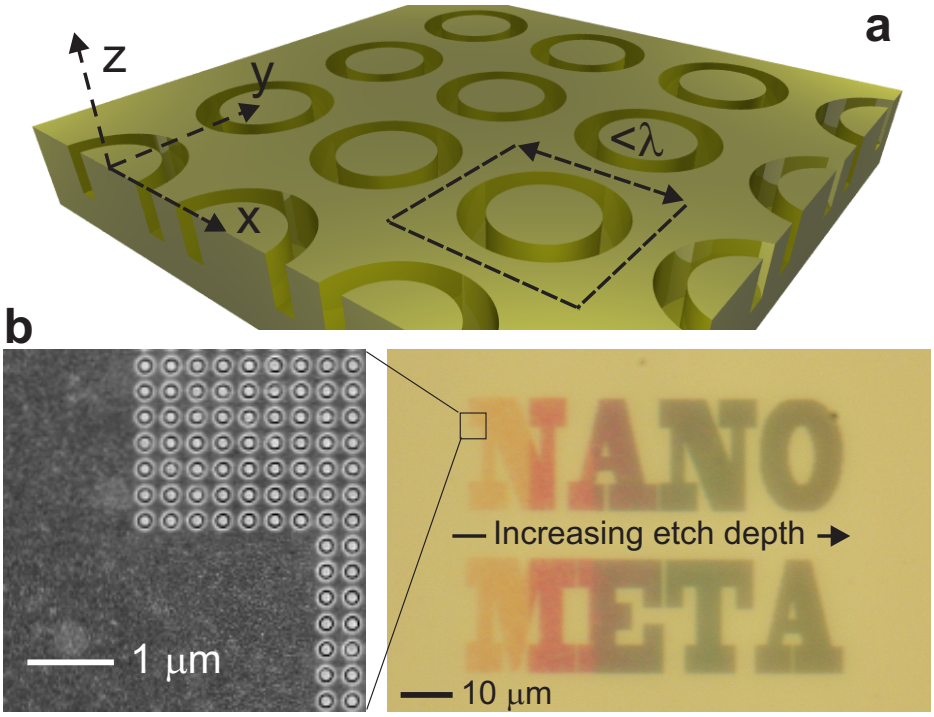

Figure 3.8: Metallic structural colour. (a) Artistic impression of a generic intaglio metamaterial array of sub-wavelength single ring meta-molecules inscribed into a metal surface; (b) The realization of this concept in gold: The words 'NANO META' seen under an optical microscope on the right are formed from arrays of 170 nm diameter rings (as shown in the electron microscope image, left) milled to a depth that increases in six steps from 60 to 200 nm across the sample.

In the natural world, many plants and animals display dramatic 'structural colours' derived from astonishingly intricate three-dimensional assemblies of intrinsically colourless bio-materials [80] and while the physics of these colours is increasingly well un-

derstood, replicating them remains a significant challenge [81–83], typically requiring complex (multi- or atomic) layer deposition and etching fabrication procedures. In contrast, the intaglio/bas-relief metamaterials provide a flexible paradigm for structural colouring of pure metals that can be applied equally to bulk and thin-film surfaces and may ultimately be implemented via a single-step imprint process.

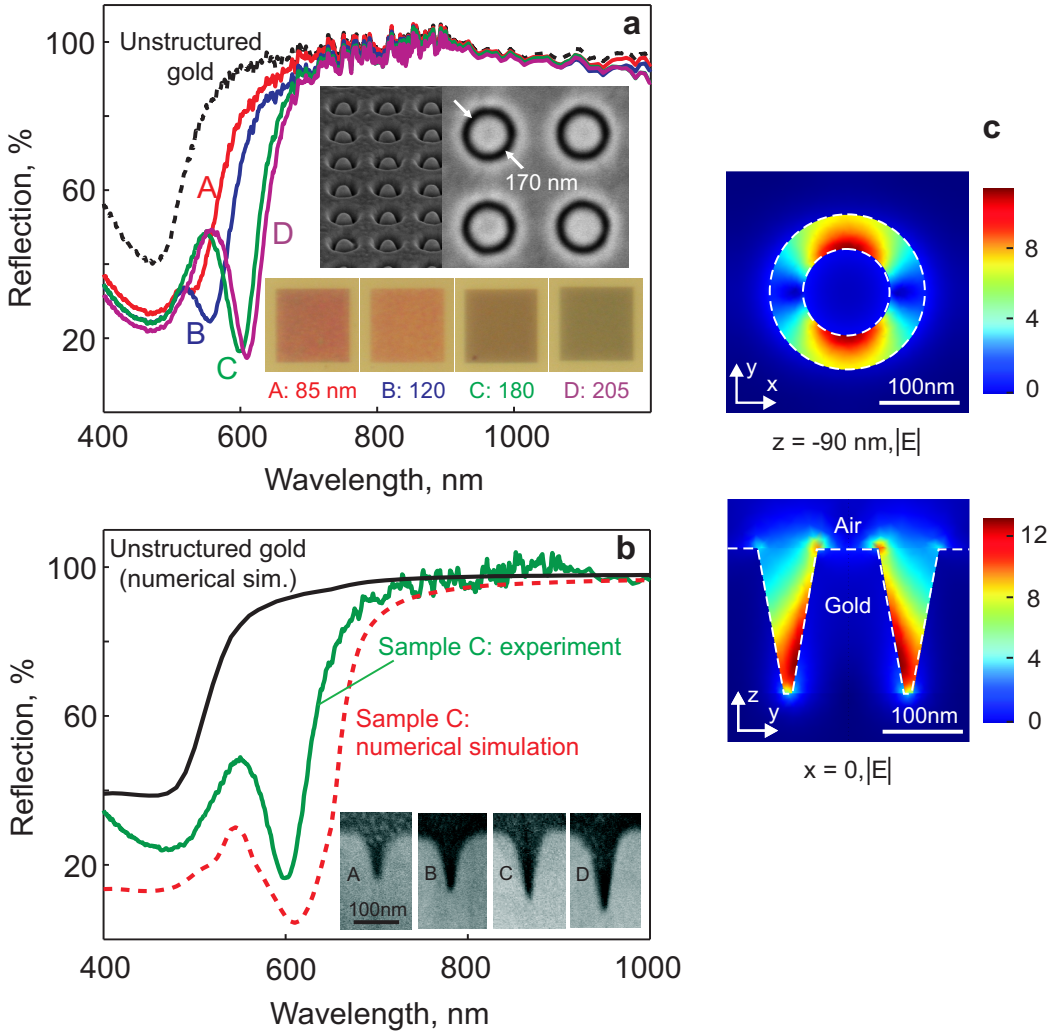

Figure 3.9: Changing the colour of gold. (a) Normal incidence reflection spectra for an unstructured gold surface and for the same surface patterned with intaglio metamaterial arrays of 170 nm diameter rings cut to depths ranging from 85 to 205 nm (as labeled, depths derived from FIB calibration). The insets show electron microscope images of the design (at oblique incidence and in plan view) and optical microscope images of the different patterned domains; (b, c) Numerical modeling of gold intaglio metamaterials: (b) Comparison between simulated and experimentally measured reflection spectra. For clarity, data for one of the four designs presented in part (a) are shown on a magnified wavelength axis; (c) Maps of total electric field intensity in a z-plane 90 nm below the top surface of the metal (left) and in the x-plane diametrically bisecting a ring (right). The structure is illuminated at normal incidence with y-polarized plane waves at 610 nm.

In experiment, again a microspectrophotometer (CRAIC QDI2010) was employed to measure normal incidence reflection spectra for a variety of gold and aluminum intaglio and bas-relief metamaterial designs: Gold intaglio metamaterial patterns were fabricated by focused ion beam milling (FEI Helios NanoLab 600) on 250 nm thick gold films evaporated on optically polished quartz substrates. Fig. 3.9a shows spectra for square metamaterial arrays of 170 nm single rings milled to four different depths into a gold film, alongside the reflection spectrum for the adjacent unstructured gold surface. The red-shift of absorption resonance with increasing etch depth is clearly seen and the associated changes in the colour of gold are strikingly illustrated by the inset optical microscope images.

These intaglio metamaterial designs have been numerically modeled using the COMSOL MultiPhysics, employing dielectric parameters for gold from Ref [60]. With account taken of the characteristic v-shaped slot profile produced by focused ion beam milling, there is excellent agreement between experimental and simulated reflection spectra. This is illustrated in Fig. 3.9b, which presents curve C from Fig. 3.9a alongside the corresponding simulated spectrum for an array of 180 nm deep, 170 nm diameter single rings and the simulated reflection spectrum for unstructured gold. Detail of the model meta-molecule geometry is shown in Fig. 3.9c, which shows horizontal and vertical cross-sections of the field distribution within the plasmonic ring resonator mode responsible for the 610 nm absorption resonance.

Controlling the colour of silver using intaglio metamaterials has also been experimentally demonstrated. Fig. 3.10 shows optical microscope images as well as spectra for square metamaterial arrays of 300 nm slots cut to a range of depths into a 300 nm thick silver film. The patterned area shows striking colour compared to unstructured silver in the surrounding area. There are two absorption resonance in the optical spectra. As the depth of slot increases, the second resonance red-shifts and broadens, leading to a significant change of colour.

Aluminum bas-relief structures were fabricated at an interface between the metal and an optically polished fused silica substrate using electron beam lithography and anisotropic reactive ion etching(Al samples were manufactured by Dr. Yifang Chen [Rutherford Appleton Laboratory]): A 100 nm PMMA resist layer on the substrate was patterned by electron beam exposure at 100 keV via a high-resolution vector beam

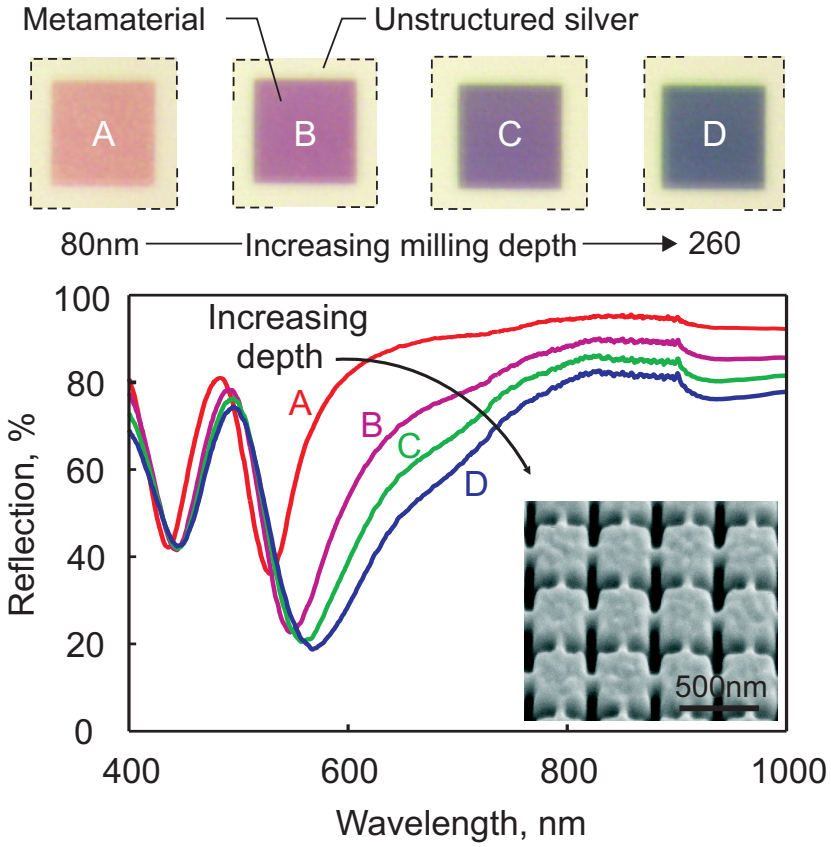

Figure 3.10: Controlling the colour of silver: normal incidence reflection spectra for a silver surface patterned with intaglio metamaterial arrays of crossed 300 nm slots (unit cell size 400 nm) cut to a range of depths to achieve a variety of polarization- and viewing-angle-independent colours as shown in the upper row of optical microscope images, where each patterned (coloured) area measures 20 μm × 20 μm and is surrounded by unstructured silver. The inset shows an electron microscope image of a section of such a meta-surface (viewed at oblique incidence).

pattern generator (Vistec Lithography VB6HR) to form a mask for reactive ion etching in a fluorine-based plasma (Oxford Plasma Technology System90). The metamaterial design was etched into the silica to a nominal depth of 70 nm then coated by evaporation with a 250 nm layer of aluminum. Fig. 3.11 shows spectra for an aluminum bas-relief design of asymmetric split rings (ASRs). Such patterns are routinely employed in conventional (discrete resonator) photonic metamaterials where they deliver collective 'closed-mode', polarization-sensitive transmission/reflection/ absorption resonances [38]. In the bas-relief form they provide dramatic changes in colour from that of the unstructured metal, which are by virtue of the design anisotropy dependent on the polarization of incident light.

Fig. 3.12 presents a numerical analysis (based on material parameters from Ref [60].)

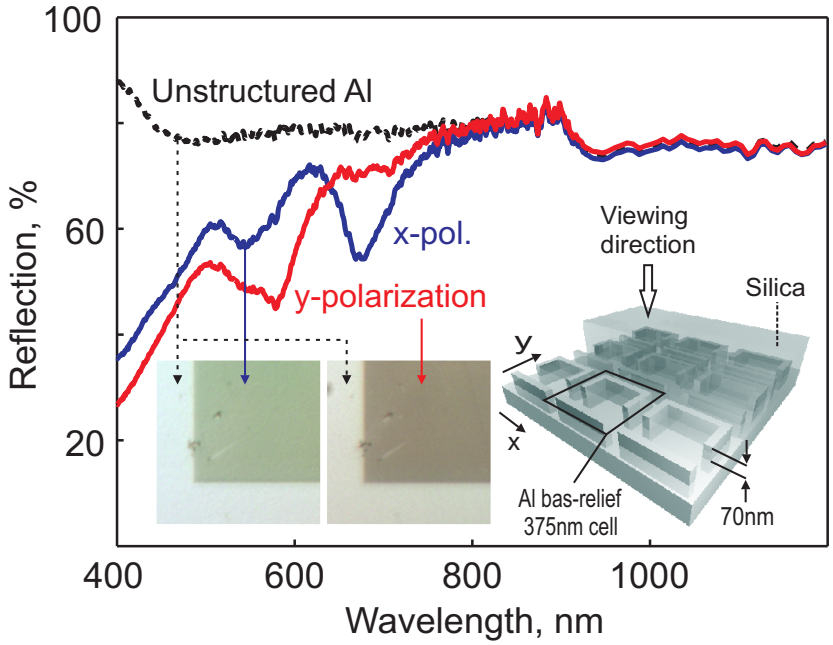

Figure 3.11: Anisotropic colour control on aluminum. (a) Normal incidence reflection spectra for an unstructured aluminum/silica interface and for the same surface patterned with a bas-relief metamaterial array of 375 nm asymmetric split rings having a height of 70 nm. Data are presented for two orthogonal incident polarizations parallel [x] and perpendicular [y] to the split in the rings. The insets show a schematic of the sample structure [with part of the silica layer cut away] and optical microscope images of the patterned domain under the two incident polarizations.

of various single-ring intaglio designs and illustrates that one can achieve a wide palette of colours through structural engineering of the metamaterial design. In this two-dimensional representation of the CIE1931 colour space, perceived colour coordinates are derived directly from reflection spectra using Judd-Vos-modified CIE 2-deg colour matching functions [84–86] assuming in all cases an illuminating light source with the spectral radiant power distribution of a 6500 K black body and a normalized observational brightness level (for details of calculating chromaticity coordinates, see Appendix C).

Unstructured aluminum, which uniformly reflects more than 80 % of light across the range from 400 to 800 nm, occupies a position in the central white region of this map at (0.315, 0.327) [open circle symbol], while unstructured gold is found at (0.383, 0.399) [open triangle]. Metamaterial arrays of intaglio ring-resonators on these metals introduce strong absorption resonances at wavelengths dependent on the structural parameters of the meta-molecules thereby modifying the reflection spectrum, i.e. per-

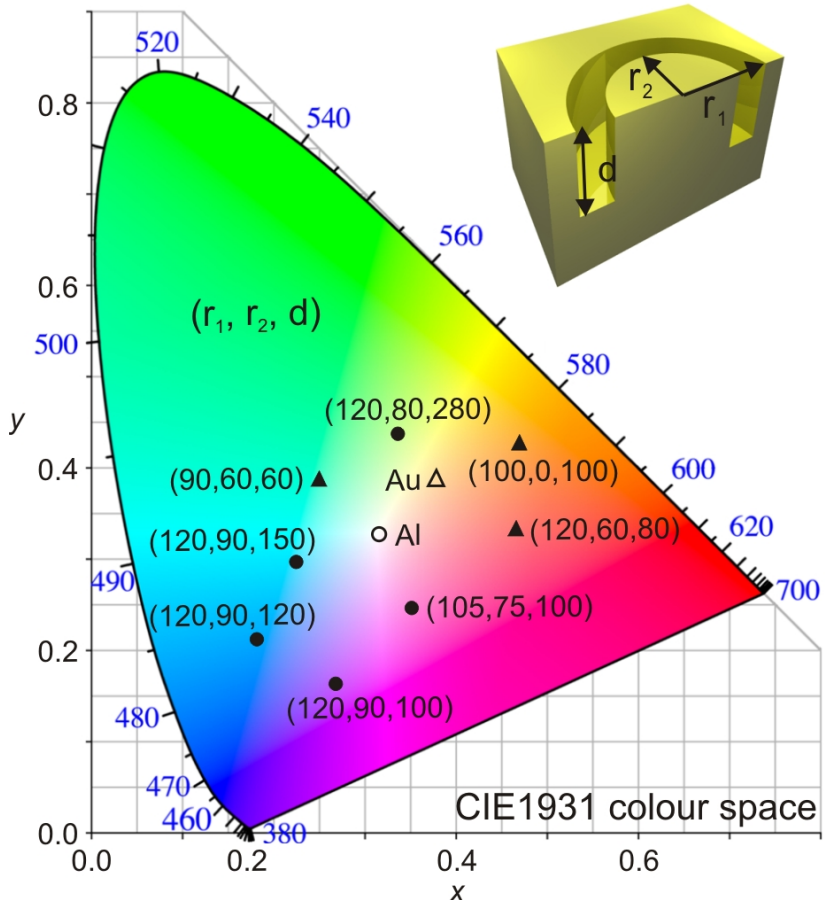

Figure 3.12: Metallic colour palette: CIE1931 chromaticity diagram overlaid with points corresponding to the simulated reflected colours of single ring intaglio metamaterial designs in aluminum (circular symbols) and gold (triangles), labeled according to their structural parameters (external radius r1, internal radius r2, depth d, array period = 300 nm in all cases). Points for the unstructured metals are indicated by open symbols.

ceived colour, of the surface. A selection of geometries have been assessed through numerical simulation (as shown by the filled symbols in Fig. 3.12, labeled according to the outer/inner radii and depth of the rings) illustrating that this simple design alone can provide access to a significant proportion of colour space. The available parameter space for meta-molecule design and distribution is obviously almost unlimited and, as the above experimental results show, one has the option of introducing anisotropy through design asymmetry.

It should be emphasized that the experimentally observed colours presented in Figs. 3.8, 3.9, 3.10, 3.11 cannot be mapped directly to colours in Fig. 3.12 because neither the illumination spectrum nor the uniform observational brightness assumed in this 2D chromaticity diagram correspond to experimental conditions. Nevertheless,

(x, y) chromaticity coordinates derived from experimental spectra on the basis of an assumed light source (i.e. a 6500 K black body) do provide an approximate quantitative measure of structurally induced colour change: For example, sample A in Fig. 3.9 has coordinates of (0.419, 0.362) and at progressively decreasing brightness sample B = (0.415, 0.342); C = (0.340, 0.374); D = (0.342, 0.386); the coordinates of the unstructured gold surface are (0.383, 0.385).

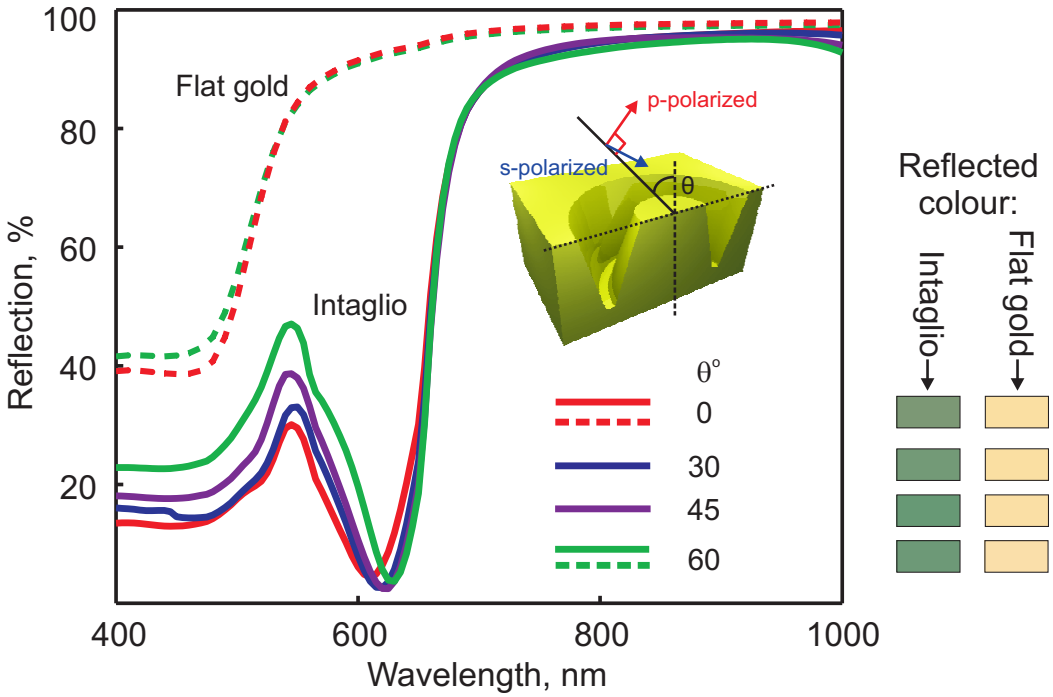

Figure 3.13: Colour invariance with viewing angle: Numerically simulated reflection spectra and associated perceived colours for a gold intaglio metamaterial array of 170 nm diameter rings with a depth of 180 nm viewed at normal incidence and a selection of oblique angles (as labeled, averaged over incident s- and p-polarizations). Here the reflection includes reflected light of all angles at a specific incident angle. For comparison, the corresponding perceived colour of an unstructured gold surface is shown for each viewing angle and reflection spectra for the unstructured metal at 0 and 60 degree angles are plotted.

While spectrophotometric experiments are instrumentally restricted to normal incidence illumination, numerical analyses are readily extended to oblique incidence configurations. These reveal, as shown in Fig. 3.13, that the colours derived from metamaterial relief structuring are essentially independent of viewing angle, with variations in colour being no larger than those observed for the unstructured metal. This angle invariance results from the fact that absorption is linked to localized plasmon modes of the metamaterial unit cells rather than diffraction effects or the coupling of incident en-

ergy to propagating surface plasmon polaritons (both excluded by the sub-wavelength periodicity of the metamaterial arrays). Indeed, here the unit cell period of 300 nm is not much smaller than the wavelength of visible light and diffraction may happen at big oblique incident angles. However, the absorption of gold is quite strong for light with wavelength shorter than 500 nm and diffraction feature is not observed in the reflection spectra of Fig. 3.13. By decreasing period of metamaterial unit cell, we may further preclude diffraction effects and reduce the variations of colour at different viewing angles.

3.4 Dielectric loaded metamaterials

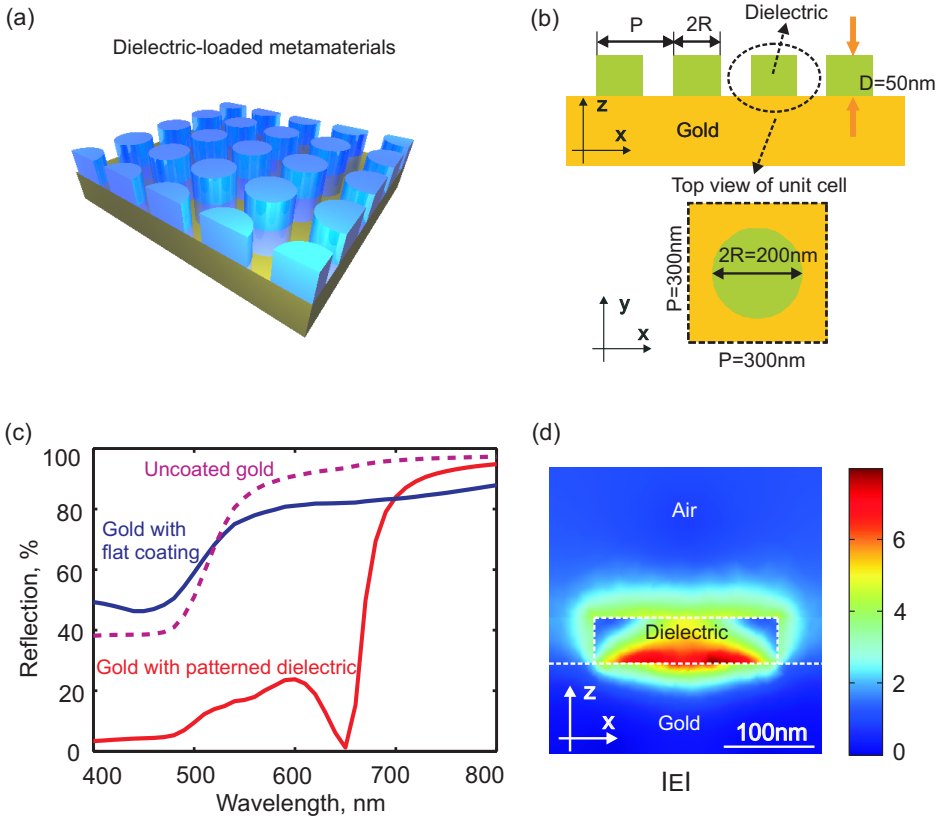

Figure 3.14: Dielectric-loaded relief metamaterials: (a) Artist's impress of a dielectric loaded metamaterial; (b) Structural geometry and dimensions - a flat gold surface loaded with a 300 nm period square array of 200 nm diameter, 50 nm thick dielectric disks; (c) Numerically simulated reflection spectrum of the structure in (b) alongside the spectra for unstructured, uncoated gold and gold with a continuous thin film dielectric coating; (d) Cross-sectional map of electric field intensity in the y symmetry plane of a nanodisk. The structure is illuminated at normal incidence with x-polarized plane waves.

As an extension to the bas-relief metamaterials family, another new type of meta-

materials comprising sub-wavelength patterns of thin-film dielectrics on planar metal surfaces in introduced here (see Fig. 3.14a). Borrowing the terminology from plasmonic waveguides, these are called 'dielectric loaded' metamaterials [87]. Fig. 3.14 illustrates the significant changes in the reflection spectrum of gold that may be brought about by the application of a patterned dielectric layer only 50 nm thick. As Fig. 3.14c shows, a continuous dielectric layer of this thickness (assumed to be lossless, with a refractive index of 2.5) has relatively little effect. But a nanostructured layer (in the present case an array of 200 nm diameter disks), supporting localized surface plasmon modes with strong field enhancement at the metal/nanodisk interface as shown in Fig. 3.14d, can substantially modify the reflection spectrum of the metal.

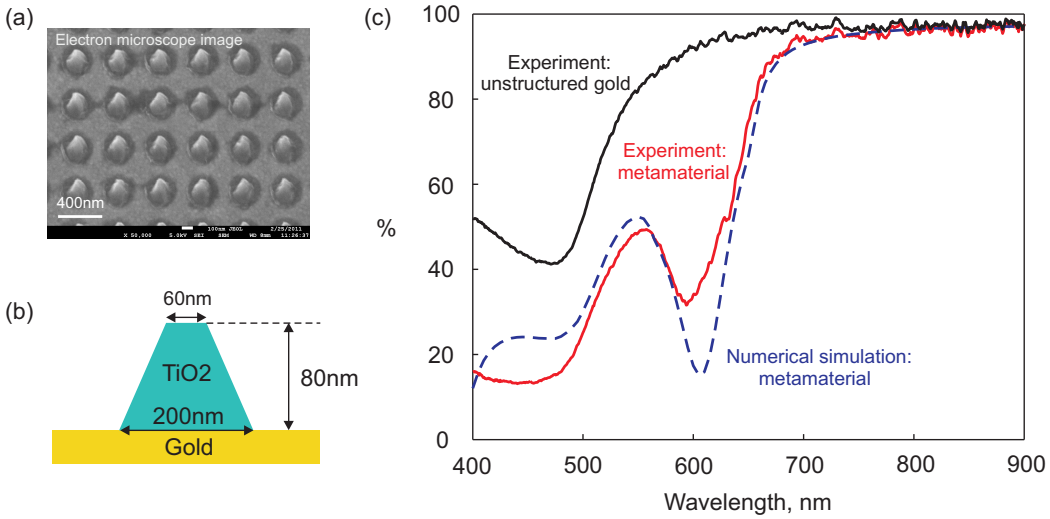

Figure 3.15: Experimental realization of a dielectric-loaded relief metamaterial: (a)Scanning electron microscope image of a dielectric metamaterial sample.(b) Structural geometry and dimensions for numerical simulation - a flat gold surface loaded with a 400 nm period square array of 80 nm thick dielectric disks; The diameter of dielectric disks is 200 nm at the bottom and 60 nm at the top.(c)Measured spectra for metamaterial in (a) and unstructured, uncoated gold alongside simulated spectrum for metamaterial in (b); The structure is illuminated at normal incidence with x-polarized plane waves.

Dielectric-loaded metamaterials are fabricated by E-beam lithography with a lift off process as follows (The E-beam lithography and lift off process was conducted with the assistance of Jun-Yu [Bruce] Ou and Takashi Uchino): First, 5 nm of chromium and 250 nm of gold were deposited on an optically polished fused silica substrate by thermal evaporation. Then polymethylmethacrylate (PMMA) was spin-coated on the gold surface with a thickness of 600 nm. Nanoholes with a diameter of 200 nm and period of 400 nm were patterned on PMMA by E-beam lithography. After the patterns

were developed, 80 nm of titanium dioxide (TiO_2) was deposited on the sample by e-beam evaporation. Finally, PMMA mask was removed in acetone and TiO_2 was left on gold surface after this lift off process. Fig. 3.15 shows an electron microscope image of a dielectric metamaterial sample and corresponding optical spectra. Due to the localized plasmon resonance, measured reflection spectrum of the sample display a clear dip at around 595 nm, which agrees well with the simulation results using estimated geometric dimensions.

3.5 Summary

A new family of continuously metallic metamaterials has been demonstrated in simulations and experiments. They are formed of indented or raised sub-wavelength patterns with depth/height of the order 100 nm. We borrow terminology from the art world here and call these 'intaglio' and 'bas-relief' designs. Localized surface plasmons could be excited in the indented grooves or raised patterns under the illumination of visible or IR electromagnetic radiation. Near the plasmonic resonance, the incident light are strongly coupled into the plasmonic modes, leading to dramatic absorption, enhancement of electromagnetic field in the subwavelength patterns and a zero change in the phase of reflected light. Intaglio and bas-relief metamaterials bring the functionality of FSS into the optical range and several novel phenomena such as perfect absorption and optical magnetic mirror effects have been demonstrated. Further more, their optical properties could be engineered with considerable freedom by changing the geometry of the indented or raised patterns (width, depth or cross section) or the refractive index of surrounding media, providing opportunities for achieving desired functionalities or controlling over their properties via hybridization with active media.

Structural control over the visible colour of pure metal surfaces has been dramatically demonstrated in experiments. Controlling the colour of metals by both intaglio and bas-relief metamaterials has been shown. We patterned a 250 nm gold film with intaglio metamaterial arrays of 170 nm diameter rings (period=300 nm) cut to depths ranging from 85 to 205 nm and show that the colour of structured gold surfaces could be tuned from the general 'gold yellow' to 'red' and even 'green' under specific experimental illumination condition. This is realized by controlling the absorption and

reflection spectra response of structured surface in the visible range. As the structural colour is attributed to localized plasmon resonance and the subwavelength arrangement of the indented and raised patterns effectively excludes diffraction, it is not sensitive to the incidence angle of light. While the structural colours displayed by the gold intaglio ring metamaterial are polarization insensitive, polarization dependent colours were also demonstrated using anisotropic pattern designs in aluminium. Finally, assuming the illumination of a 6500K blackbody radiation, we theoretical calculated the colours of gold and aluminium with indented rings and show a variety of striking colours by simply changing the radius, width and depth of ring design. Intaglio/bas-relief photonic metamaterials offer a robust and flexible paradigm for controlling the spectral response of metals in the visible domain and thus the colour of metals, with potential applications ranging from aesthetic (e.g. jewelry) to optical sensing and security (e.g. in banknote/document anti-forgery features that must be difficult to imitate without substantial up-front investment in design and fabrication technology).

We have introduced concept of dielectric loaded metamaterials that comprises subwavelength patterns of thin-film dielectrics on planar metal surfaces. The strong resonances in dielectric metamaterials lead to field and loss enhancements, making the patterned dielectric a 'super coating'. This concept may lead to interesting applications including the enhancement of linear and nonlinear optical properties of dielectrics. More broadly, the ability of control the absorption of metal surface has many potential applications in perfect absorbers/emitters, sensors, and solar cell designs.

Chapter 4

Controlling light-with-light without nonlinearity

4.1 Introduction

In 1678, Christiaan Huygens stipulated that '...light beams traveling in different and even opposite directions pass though one another without mutual disturbance' [88] and in the framework of classical electrodynamics, this superposition principle remains unchallenged for electromagnetic waves interacting in vacuum or inside an extended medium [89]. Since the invention of the laser, colossal effort has been focused on the study and development of intense laser sources and nonlinear media for controlling light with light, from the initial search for optical bistability [90] to recent quests for all-optical data networking and silicon photonic circuits [91]. As the nonlinear coefficients of natural materials are usually small, there has been lots of interests in engineering structures for enhancement of nonlinear effects. Significant progress has been made in this field by using nanostructured artificial materials such as photonic crystal cavities and slow light waveguides [92, 93], plasmonic nanorods [35] as well as plasmonic metamaterials [48]. However, quite intensive laser sources are still required to realized visible nonlinearities in such structures. This chapter shows that, via coherent interactions, an interesting way of controlling light with light is realized without nonlinearity.

Coherent interactions have been a very powerful tool for decades in many applications, e.g., phased array antennas [96, 97]. In atomic and solid-state physics, study

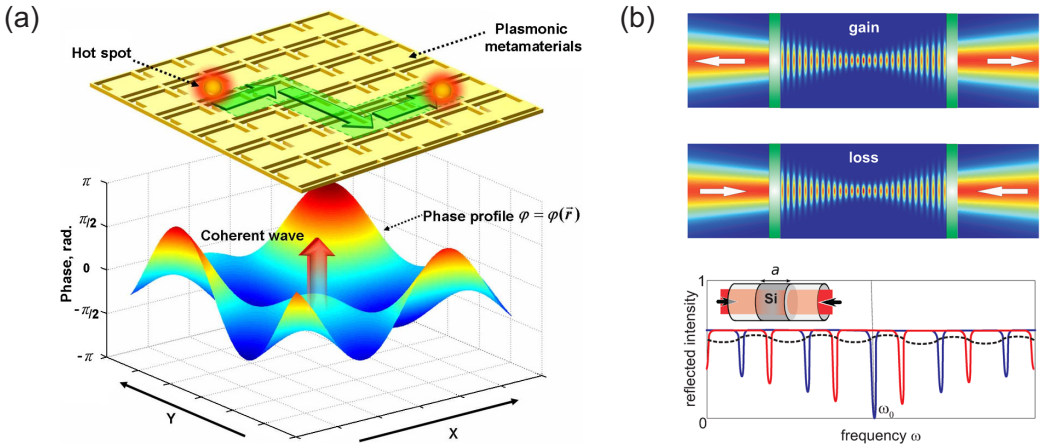

Figure 4.1: Applications of coherent interactions. (a) Coherent control of nanoscale light localization [94]; (b) Coherent perfect absorption [95]. Figure reproduced with permission from: (a), ref. [94], ©2011 APS; (b), ref. [95], ©2010 APS.

of coherent light-matter interactions has led to the finding of electromagnetically induced transparency (EIT) [98, 99], which has been at the forefront of experimental study in the past two decades for its ability of slowing and stopping light with potential applications in modern optical networks [100] and future quantum networks [101]. There have also been many interests in studying coherent interactions and interference between nano-optical resonators and all-optical analogs of EIT have been experimentally demonstrated in various nano-optical systems such as waveguide-resonator systems [102,103], plasmonic meta-atoms [104–106] and optomechanical devices [107,108]. Furthermore, coherent interactions are increasingly being explored and exploited on the nanoscale for imaging, surface plasmon focusing and light focusing and localization (see Fig. 4.1a) [94,109–112].

Most recently, the idea of coherent perfect absorption has attracted lots of attentions [113, 114]. In what can be seen as a time-reversed analogue of lasing, 100% of incident light in two counter-propagating beams is absorbed in a bulk silicon cavity due to interplay of interference and absorption (see Fig. 4.1b). Coherent perfect absorption has also been theoretically proposed in systems such as composite metallic films [115, 116], plasmonic nanoparticles [117] and even epsilon-near-zero metamaterials [118] and metamaterials with negative refractive index [119]. However, most of these designs could only be realized with strict requirements and at limited frequency ranges as they rely on the natural properties of materials while others may be difficult

to be implemented practically due to complexity of design. At the same time, coherent perfect transparency, an opposite phenomena of coherent perfect absorption, has been ignored and the ability of dynamically manipulating the absorption and transmission hasn't been fully explored. In this chapter, coherent control is applied to manipulate interactions between light and a metamaterial layer of nanoscale thickness and it is demonstrated that two coherent beams of light of arbitrarily low intensity can interact on the metamaterial in such a way that one beam modulates the intensity of the other. It's shown that the interference of beams can eliminate the plasmonic Joule losses of light energy in the metamaterial or, in contrast, can lead to almost total absorption of light [120].

4.2 Methods and materials

Consider a thin light-absorbing film of sub-wavelength thickness: the interference of two counter-propagating incident beams A and B on such a film is described by two limiting cases illustrated in Fig. 4.2: in the first, a standing wave is formed with a zero-field node at the position of the absorbing film. As the film is much thinner than the wavelength of the light, its interaction with the electromagnetic field at this minimum is negligible and the absorber will appear to be transparent for both incident waves. On the other hand, if the film is at a standing wave field maximum, an antinode, the interaction is strong and absorption becomes very efficient. Altering the phase or intensity of one beam will disturb the interference pattern and change the absorption (and thereby transmission) of the other. For instance, if the film is located at a node of the standing wave, blocking beam B will lead to an immediate increase in loss for beam A and therefore a decrease in its transmitted intensity. Alternatively, if the film is located at an antinode of the standing wave, blocking beam B will result in a decrease of losses for beam A and an increase in its transmitted intensity. In short, manipulating either the phase or intensity of beam B modulates the transmitted intensity of beam A.

To optimize the modulation efficiency the film should absorb half of the energy of a single beam passing through it (see Fig. 4.2c). Under such circumstances 100% light-by-light modulation can be achieved when signal A is modulated by manipulating the phase

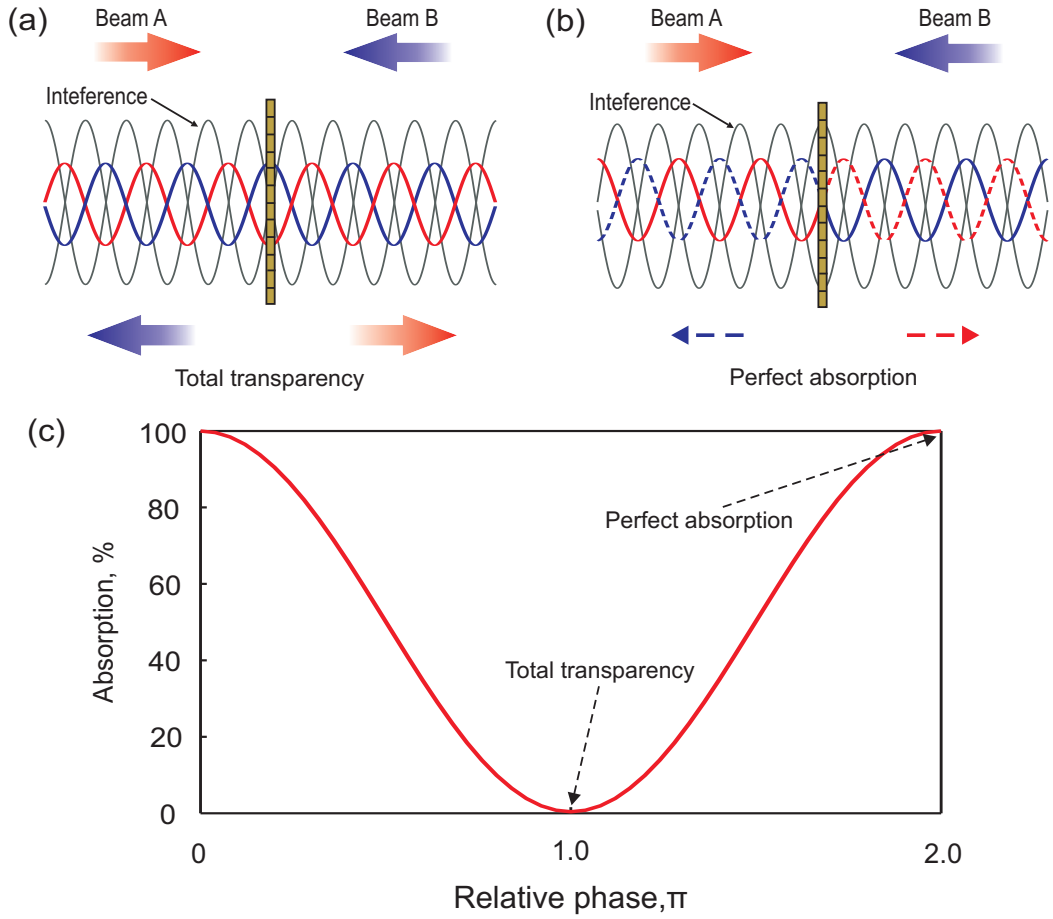

Figure 4.2: Interaction of light with light on a nanoscale absorber. Two coherent counter-propagating beams A and B are incident on an absorber of sub-wavelength thickness, for instance a lossy plasmonic metamaterial film. Two limiting regimes of interaction exist wherein the beams at the film interfere either (a) destructively or (b) constructively to effect total transmission or total absorption respectively. (c) Coherent absorption as a function of the mutual phase of two counter propagating coherent beams with equal intensities. The thin film is assumed to infinitely thin with a single beam absorption of 50% while both reflection and transmission are 25%.

of beam B and 50% modulation can be achieved if control is encoded in the intensity of beam B. Moreover, one will observe that when the intensities of the two beams are equal and the film is located at an antinode, all light entering the metamaterial will be absorbed, while at a node light transmitted by the film will experience no Joule losses. Actually, as the thin film is a symmetric and linear system, a single beam can be viewed as a superpositon of two counter propagating beams with anti-phases and two counter propagating beams with same phases. So the maximum coherent absorption equals two times the single beam absorption subtracts the minimum coherent absorption. As a result, the single beam absorption shouldn't be lower than 50% if coherent perfect

absorption is going to be realized.

Here, it should be noted that an infinitely thin film in symmetric environment can absorb *not more than* half of the energy of an incident single beam [121, 122]. According to the continuity equation of electromagnetic field, the reflection coefficient r and transmission coefficient t of a 'zero' thickness layer (much thinner than λ) in a symmetric environment are related to each other as: $t = 1 \pm r$(upper and lower signs are for s- and p-polarized light, respectively). Therefore, the maximum absorption ($A = 1 - \mid r \mid^2 - \mid 1 \pm r \mid^2$) is limited to 50% (corresponding to $r = \mp\frac{1}{2}$). This value can be increased when the environment is asymmetric, such as a metamaterial film on a dielectric substrate, which shows different reflection and absorption for light impinging from different sides. Detailed discussions about absorption limitation in an ideal 'zero' thickness film can be found in ref [122].

At the same time, a level of absorption of 50% is difficult to achieve in thin unstructured metal films: across most of the optical spectrum incident energy will either be reflected or transmitted by such a film. Recently reported much higher absorption levels have only been achieved in layered structures of finite thickness [64, 68, 71, 123, 124] that are unsuitable for implementation of the scheme presented in Fig. 4.2. However, in the optical part of the spectrum a very thin plasmonic metamaterial can deliver strong resonant absorption approaching the 50% target at a designated wavelength.

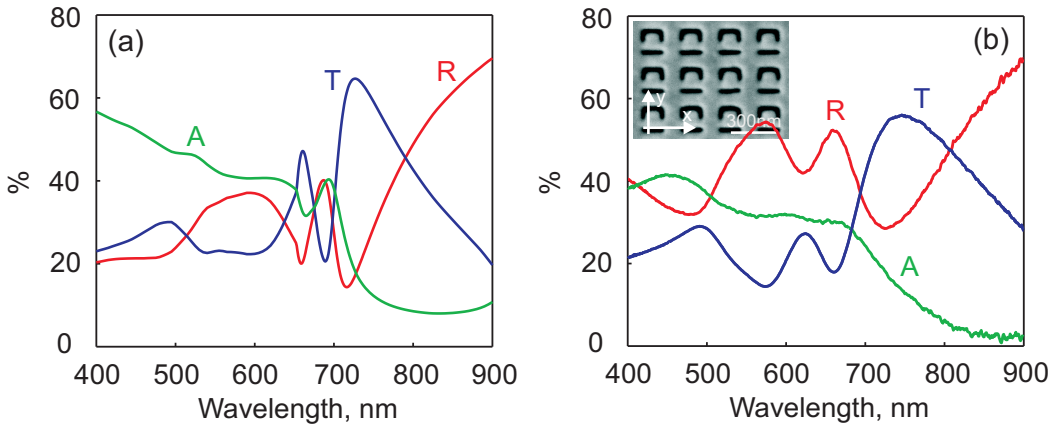

Figure 4.3: Optical spectra for the metamaterial. (a) Numerically simulated spectra for the metamaterial (b) Experimentally measured spectra for the metamaterial sample.Light impinges from the air side (no-substrate side) with y-polarization.

As the key element for light-by-light modulation, a metamaterial with a thickness of $\lambda/13$ - a two-dimensional array of asymmetric split-ring plasmonic resonators milled

through a 50 nm gold film, is employed in the present experiment. This nanostructure supports a Fano-type plasmonic mode [38,40] that leads to strong resonant absorption. The pitch of metamaterial array, with a unit cell size of 250 nm × 250 nm smaller than the wavelength, is such that it does not diffract light. Fig. 4.3 shows numerically simulated(a) and measured (b) transmission, reflection and absorption spectra of the metamaterial on silica substrate utilized for our experiment. The light impinges on the metamaterial from the air side at normal incidence with y-polarization.

Numerical results are obtained using fully three dimensional finite element package by COMSOL Multiphysics (see Appendix A for details of COMSOL modeling). Experimental values of the complex dielectric parameters for gold are utilized [60]. At $\lambda = 633\ nm$, $\epsilon_{gold} = -9.51588 - 1.12858i$ is used for gold permittivity, $\epsilon_{silica} = 2.1316$ for silica substrate permittivity, and $\epsilon_{air} = 1$ for air permittivity. At $\lambda = 1550.5\ nm$, permittivity of gold is $\epsilon_{gold} = -132.024 - 12.6637i$. The metamaterial sample was prepared using the following procedure: A cleaned silica cover slip with a thickness of about 170 μm and surface roughness less than 0.5 nm is chosen as the substrate. 50 nm gold is deposited on the silica substrate using high vacuum $10^{-7}\ mbar$ thermal evaporation at a deposition rate of 0.05 nm/s. Metamaterial structures are fabricated by direct milling with focused ion beam. Metamaterial spectra are characterized using a microspectrophotometer by CRAIC technology. As $\lambda = 633\ nm$ is near the absorption band of gold, the metamaterial resonance is hampered by the gold loss. However,clear plasmonic resonances can still be clearly observed in the spectra. Experiment results agree well with simulations.

The experimental arrangement presented in Fig. 4.4 was employed to demonstrate light-by-light modulation and total absorption/transparency for a plasmonic metamaterial. A linearly polarized beam of light from a HeNe laser (wavelength $\lambda = 632.8$ nm) is divided by a pellicle beam-splitter $BS1$ into two beams A and B, denoted as 'signal' and 'control' beams respectively, which are adjusted to equal intensity by an attenuator in path B. The beams are focused at normal incidence onto the plasmonic metamaterial (PMM) from opposing directions by parabolic mirrors. The array is placed where the travel distances of both beams are equal so they can efficiently interfere on the array. The phase of control beam B is manipulated via a piezoelectrically actuated optical delay line while a mechanical chopper provides for modulation of its intensity.

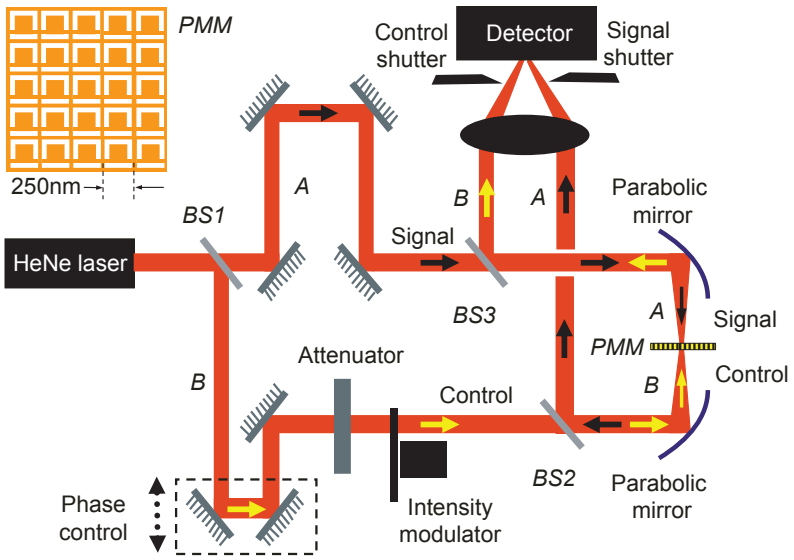

Figure 4.4: Experimental arrangement for demonstration of optically-controlled transparency/absorption in a plasmonic metamaterial. Black and yellow arrows respectively indicate the paths of 'signal' and 'control' beams A and B from beam-splitter $BS1$ where they are generated from a single source beam to the metamaterial sample PMM and from there to the photodetector. Changes in the phase or intensity of the control beam B can be used to switch between regimes of total transmission and total absorption at the plasmonic metamaterial, and to modulate the intensity of the signal beam A with the control beam B. The inset shows an artistic impression of the plasmonic metamaterial - a gold film perforated with an array of asymmetric split-ring slits.

The intensities of the beams transmitted by the metamaterial are monitored by a single photodetector, which may register the combined intensity of both beams (the difference in path length from metamaterial to detector for the two beams being much longer than the coherence length of the laser radiation so there is no optical interfere at the detector) or that of either single beam (the other being shuttered accordingly). The position of beam splitters BS2 and BS3 are carefully adjusted to make sure that the scattered lights don't interfere with incident beams.

4.3 Results and discussions

Fig. 4.5 illustrates the modulation of signal intensity via manipulation of control beam phase φ (Figs. 4.5a and 4.5b) or intensity (Fig. 4.5c). The phase of the control beam is changed using the delay line in arm B. Continuously changing the phase has the effect of translating the metamaterial film between nodes ($\varphi = \pi, 3\pi, ...$) and anti-nodes

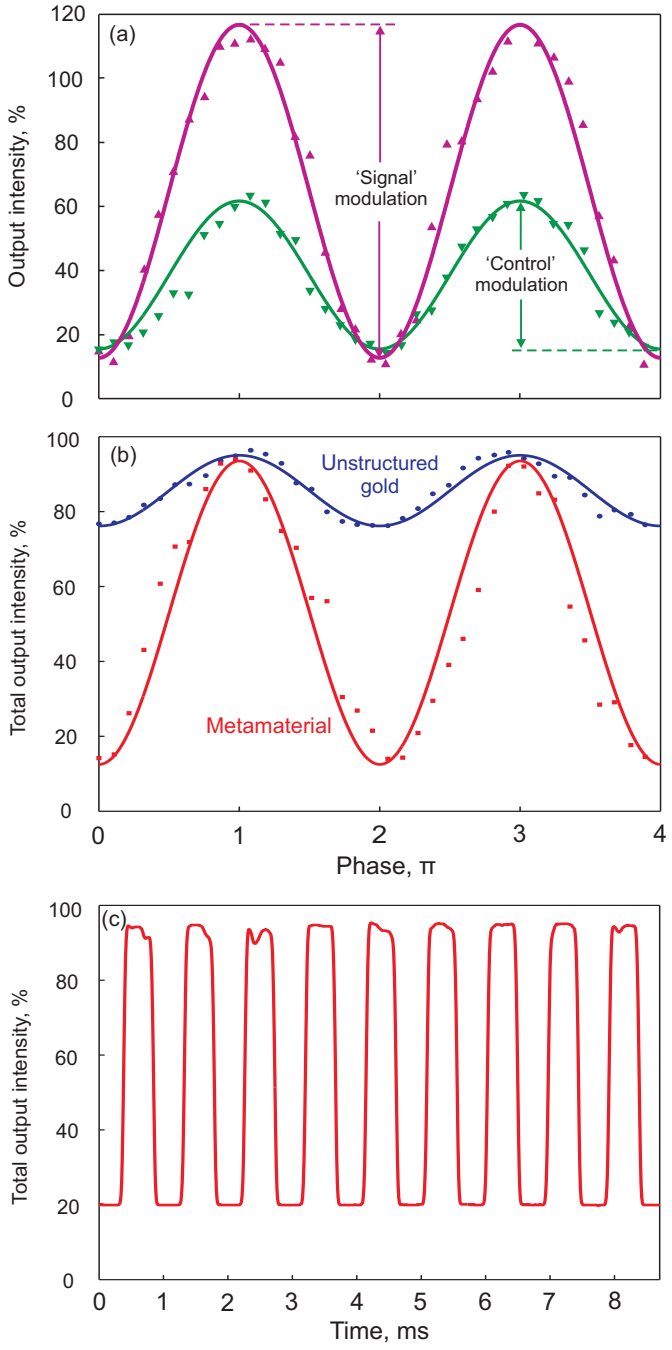

Figure 4.5: Controlling light-with-light in a plasmonic metamaterial. (a) Output intensity in signal and control channels, relative to their respective input intensities, as functions of the mutual phase of the input beams at the metamaterial film. (b) Combined output intensity of the signal and control channels, relative to combined input intensity, as a function of the mutual phase of the incident beams for the plasmonic metamaterial absorber and for an unstructured 50 nm gold film. (c) Time domain trace of output (combined intensity) modulation effected via intensity modulation of the input control beam (mechanically chopped at 1.07 kHz). In (a) and (b), points are measured data and solid lines are fits to the data, not theory curves.

($\varphi = 0, 2\pi, ...$) of the standing wave, bringing about a modulation of the detected signal (channel A) intensity between levels at 115% and 10% of the incident level (Fig. 4.5a). Experimental results agree very well with numerical simulations (see Fig. 4.6) even though measured modulation is slightly lower than simulated results.

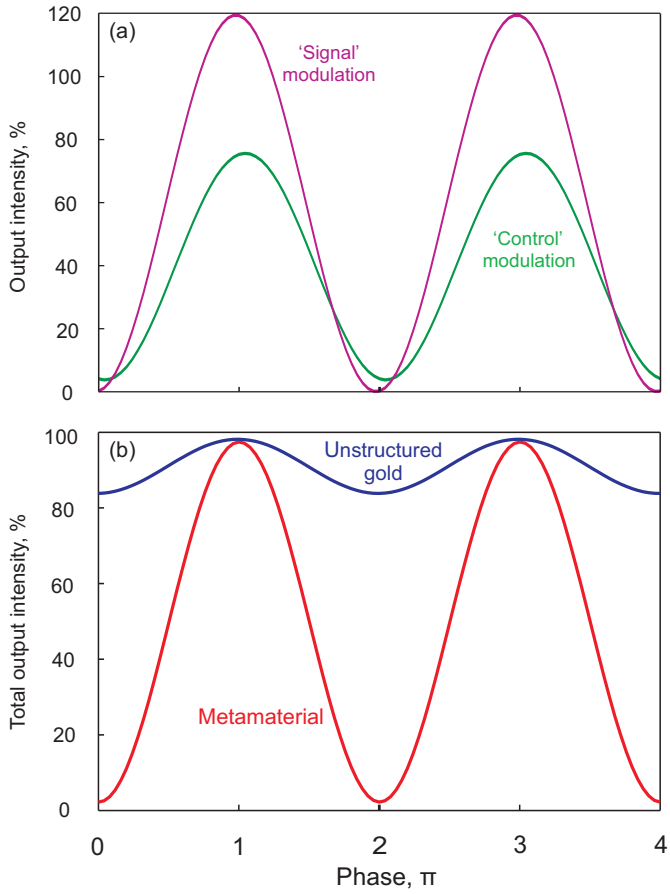

Figure 4.6: Simulated results of controlling light-with-light in the plasmonic metamaterial used for the experiment. (a) Output intensity in signal and control channels, relative to their respective input intensities, as functions of the mutual phase of the input beams at the metamaterial film. (b) Combined output intensity of the signal and control channels, relative to combined input intensity, as a function of the mutual phase of the incident beams for the plasmonic metamaterial absorber and for an unstructured 50 nm gold film.

For an ideal, free-standing, zero-thickness 50% absorber one would see the signal beam modulated between 0% and the full 100% incident intensity level. The somewhat different limits between which experimental modulation is observed are explained by a number of factors: First, the sample's absorption level at the laser wavelength is not exactly 50%. Indeed, due to the presence of a substrate, it shows differing levels of absorption for the two opposing propagation directions and the fabrication-related

asymmetry/imperfection of the slots milled into the gold film further increases the asymmetry of measured absorption levels (34% and 57%); Second, although the metamaterial is very thin it does have a finite thickness of $\lambda/13$; And finally, the laser source is not perfectly coherent - its emission includes an incoherent luminescence component.

Fig. 4.5b compares phase modulation of total output intensity for the metamaterial array and an unstructured area of the same gold film. The modulation amplitude for the unstructured metal is severely limited because it is highly reflective and therefore presents single-beam absorption far below the optimal 50% level. Through metamaterial patterning, one can manipulate the balance among absorption, transmission and reflection in sub-wavelength plasmonic films to achieve desired levels at any visible/infrared wavelength.

Fig. 4.5c shows modulation of total output intensity resulting from modulation of control intensity in the time domain. When the control beam is blocked only the signal wave is present at the metamaterial and the standing wave regime of light-metamaterial interaction is replaced by the traveling wave regime: In this example the metamaterial is initially located at a node of the standing wave where absorption is minimal (combined output intensity = 95% of input); interruption of the control beam 'switches on' signal beam absorption and the output drops to 20%. This proof-of-principle demonstration employs a mechanical chopper running at only 1.07 kHz. However, the cross-beam modulation bandwidth will be limited only by the width of the resonant absorption peak, and as such will be in the THz range (see below).

To further illustrate the potential for application of coherent control over metamaterial absorption in real-world devices, Fig. 4.7 shows the simulated performance of a free-standing (no substrate) 50 nm gold metamaterial film with an absorption line engineered for the telecommunications band centered at 1550.5 nm. The metamaterial exhibits a trapped mode resonance around 1550.5 nm for y-polarization and single-beam absorption of 50.18% at the resonance (slightly higher than 50% due to the finite thickness of metamaterial film).

Fig. 4.8 shows the simulated modulation of total metamaterial absorption and scattered intensities as a function of mutual phase between two counter propagating coherent beams with equal intensities at resonant (a) and non-resonant (b) wavelengths while the case for an unstructured gold film is also shown as a reference (c). Perfect

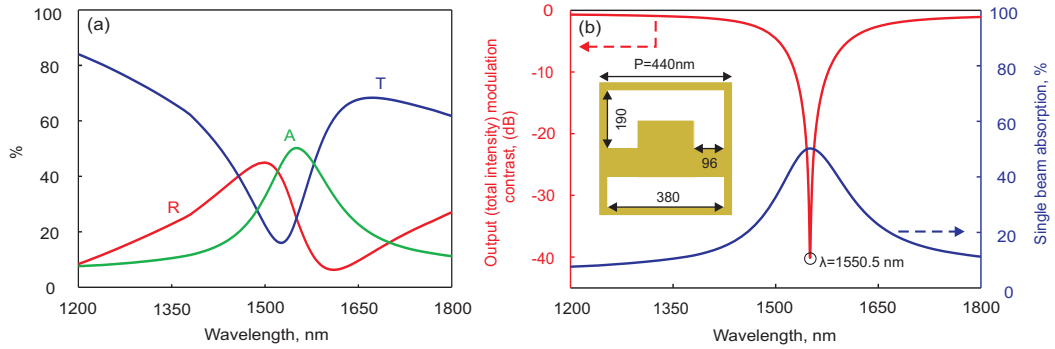

Figure 4.7: Metamaterial modulator for telecommunications. (a) Simulated reflection, transmission and absorption spectra of an asymmetric split ring(ASR) metamaterial for y-polarized plane wave at normal incidence. (b) Dispersion of the cross-intensity modulation contrast (red) and traveling wave absorption (blue) of a plasmonic metamaterial engineered to function as a coherently-controlled absorber at 1550.5 nm. The metamaterial unit cell geometry is shown inset; a free-standing gold film thickness of 50 nm is assumed.

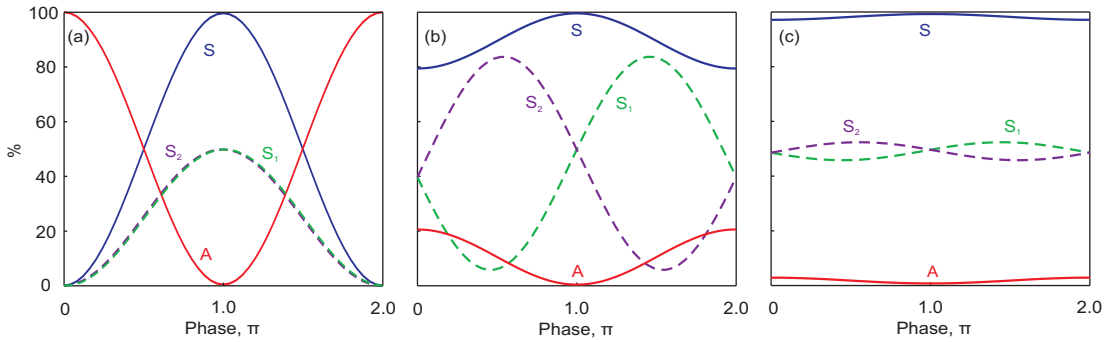

Figure 4.8: Light-controlled perfect plasmonic transparency and absorption on a telecommunication wavelength. (a) At absorption resonance wavelength ($\lambda = 1550.5\ nm$), simulated total absorption of plasmonic metamterial changes from 0.38% to 99.99% as the relative phase of two incident coherent beams varies;. (b) At non-resonance wavelength($\lambda = 1350\ nm$), numerical simulation shows that metamaterial absorption and total output intensities doesn't change much as the relative phase varies but the energy transfers between the two output ports.(c)At 1550.5 nm, the absorption of unstructured gold film varies only a few percent as the mutual phase changes

plasmonic transparency and absorption can be realized at the resonance wavelength by controlling the mutual phase of two counter-propagating coherent beams (Fig. 4.8a). As such, it will deliver phase-controlled total absorption of between 0.38% and 99.99% and total output intensity modulation between levels of 99.62% and 0.01% of total (combined) input intensity. At the non resonant wavelength $\lambda = 1350\ nm$, the metamaterial absorption is much smaller and transmission is high. So the metamaterial behaves like a normal interferometer with energy transfers between the two output ports as the relative phase of incident beams varies (Fig. 4.8b). At $\lambda = 1550.5\ nm$, the absorption of

50 nm thick unstructured gold film varies only about 2% as the relative phase changes (Fig. 4.8c). It's not surprising as 50 nm thick gold film is a good mirror in the near infrared range with little light transmitted or absorbed. The relatively broad nature of the metamaterial resonance provides for absorption modulation between 1% and 90% of input intensity levels across the entire spectral range from 1530 to 1575 nm, giving a bandwidth of 5.6 THz.

4.4 Summary

In summary, it has been demonstrated for the first time that a plasmonic metamaterial - a single layer of nanostructured metal much thinner than the wavelength of light - can be used to modulate light with light. A plasmonic metamaterial with period of 250 nm has been fabricated and interferometric control of metamaterial absorption from less than 5% to nearly 90% using a 630 nm Ne-He laser has been experimentally demonstrated. Manipulating either the phase or intensity of one beam can be used to control the transmitted intensity of the other beam. The phenomenon relies on the coherent interaction of light beams on the metamaterial and provides functionality that can be implemented freely across a broad visible to infrared range by varying the structural design.

The potential applications of the effect are manifold and of considerable technological importance. The high sensitivity of absorption to the mutual phase of beams may be harnessed for applications in sensors (i.e. a relative phase change between two coherent beams results in a variation of absorption signal) and the effect may find use in laser spectroscopy. However, the most striking applications may lie in the domain of signal processing (Fig. 4.9), for example in:

- Photonic 'pulse restoration' (Fig. 4.9a). In optical data systems, signal pulses become distorted through dispersion and nonlinear interactions, slowing down data distribution and processing. For a coherent optical network, incoherent noises in a distorted pulse may be 'cleaned up' through interaction with a clock pulse (or a duplicated pulse produced by splitting the distorted pulse into two and introducing a phase delay) at a nanoscale metamaterial absorber. Indeed, in the total transmission regime (i.e. the two pulses have a phase difference of π) spectral components of the distorted pulse

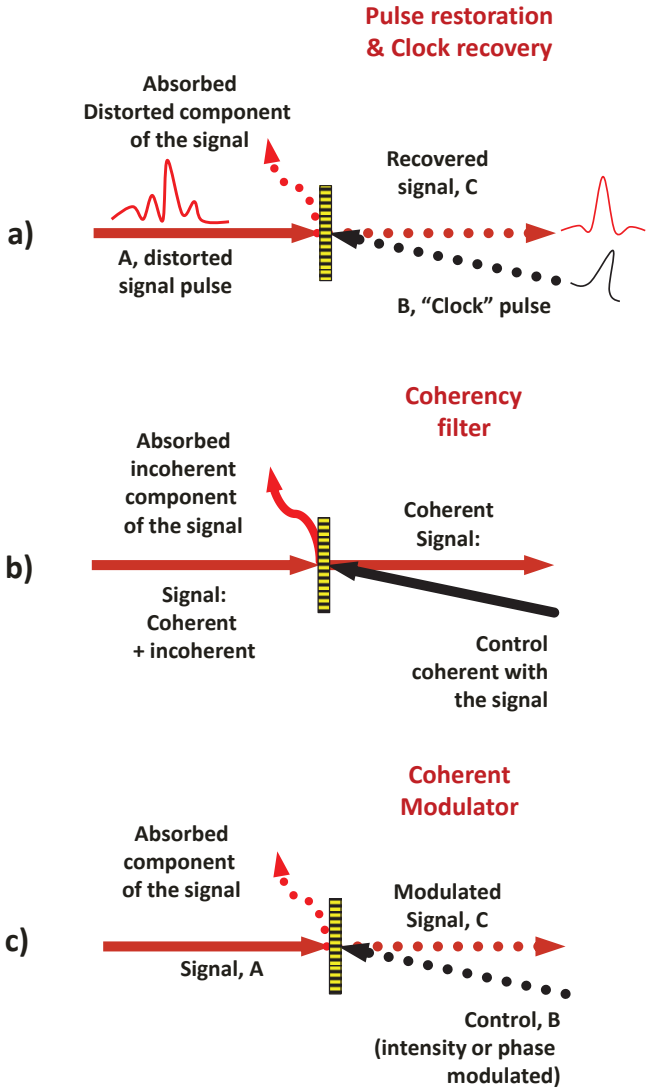

Figure 4.9: Applications. (a) A pulse restoration device to restore the form of distorted signal pulses according to that of a clock (control) pulse; (b) A coherence filter that improves the coherence of light beams by absorbing incoherent components; (c) A coherent light-by-light modulator wherein a digital or analogue intensity- or phase-modulated control input governs signal channel output.

that have the same intensity and amplitude as the clock pulse will be transmitted with negligible loss while distorted components are strongly absorbed, thereby restoring the temporal and spectral profile of the signal.

- Coherence filtering (Fig. 4.9b). Following the same principle as behind 'pulse restoration', i.e. that the absorption of the coherent part of a signal can be enhanced

or eliminated, one may realize a filter with the unique ability to increase or decrease the mutual coherence of two light beams [125].

- Optical gating (Fig. 4.9c). Coherent control of absorption provides functionality for analogue and digital, all-optical (light-by-light) modulation/switching without any optically nonlinear medium, thereby delivering this functionality at extremely low power levels. The coherent control approach promises extremely high, terahertz frequency modulation bandwidth, which is determined by the width of metamaterial plasmonic resonance. Using plasmonic metal nanostructures the approach may be implemented across the entire visible and near-IR spectral range, where resonances can be engineered by design and metallic Joule losses are substantial.

For all the above applications, it is critical to realize a stable relative phase between two coherent beams. Since a modulation in the relative phase will be turned into an intensity modulation of the absorption/scattering signal, we may use this phase-amplitude coupling effect as a feedback mechanism for phase control.

Chapter 5

Optomechanical forces in metamaterials

5.1 Introduction

The fact that light exerts forces upon any surface exposed to it was deduced theoretically by James Clerk Maxwell in 1871 and proven experimentally in 1901 by Lebedew [126] and in 1903 by Nichols & Hull [127]. There are two major categories of optical forces: optical radiation pressure and the optical gradient force. Optical radiation pressure can be regarded as a consequence of the momentum transfer from the radiating field to the dielectric medium while the optical gradient force originates from the intensity gradients of electromagnetic field. In various guises, optical forces are extremely important in mesoscopic systems: They are exploited in all forms of optical tweezing, manipulation and binding [128–131], and recently in optomechanical photonic devices [132–139].

Photonic metamaterials provide an unique platform for manipulating electromagnetic field and thereby optical forces, on the nanoscale. Indeed, there have been quite a lot of interests to demonstrate negative radiation pressure in artificial medium exhibiting negative refractive index [140, 141]. Besides there are also many other interesting phenomena and functionalities that could be achieved by harnessing optical forces via metamaterials. Their ability of trapping light through plasmonic resonances and generating strong variations of the electromagnetic field, for example, can be utilized for

efficient enhancement of optical forces [38]. And the complex electromagnetic fields and nanoscale localization of light produced by metamaterials show potentials for optical manipulation at unprecedented capabilities [94,142]. Moreover, optical forces, via suitable mechanical designs, can be harnessed to drive the reconfiguration of metamaterials, providing opportunities for all optically controlled active metamaterials and for optomechanical metamaterials displaying novel nonlinear effects via mutual interactions between light and mesoscopic structures [139,143].

5.2 Calculating optical forces using Maxwell stress tensor

Within the framework of classical electrodynamics the components of the total time-averaged force **F** acting on a metamaterial structure illuminated with light can be calculated using a surface integral [89]:

$$\langle F_i \rangle = \oiint_S \langle T_{ij} \rangle \, n_j \, \mathrm{d}S \tag{5.1}$$

where S is a bounding surface around the metamaterial, n_j is the unit vector pointing out of the surface and T_{ij} is the time-averaged Maxwell stress tensor defined by:

$$\begin{aligned} \langle T_{ij} \rangle = \frac{1}{2} \mathrm{Re} \Bigg[& \varepsilon\varepsilon_0 \left(E_i E_j^* - \frac{1}{2} \delta_{ij} |E|^2 \right) \\ & + \mu\mu_0 \left(H_i H_j^* - \frac{1}{2} \delta_{ij} |H|^2 \right) \Bigg] \end{aligned} \tag{5.2}$$

The stress tensor integral equation (5.1) encompasses both the radiation pressure and near-field gradient force - the focus of this study. It does not include Casimir forces, which are derived from vacuum quantum fluctuation and thus exist even in the absence of illumination [144].

Radiation pressure arises through transfer of momentum between photons and any surface on which they impinge. It depends on the reflection R and absorption A coefficients of the surface according to the equation $F_r = (2R + A)P/c$, where c is the speed of light in vacuum and P is the power of the incident light, and assumes a maximum value of $2P/c$ when the reflectivity of a surface is 100%.

In this chapter, forces acting on metamaterial structures are evaluated via the Maxwell stress tensor integral Eq. (5.1) with electric E and magnetic H field distribu-

tions obtained from fully three-dimensional finite element Maxwell solver simulations (Comsol MultiPhysics, see Appendix A for details of COMSOL modeling). This analysis utilizes established experimental values of the complex dielectric parameters for gold (see Appendix B) [60], excludes losses in dielectric media and assumes normally incident, narrow-band coherent illumination. By modeling a single 'meta-molecule' (translation unit cell of the metamaterial design) with periodic boundary conditions, calculations assumed a planar metamaterial array of infinite extent. The surface of integration S was defined as a rectangular parallelepiped enclosing the meta-molecule, with walls along each of the four periodic boundaries and *outside* each of the two free surfaces of the metamaterial film (or enclosing each constituent element of the meta-molecue, with walls outside the surfaces of the element, to evaluate forces on elements within a meta-molecule). The same numerical model provides data on the transmission T and reflectance R of the structure.

5.3 Optical gecko toe: Optically-controlled attractive near-field forces between plasmonic metamaterials and dielectric or metal surfaces

In this section, optical forces in plasmonic metamaterials are studied while optical forces in all-dielectric nanostructures will be discussed in Section 5.4 and Section 5.6. In recent years it has become clear that plasmonic systems can provide unprecedented control over optical fields on the nanoscale, offering gigantic field enhancement, subwavelength light localization and strongly enhanced interactions between nano-objects [145–148]. They show potentials to generate strong optical forces on objects with nanoscale dimensions and present opportunities, for example, to extend/enhance the functionality of optical tweezers/traps [149].

In nature, van der Waals interactions underpin the gecko's remarkable ability to overcome gravity by sticking to walls and ceilings [150]. Here it is shown that in addition to the conventional, well-understood force of radiation pressure a much stronger light-driven near-field force may be generated between an illuminated planar plasmonic metamaterial and a dielectric or metallic surface [151]. This newly identified near-field force has a resonant nature linked to the excitation of the metamaterial's plasmonic

mode and acts to close the gap between the metamaterial film and the surface (Fig. 5.1). This 'optical adhesion' force exists alongside interfacial Casimir forces and can outmatch both radiation pressure and, like the gecko toe, gravity.

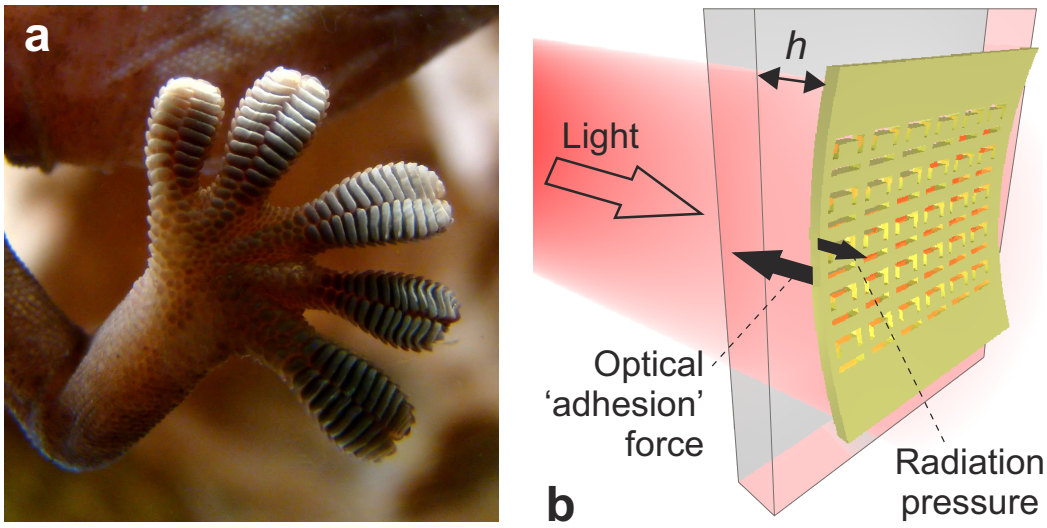

Figure 5.1: Gecko toes and their optical analogue. (a) Gecko toes sticking to a smooth glass wall [152]. (b) Artistic impression of a metamaterial film attracted by a beam of light to a dielectric surface.

This near-field optical force emerges when a metamaterial is placed in close proximity to another object and the evanescent field of the nanostructure encounters that object. The magnitude of this force depends on how strongly optical energy is trapped in the metamaterial and on the electromagnetic properties of the nearby object. In general, the higher the refractive index of the nearby object is, the stronger the interaction will be and in all cases studied here the near-field optical force is attractive. In what follows, the ratio $|\mathbf{F}| : P/c$ is employed as a dimensionless measure of optical force [153].

Firstly, optical forces between a gold metamaterial film and the surface of a semi-infinite transparent dielectric are studied (Fig. 5.2). The metamaterial here is taken to comprise a two-dimensional square array of asymmetric split rings - a popular design recognized for its strong light confinement and simplicity of fabrication [38, 40]. Dimensional details are shown inset to Fig. 5.2a.

For a plasmonic metamaterial both the radiation pressure and near-field forces are resonant (Fig. 5.2b). The dispersion of the radiation pressure force F_r is linked to variations in the metamaterial's absorbtion and reflection coefficients (Fig. 5.2a) and

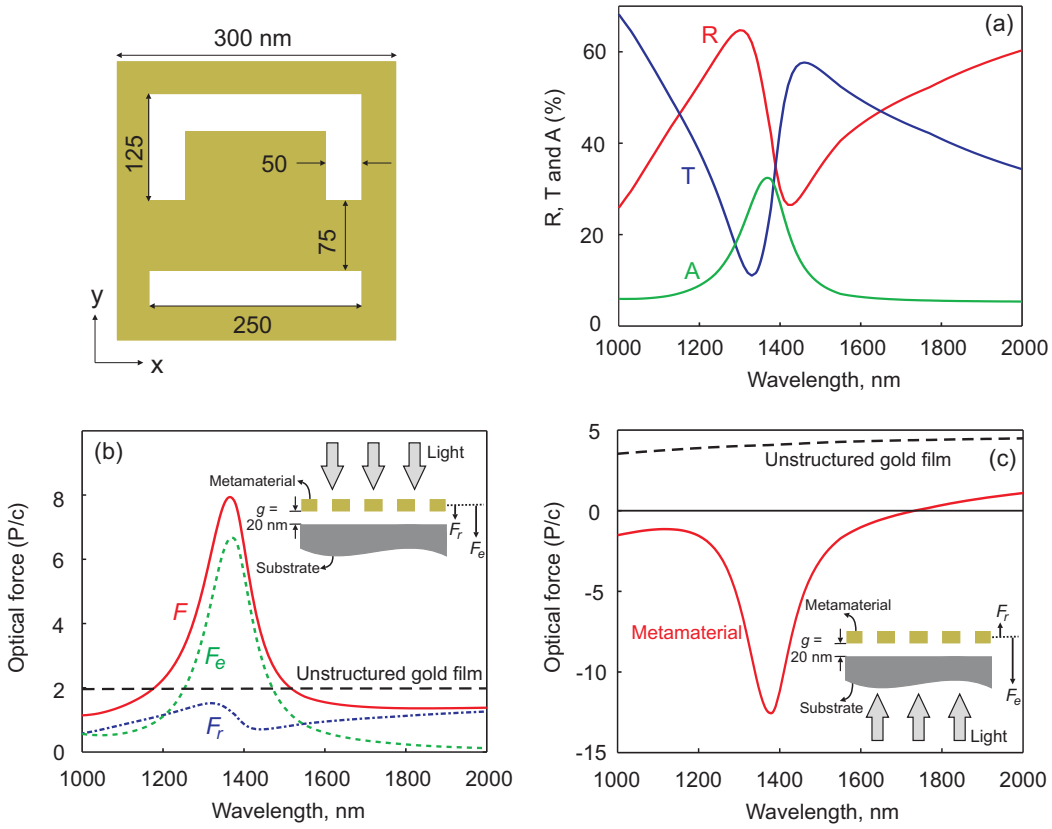

Figure 5.2: Optical forces between a plasmonic metamaterial and a dielectric surface. (a) Reflection R, transmission T and absorption A spectra of a 50 nm thick gold metamaterial located at a distance $h = 20$ nm from the surface of a dielectric with refractive index $n = 2.5$ for y-polarized light normally incident from free space. The inset shows the metamaterial unit cell geometry. (b) Total optical force F acting on a metamaterial illuminated from free-space as illustrated inset. Dashed lines show the evanescent F_e and light pressure F_r components of F. (c) Total optical force acting on a metamaterial illuminated through the dielectric. For comparison, the total force acting on an *unstructured* gold film in place of the metamaterial is shown in both (b) and (c). In all cases, positive values denote forces acting in the direction of incident light propagation.

has a local maximum at a wavelength of 1320 nm corresponding to the reflectivity peak. When the structure is illuminated from free space the radiation pressure F_r and near-field evanescent F_e forces act in the same direction to reduce the gap h between the metamaterial and the dielectric surface. The evanescent force is resonant at 1370 nm, the wavelength of the absorption peak, and exceeds the radiation force across the entire spectral range from 1210 to 1550 nm, reaching a peak magnitude of approximately $6.7P/c$ as compared to only $1.2P/c$ for the radiation force. When light impinges on the sample through the transparent dielectric (Fig. 5.2c) the evanescent force acts *in opposition* to the radiation pressure and again acts to reduce h. In this configuration,

if the gold film were unstructured the total light force would push it away from the dielectric surface, but for a metamaterial the attractive near-field force is dominant and pulls the metamaterial film towards the dielectric.

The near-field force is related to the non-propagating evanescent field of localized plasmons in the nanostructure, which possesses no momentum. As such it does not contribute directly to the momentum balance with incident light; it simply adds to or subtracts from the radiation pressure force depending on the direction of the later. The evanescent force works to change the energy trapped in the nanostructure when the metamaterial is brought into close proximity with a surface. As the eigenfrequencies of a metamaterial are always red-shifted relative to their free-space values when the structure is close to or embedded in another medium with a refractive index exceeding unity, the closest possible presence of such a medium is energetically preferable. As a consequence, the evanescent force between a metamaterial and nearby surface is always attractive. This attractive near-field force can also be understood in a microscopic picture. Since the evanescent field decreases from the metamaterial surface and the permittivity of the dielectric is higher than that of air, the Coulomb force on the induced electric dipole in the dielectric should drive the dielectric surface towards the metamaterial.

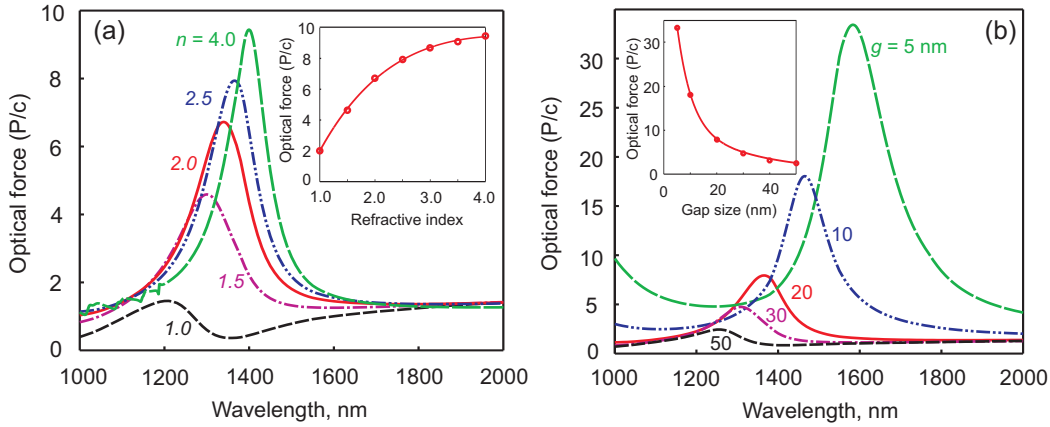

Figure 5.3: Optical forces between a plasmonic metamaterial and a dielectric surface. Spectral dispersion of the total optical force (under illumination from free space as illustrated inset to Fig. 5.2b) for different values, as labeled, of: (a) dielectric refractive index n (at h = 20 nm); (b) gap size h (n = 2.5). Insets show peak optical force as a function of n and h respectively.

Both the radiation pressure and evanescent forces are stronger when the metamaterial is illuminated through the dielectric than when light is incident on the structure

from free space. Higher values of F_r result from the fact that photons traveling in a dielectric have higher momentum p than in free space ($p = nh/\lambda$, where h is the Plank constant and n is the refractive index of the dielectric). Higher values of $|F_e|$ (stronger evanescent fields between metamaterial and dielectric) are a consequence of the metamaterial's higher absorption coefficient under illumination through the dielectric [65] (the increase in $|F_e|$ being proportional to that in A).

Fig. 5.3 shows the dependence of total optical force on dielectric refractive index n and gap size h for free space illumination (as in Fig. 5.2b). As the refractive index of the dielectric increases from $n = 1$ to 4, the magnitude of the optical force increases and the resonance red-shifts. A similar trend is seen with decreasing gap size: at $h = 5$ nm the evanescent force is 33 times stronger than the radiation pressure. Both trends reflect the strong influence of the near-field environment on the metamaterial resonances.

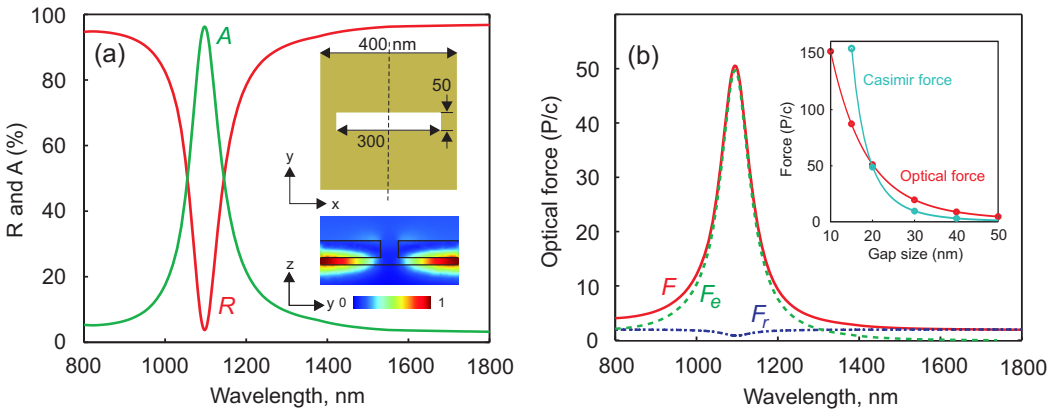

Figure 5.4: Optical forces between a plasmonic metamaterial and a metallic surface. (a) Normal incidence reflection R and absorption A spectra of a 50 nm thick gold metamaterial located at a distance $h = 20$ nm from a gold surface (incident light propagation in the $-z$ direction as defined inset). The insets show the metamaterial unit cell geometry and a map of the normalized magnetic field intensity distribution at the 1095 nm resonance wavelength for a cross-section along the dashed line in the y-z plane. (b) Evanescent F_e, radiation pressure F_r and total optical force F acting on the metamaterial. The inset shows peak optical force as a function of gap size h and the corresponding dependence on h of the Casimir force between two perfectly conducting plates (scaled assuming $I = 50$ mW/μm^2).

Near-field optical forces are even greater at metallic surfaces. In this case a metamaterial comprising a square array of rectangular slots is considered (see inset to Fig. 5.4a). With a metallic backplane this structure supports a 'magnetic resonance' (where anti-symmetric currents are excited in the metamaterial and backplane) at which light is trapped (see inset to Fig. 5.4b) and strongly absorbed. Indeed, similar systems have

previously been analyzed for 'perfect' absorption applications [68, 69, 154]. Fig. 5.4 shows the normal incidence reflection and absorption spectra of the structure and the dispersion of the optical forces acting on the metamaterial film. In this case the magnitude of the total optical force reaches $\sim 50P/c$ at the absorption peak around 1095 nm. The origin of attractive near-field optical forces at metallic surfaces can be explained using similar pictures as the forces at dielectric surfaces both in the macroscopic scale where a decrease of the gap size leads to a redshif of resonance position and in the microscopic scale where the Coulomb force on the induced electric dipole in the metal drives the metal surface towards the plasmonic metamaterial. Indeed, the picture may be more complicated in the microscopic scale if we consider Lorentz forces as well as high order dipole-dipole interactions, especially for high order resonances.

It is interesting to compare the enhanced optical forces between a metamaterial and metallic-surface with the force of gravity on the metamaterial film. The gravitational force on a 50 nm thick gold film is of order 1×10^{-14} N/μm^2. An optical force of the same magnitude can be achieved between a metallic (gold) surface and a metamaterial 20 nm away when the metamaterial is illuminated at the 1095 nm resonant wavelength at an intensity of around 60 nW/μm^2. Under such conditions the optical force will be sufficient to pull a metamaterial against gravity towards a surface. At shorter distances the pulling force becomes even stronger but other micro-/nanoscale forces also become important. The Casimir force $F_c = -(\pi^2 \hbar c)/(240 d^4)$ between two perfectly conducting plates separated by 20 nm is (at $\sim$8 nN/μm^2) equivalent to the optical force achieved at the same separation between a gold metamaterial and planar gold surface for an illumination intensity I of approximately 50 mW/μm^2 (see inset to Fig. 5.4b). However, for a perforated real metal thin film the Casimir force may easily be an order of magnitude smaller than the above estimate [155–157], in which case it would be surpassed by the near-field optical force at much lower intensities.

Indeed, as the Casimir and near-field forces depend differently on distance: $F_c \propto h^{-4}$ (or h^{-3} for realistic metallic plates at values of h smaller than the metal's plasma wavelength [156]) while $F_e \propto I\ e^{-h/a}$ (where a is the characteristic dimension of the nanostructural pattern), above a threshold value of intensity I there will be a range of distances h where the near-field force is dominant, and this range will broaden with increasing intensity. As a result, the near-field force is likely to prevail where conditions

such as surface roughness limit the proximity of two objects.

With regard to the experimental observation of the evanescent force described here, photonic metamaterials can readily tolerate mW/μm^2 illumination intensities whereunder F_e would exceed the gravitational force by several orders of magnitude. The great advantage of this near-field force for nanoscale manipulation is that it depends on both light intensity and wavelength, thereby offering dynamic controllability and spectral selectivity. Such forces could manifest themselves in a variety of resonant structural configurations including, for instance, single meta-molecules or plasmonic elements and may serve applications in optical trapping/tweezing and in the control of light with light via optically reconfigurable metamaterials. For example: an optical fibre scanning probe tip capped with a plasmonic metamaterial may be employed to pick up and re-position individual nano-objects; an array of optically switchable adhesion elements may dynamically control patterns of particles/flakes; optically tuning the position of a metamaterial elastically suspended near a metal surface (varying illumination intensity to adjust the balance between near-field and mechanical forces) will deliver broadband changes in the reflectivity of the structure.

5.4 Giant resonant optical forces in planar dielectric metamaterials

In the previous section, enhanced optical adhesion forces between plasmonic metamaterial and unstructured dielectric or metallic surface have been demonstrated. Resonant optical forces can also be obtained between metallic nanowires [145]. However, the enhancement of optical forces in metallic metamaterials are generally hampered by high inherent energy dissipation due to resistive losses of metals. Moreover, the rapid attenuation of electromagnetic field away from plasmonic structures means optical near field forces decrease quickly with increasing distance between interacting objects and become quite weak if the distance goes to hundreds of nanometers, which limits the pursuit of this type of optical forces for some applications.

Recently, dielectric particles have been proposed as building blocks for metamaterials [158–161]. Dielectric metamaterials can avoid the high inherent loss from material absorption and thus show high quality resonances that are not available in metallic

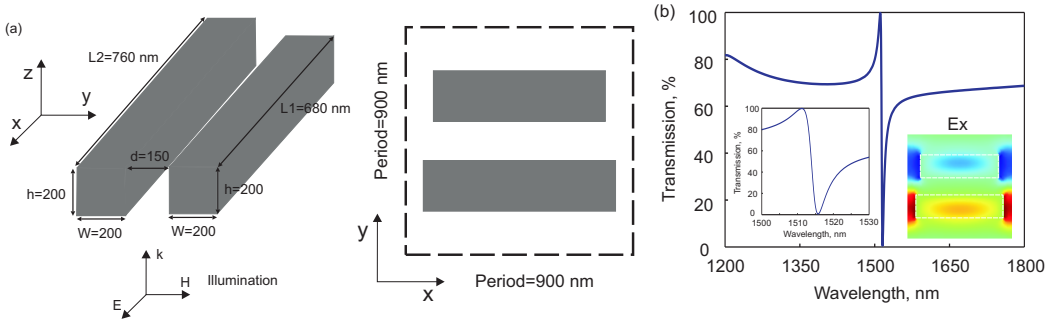

Figure 5.5: Schematic and dimensions of a dielectric metamaterial along with its optical spectrum. (a) Schematic and dimensions of dielectric metamaterial. A metamaterial unit cell consists of two silicon (n=3.48) bars with same cross section and slightly different lengths. The period of unit cell is 900 nm. (b) Simulated transmission spectra of the dielectric metamaterial for x-polarized plane wave at normal incidence. Insets show the zoomed transmission spectrum near the resonance and the electric field distribution (x-direction) in the plane z=25 nm (middle of the rods) at the resonant wavelength $\lambda = 1516\ nm$.

metamaterials. In this section, it will be shown that under illumination of electromagnetic radiation, strong resonant optical forces arise within dielectric planar metamaterials composed of asymmetric silicon nano-rods (see Fig. 5.5(a, b)). There are optical forces exerting on the silicon nano-rods perpendicular to the metamaterial plane, which has the same (or opposite) direction as radiation pressure, as well as optical forces in the metamaterial plane, which act as attractive or repulsive forces between the nano-rods. Furthermore, it will be shown that the relatively less localized field in the dielectric metamaterials makes it possible to have strong interactions between nearby resonators constructing metamaterials with separations of hundreds of nanometers.

Fig. 5.5 shows the schematic and dimensions of the idealized dielectric metamaterial under study. The metamaterial unit cell consists of two silicon (n=3.48) rods with same cross section and different lengths and the period is 900 nm. The cross section of the silicon rods is $200\ nm \times 200\ nm$. The long rod is 760 nm long and the short rod is 680 nm long. Under the illumination of x-polarized plane wave, there is a sharp Fano resonance around 1515 nm. Similar to the metallic asymmetric split ring (ASR) structures, this sharp resonance is attributed to the structural symmetry breaking between the two silicon rods [40, 161]. The electric field distribution reveals that the oscillations in the two dielectric rods are anti-phase at the resonance (see insets in Fig. 5.5(b)). The electric dipole radiation of displacement currents oscillating in the two dielectric bars is largely cancelled out within the unit cell while magnetic dipole radiation is suppressed

among neighboring cells. As a result, the radiation loss is effectively suppressed, leading to a magnetic resonance akin to the well-known 'trapped mode' resonances of metallic asymmetric split ring (ASR) structures. (Note: More details about the mechanism and properties of this resonance will be discussed in Section 5.6).

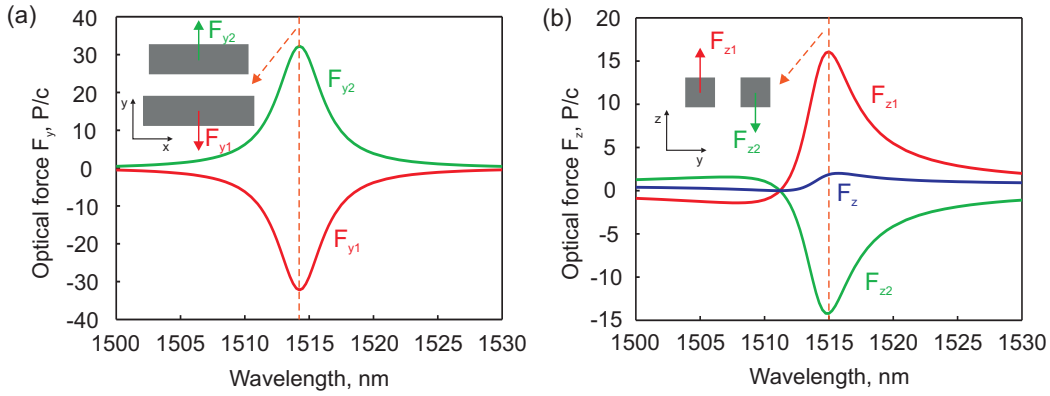

Figure 5.6: Optical forces on dielectric rods within the dielectric planar metamaterial. (a) In plane(y-direction) optical forces on dielectric rods. (b) Out of plane(z-direction) optical forces. Giant near field optical forces are generated around the metamaterial trapped mode resonance. Optical forces are normalized to the radiation pressure P/c, where P is the power of light on each metamaterial unit cell and c is the vacuum velocity of light.

Near the resonant wavelength, electromagnetic energy is trapped in the metamaterial and the electromagnetic field is greatly enhanced. As a result, giant optical forces that are tens of times stronger than radiation pressure are generated in the metamaterial. Fig. 5.6(a) shows optical forces in the metamaterial plane (y-direction). Here F_{y1} and F_{z1} are defined as the y-direction force and z-direction force on the long rod, respectively, and F_{y2} and F_{z2} as the y-direction force and z-direction force on the short rod, respectively. Obviously, the in plane forces on long rod and short rod have the same amplitude but opposite directions. Near the resonance,in plane forces between the two rods are repulsive and the relative force could be $64P/c$ at $\lambda = 1514\ nm$. (Simulation shows that in plane forces could be attractive though they are not shown in this spectrum range).

Besides, there are also out of plane optical force (z-direction) in the dielectric metamaterial. The out of plane optical forces in dielectric rods consists of both radiation pressure and near field force and near field force and reaches $16.08P/c$ on the long rod and $-14.2P/c$ on the short rod at $\lambda = 1515\ nm$ around the resonance. The total optical force $F_z = 1.88P/c$ on unit area of dielectric metamaterial comes from radiation

pressure and is determined only by reflection $F_z = 2R * P/c$. In plane optical forces can be precluded if all the dielectric unit rods are arranged with the same separation and only vertical forces work on the dielectric rods. In plane optical forces can be understood intuitively by considering the Coulomb force and Lorentz force between the two silicon rods. Near the resonance, the repulsive Lorentz force of anti-phase displacement currents in the two rods is stronger than the attractive Coulomb force of dipole-dipole interactions, leading to the repulsive optical force between the nanorods. Out of plane optical forces on the rods can be understood as the Lorentz force of oscillating displacement currents in the field of incident light combined with the radiation pressure. The former is much stronger than the later near the resonance and the anti-phase displacement currents on the two rods lead to out of plane forces in oppositive directions.

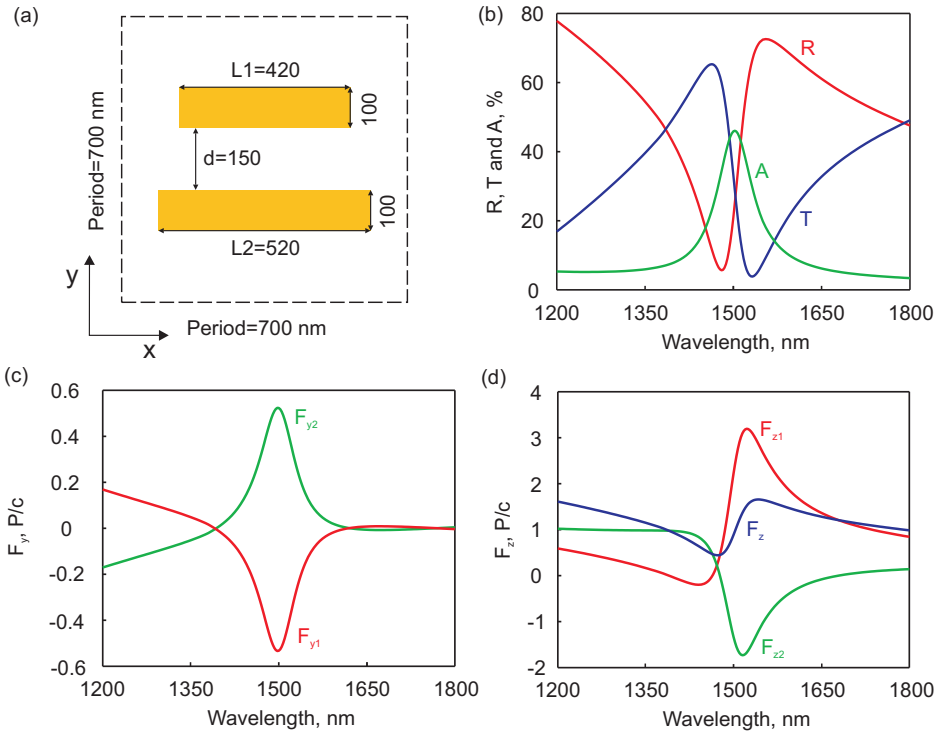

Figure 5.7: Optical forces in a plasmonic metamaterial. (a) Schematic and dimensions the plasmonic metamterial with unit cells consisting of two gold rods with slightly different lengths. Period of metamaterial unit cell is 700 nm. The cross section of gold rods is 100 $nm \times 100$ nm (thickness=100 nm) and the length are 520 nm and 420 nm, respectively; (b) Simulated reflection, transmission and absorption spectra of the plasmonic metamaterial. The incident radiation is x-polarized plane wave at normal angle. (c) In plane (y-direction) and (d) out of plane (z-direction) optical forces on metallic bars.

As a comparison, optical forces in a plasmonic metamaterial composed of periodical

resonator unit cells are calculated. The unit cell consists of two gold rods with slightly different lengths, which supports trapped mode Fano-resonances (Fig. 5.7(a)). Here the optical spectra show that there is a trapped mode resonance near 1500 nm (Fig. 5.7(b)). Both in plane and out of plane optical forces show resonances near the trapped mode (Fig. 5.7(c) and (d)). The maximum relative in plance optical force reaches $1.05P/c$ at $\lambda = 1500\ nm$. Maximum out of plance optical force on long rod is $3.19P/c$ at $\lambda = 1523\ nm$ and that on short rod is $-1.73P/c$ at $\lambda = 1515\ nm$. Even though the near field optical forces are quite remarkable in plasmonic metamaterials, the plasmonic loss, relatively low quality factor of resonance and high confinement of EM field near the metallic rods make the resonant optical forces one order smaller than that in dielectric metamaterials.

5.5 Nonlinear dielectric optomechanical metamaterials

Dynamic back-action caused by optical forces have been proposed for optomechanical laser cooling and amplification and leads to the emerging research field known as cavity optomechanics and enormous progress has been made in this field in the past few years [132]. Optical forces have also be harnessed for actuation and operation of nanophotonic devices [139]. The convergence of nanophotonics and nanomechanics via optical forces presents considerable potential for all-optical operation of nanomechanical systems, reconfigurable and ultra-widely tunable nanophotonic devices, and novel nonlinear and self-adaptive nanomechanical photonic functionalities [107,108,162–165].

In this section, the concept of optomechanical metamaterials in introduced. Here optomechanical metamaterials are susceptible to optical forces within the structure with the introduction of nano-beams, which bend and lead to reconfiguration of the metamaterial when forces are applied. Numerical analyses reveal that optomechanical forces, acting within and among the constituent cells of a dielectric (silicon/silicon nitride) metamaterial, provide a strong nonlinear optical response mechanism delivering high contrast, near-infrared asymmetric transmission and optical bistability at intensity levels of only a few hundred $\mu W/\mu m^2$.

Fig. 5.8a shows an artistic impression and dimensions of the optomechanical metamaterial under consideration: it comprises a 12 $(x-direction) \times 24$ (y) array of 250 nm

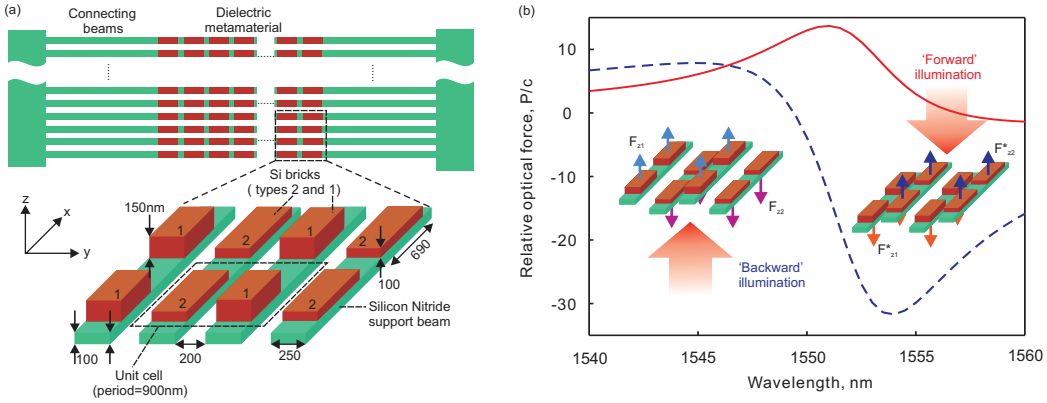

Figure 5.8: Asymmetric optomechanical forces in a dielectric photonic metamaterial. (a) artistic impression and dimensional details of the parallel silicon nitride beam, silicon nano-brick metamaterial configuration studied. (b) Spectral dispersion of the relative optical force F on the two nano-brick elements of a single metamaterial unit cell under normally-incident x-polarized illumination for both forward (-z) and backward (+z) directions of light propagation. [$F_{opt.}^{cell} = F_{z2} - F_{z1}$, where F_{z1} and F_{z2} are the optical forces on the thick and thin bricks respectively; Optical force is presented in units of P/c, where $P = P_0/N^2$ is the incident power per unit cell, P_0 being the total power incident on the metamaterial array of N^2 cells.]

wide, 690 nm long silicon 'nano-bricks' with thicknesses alternating in the y-direction between 100 and 150 nm; these are supported on parallel 100 nm thick, 250 nm wide silicon nitride strips running parallel to x and separated from each other (in y) by 200 nm; These strips extend, at a reduced thickness of 50 nm, to fixed mounting points 15 μm from the outside edges of the nano-brick array. Silicon and silicon nitride nanostructures are assumed to be lossless with refractive indices of 3.5 and 2.0 respectively. Monochromatic x-polarized plane wave is taken to be normally incident (along z) on the nano-brick metamaterial structure, which has an area of 10.8 $\mu m \times 10.8$ μm, with a total optical power P_0.

Under such illumination, optical forces are generated within the metamaterial. In-plane ('horizontal'; per-pendicular to z) optical forces are canceled and only out-of-plane ('vertical'; parallel to z) forces act on the dielectric beams. Fig. 5.8b shows the relative magnitude of optical forces acting on the unit cell pairs of adjacent thick (150 nm) and thin (100 nm) nano-bricks for light impinging on the metamaterial in the forward and backward directions, defined respectively as being incident on the silicon brick and supporting silicon nitride beam sides of the structure. A significant difference is found between these two configurations. In both cases, the optical forces will drive the supporting beams to move up or down until they are balanced by elastic restoring

forces.

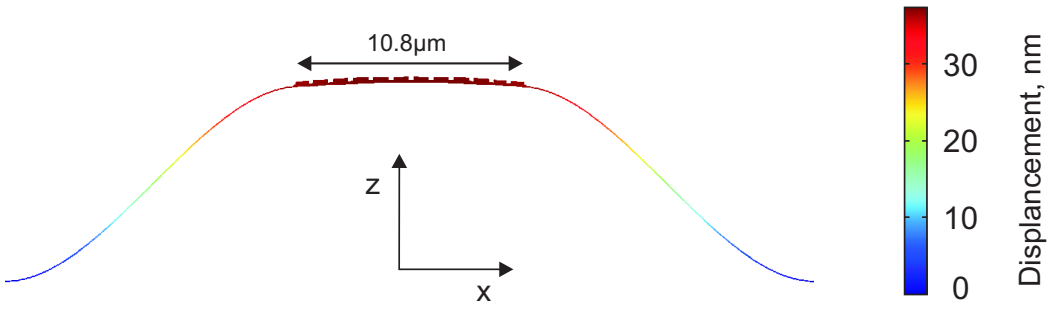

Figure 5.9: Elastic deformation of a suspended beam for a force of 100 pN. The silicon nitride beam is 40.8 μm long (x) and 250 nm wide (y). The force is uniformly applied over the central 10.8 μm long 'metamaterial' section [supporting an array of twelve 690 nm (x) $\times$ 250 nm (y) $\times$ 100 nm (z) silicon bars]. The beam has a thickness (z) of 100 nm in this central region and 50 nm over the 15 μm extension to either side. NB: the vertical scale in this figure is exaggerated by more than two orders of magnitude relative to the horizontal so that the deformation distribution can be clearly resolved.

Finite element numerical simulations (COMSOL MultiPhysics), show that the vertical (z) mechanical displacement of silicon nitride beams (as in the metamaterial structure) subject to a 100 pN applied force is of the order of 37 nm (See Fig. 5.9). Importantly, bending occurs primarily within the 50 nm thick connecting arms and there is negligible deformation of the central 100 nm thick section supporting the silicon nano-bricks. In what follows, optical forces on the nano-beams do not exceed 200 pN and vertical displace-ments are therefore confined to the tens of nanometers range. It is therefore assumed that the central nano-brick array section of each nano-beam moves up and down (in the z-direction) without changing shape and that deformation associated with this movement is confined to the peripheral supporting sections. The spring constant associated with two fixed beams is given by $\frac{2Ewt^3}{l^3}$ where E is the Young's modulus (=150 GPa for silicon nitride [166]) and w, t, and l are respectively the width (250 nm), thickness (50 nm), and length (15 μm) of the individual beams [167]. For simplicity, gravity is ignored in all cases.

Fig. 5.10a shows the dependence of relative optical force acting on two neighboring beams $F_{opt.}^{beam}$ $(= 12F_{opt.}^{cell}$, where 12 is the number of silicon bricks on each beam and $F_{opt.}^{cell}$ is the relative optical force on a unit cell brick pair) on mutual displacement D in the vertical (z) direction for a selection of incident light power levels (at a wavelength $\lambda = 1551\ nm$). To achieve stable equilibrium, not only should the optical force be equal to the elastic force $F_{elas.}$, but they should also satisfy the conditions that $F_{opt.}^{beam} >$

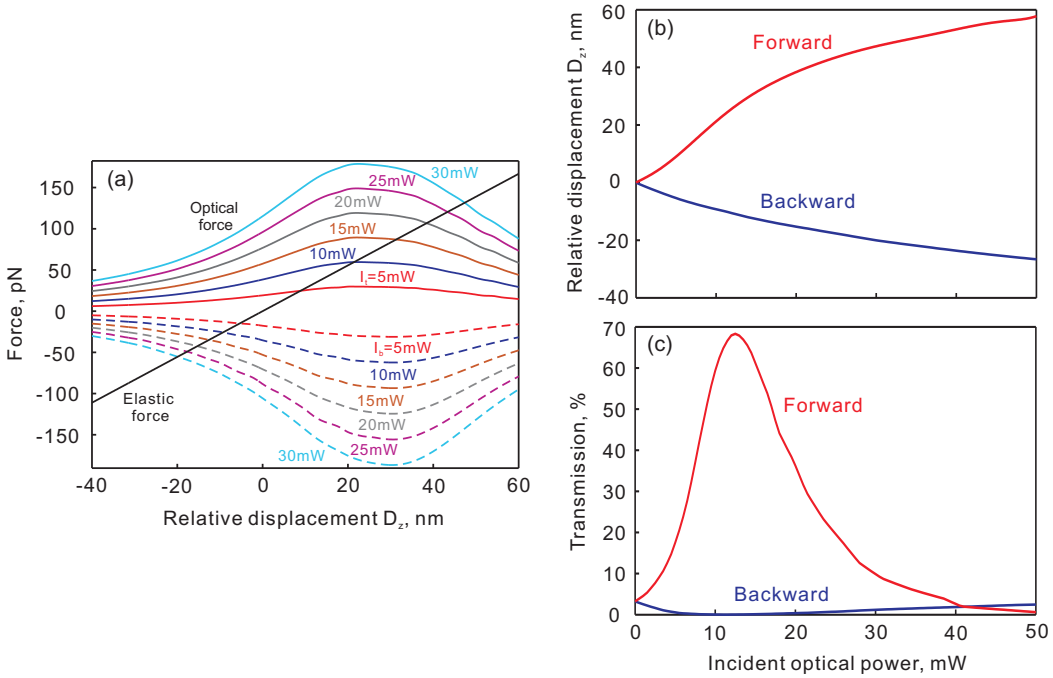

Figure 5.10: Nonlinear optical response and asymmetric transmission. (a) Dependence of the relative optical force $F_{opt.}^{beam}$ on the mutual out-of-plane displacement D of neighboring silicon nitride beams supporting thick and thin silicon nano-bricks under 1551 nm forward (solid lines) and backward (dashed lines) illumination at a range of incident power levels P_0 (as labeled). The straight black line corresponds to the opposing elastic force. (b, c) Dependencies of (b) relative nano-beam displacement and (c) metamaterial optical transmission on total incident power at a wavelength of 1551 nm.

$F_{elas.}\,|_{D-\Delta D}$ and $F_{opt.}^{beam} < F_{elas.}\,|_{D+\Delta D}$. If these last conditions are not met the equilibrium would be unstable and any perturbation would cause D to increase or decrease rapidly towards a stable balance point.

In the example shown, stable equilibrium is achieved for forward incidence of light with a power of 5 mW at a relative displacement of 9 nm (the point at which the black 'elastic force' line intercepts the solid red 5 mW optical force line). For backward incidence, the direction of relative movement is inverted and equilibrium is achieved for the same power level at a mutual separation of (-)5 nm (the intersection of black and dashed red lines).

Fig. 5.10b shows the dependence of (relative) beam displacement on optical power P0 at a wavelength of 1551 nm for forward and backward light propagation directions. As a result of this movement, the dielectric metamaterial changes its optical properties as shown in Fig. 5.10c: For forward propagation, transmission increases from a zero-illumination level of 3.2% to 68.3% at a power of 12.5 mW and then drops back to 0.6%

at 50 mW; The backward incidence optical transmission is less than 3.2% across the entirety of the 0 to 50 mW power range and at $P_0 = 12.5\ mW$ is only 0.034%, giving a forward:backward extinction ratio greater than $30dB$.

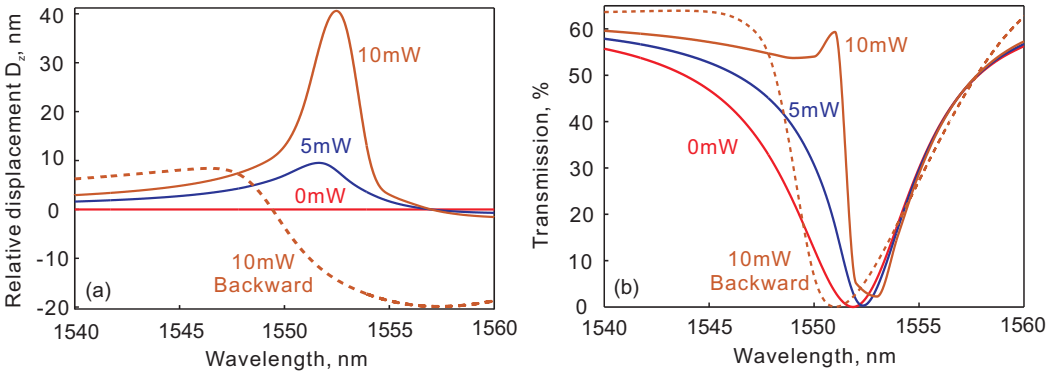

Figure 5.11: Optomechanical nonlinearity and asymmetric transmission resonances. (a) Spectral dispersion of the steady-state relative nano-beam displacement and (b) corresponding optical transmission for forward incidence of light (solid lines) at a selection of total incident power levels (as labeled) and backward incidence at 10 mW (dashed lines).

Fig. 5.11a shows the spectral dispersion of relative beam displacement under forward illumination at a selection of optical power levels and Fig. 5.11b the corresponding transmission resonances, which become increasingly narrow and asymmetric as the optical power increases from 0 to 10 mW. This figure further illustrates the property of optomechanically-induced asymmetric transmission based on differing displacement responses for forward and backward directions of light propagation: at an optical power of only 10 mW, one observes an asymmetric transmission band centered at 1551 nm wherein the forward:backward extinction exceeds 20 dB.

The dielectric nano-brick metamaterial also exhibits optical bistability based on its nano-mechanical response: Fig. 5.12a presents the relative optical force (for forward incidence at a wavelength of $\lambda = 1555\ nm$) and the corresponding elastic restoring force acting on two neighboring beams as a function of relative displacement. At both low and high incident powers the system has only one equilibrium position (the single points of intersection between $F_{elas.}$ and $F_{opt.}^{beam}$ lines at D = 6.3 nm for P0 = 14 mW and at 59 nm for 22 mW). But at intermediate levels, here between about 16 and 19 mW, the optical and elastic force lines intersect at more than one point and the system becomes bistable, as illustrated by the relative displacement and corresponding optical transmission versus power curves in Figs. 5.12b and 5.12c.

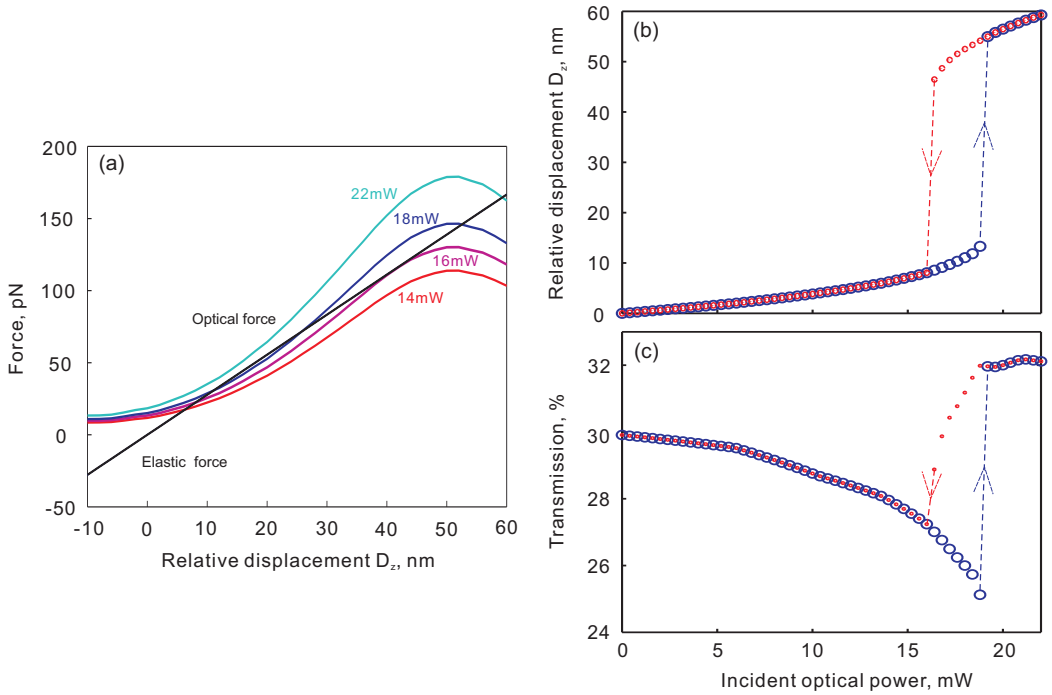

Figure 5.12: Optomechanical bistability. (a) Dependence of the relative optical force $F_{opt.}^{beam}$ and elastic restoring force $F_{elas.}$ on the mutual out-of-plane separation D of neighboring silicon nitride nano-beams under 1555 nm forward illumination at a selection of incident power levels P_0 (as labeled). (b, c) Corresponding bistable incident power dependencies of (b) mutual displacement and (c) optical transmission.

In such a highly nonlinear system the switching dynamics are complex and depend strongly on initial conditions and control input dynamics. The above study is concerned with steady-state displacements of the nanostructure (i.e. assumes constant illumination at any given incident power level) and with the associated changes in optical properties, but an indicative estimate of switching time can be obtained by numerically solving the nonlinear equations of motion for individual beams. This analysis yields a characteristic transition time, from the zero-illumination equilibrium position to maximum deflection, of order 5 μs (assuming instantaneous application of a force equivalent to that generated at $P_0 = 10\ mW$ for forward illumination at a wavelength of 1551 nm; ignoring the damping of any subsequent oscillation).

5.6 Towards dielectric optomechanical metamaterials: Experimental demonstration of optical magnetic resonances in all-dielectric metamaterials

As shown previously, dielectric metamaterials provide great potentials for optomechanical devices. In this section, sharp magnetic resonances in all-dielectric metamaterials are experimentally demonstrated, making a significant step towards high quality optical magnetism and optomechanical metamaterials.

For a decade and more, considerable effort has been focused on the engineering of metamaterials to achieve high frequency artificial magnetism, not least for applications in negative refractive media [50]. The advancement of fundamental theory and of computational and fabrication techniques has led to an increase of more than 4 orders of magnitude in the highest reported magnetic resonance frequencies over the past decade and thereby to the observation of negative permeability and negative refractive index at infrared (IR) and visible frequencies [6, 7, 168]. However, the vast majority of metamaterial structures employed here comprise arrays of sub-wavelength metallic (typically split-ring) resonators. These suffer from high inherent energy dissipation due to resistive losses in the metal, especially in the near-infrared to visible range, which severely compromise optical properties and limit potential applications. Numerous efforts have been made to incorporate gain media into metamaterials for loss compensation [169–171] but extremely high pump powers may be needed to compensate the large losses and would unavoidably introduce significant noise and heat. Consequently, there has been growing interest in the development and application of low loss alternatives to metals as plasmonic media [172].

Recently, Mie resonances of dielectric particles have been proposed as basis for the engineering of magnetic resonances [159, 173–177], and magnetic responses have been experimentally realized in metamaterials consisting of high permittivity dielectrics such as titanium dioxide and germanium, first at microwave and terahertz frequencies [158, 178–180] and more recently in the mid-infrared range [160]. Here we experimentally demonstrate a new mechanism via which visible and near-infrared magnetic resonances are achieved in purely dielectric metamaterials which have been employed in Section 5.4 and Section 5.5: Magnetic resonances akin to the well-known 'trapped mode' resonances

of metallic asymmetric split ring (ASR) structures [40, 161] are realized in dielectric metamaterials through a coupling between closely spaced, dissimilar dielectric nano-bars [161] (Figs. 5.13a, b).

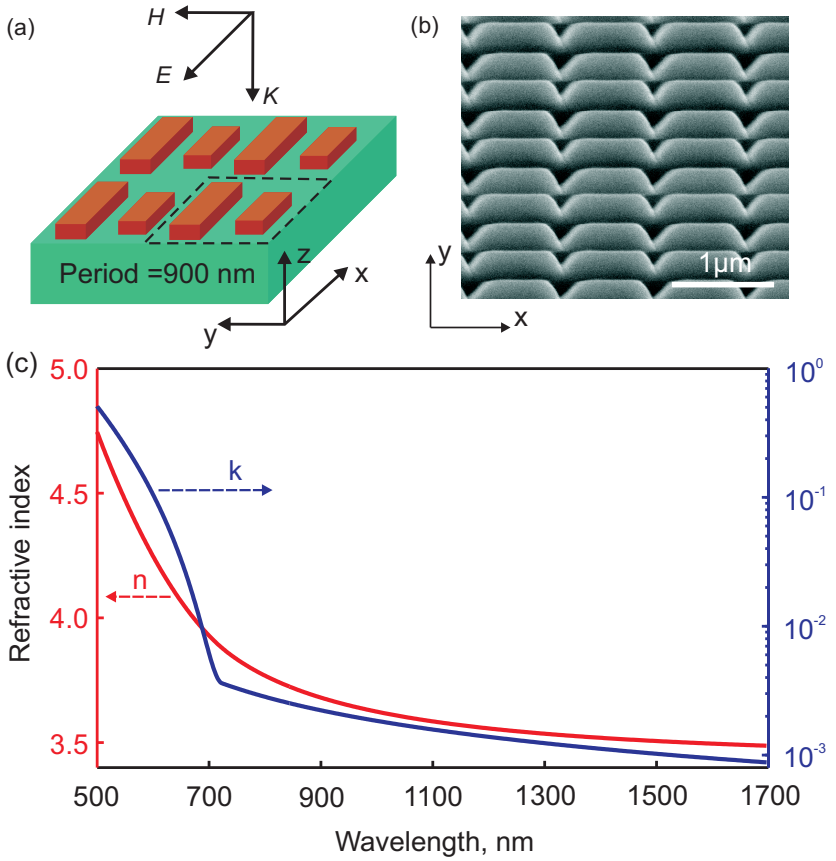

Figure 5.13: All-dielectric photonic metamaterial. (a) Artistic impression and dimensional detail of part of an all-dielectric metamaterial, composed of asymmetric silicon nano-bar pairs on silica, which exhibits sharp visible to near-IR 'trapped mode' magnetic resonances. [$h = 160$, $w = 300$, $L1 = 650$, $L2 = 750$ nm] (b) Scanning electron microscope image of the experimental implementation of this design on a 160 nm amorphous silicon film (viewed at an oblique angle to the surface normal; full array size 30 × 30 μm). (c) Refractive index of unstructured PECVD amorphous silicon obtained via spectroscopic ellipsometry.

Low-loss materials with high refractive indices must be used as a platform for the assembly of dielectric metamaterials in order to minimize absorption losses while ensuring that the metamaterial unit cells are effectively of sub-wavelength size to exclude diffraction effects. Narrow band-gap materials such as silicon, germanium, and tellurium are among the best candidates due to their high refractive indices (> 3) and relatively low absorption in the optical range. Dielectric metamaterials based on tellurium dielectric resonators have recently been demonstrated to show magnetic resonances in the mid-IR

range [160]. The present study employs silicon, which has a bandgap of 1.1 eV. 160 nm thick amorphous films, with extremely low intrinsic absorption and a refractive index of around 3.5 (Fig. 5.13(c)) in the near-IR telecommunications wavelength range, are deposited by plasma-enhanced chemical vapor deposition (PECVD) at 250 ^{o}C on glass substrates. Dielectric metamaterial structures, such as illustrated in Figs. 5.13a and b, are fabricated on these films by focused ion beam (FIB) milling. These comprise square arrays of 900 nm unit cells, each of which contains a dissimilar pair of silicon bars with the same height (the 160 nm thickness of the Si film) and width (300 nm) but different lengths (nominally 650 and 750 nm). This asymmetry within the metamaterial unit cell is crucially important to achieving a magnetic resonance.

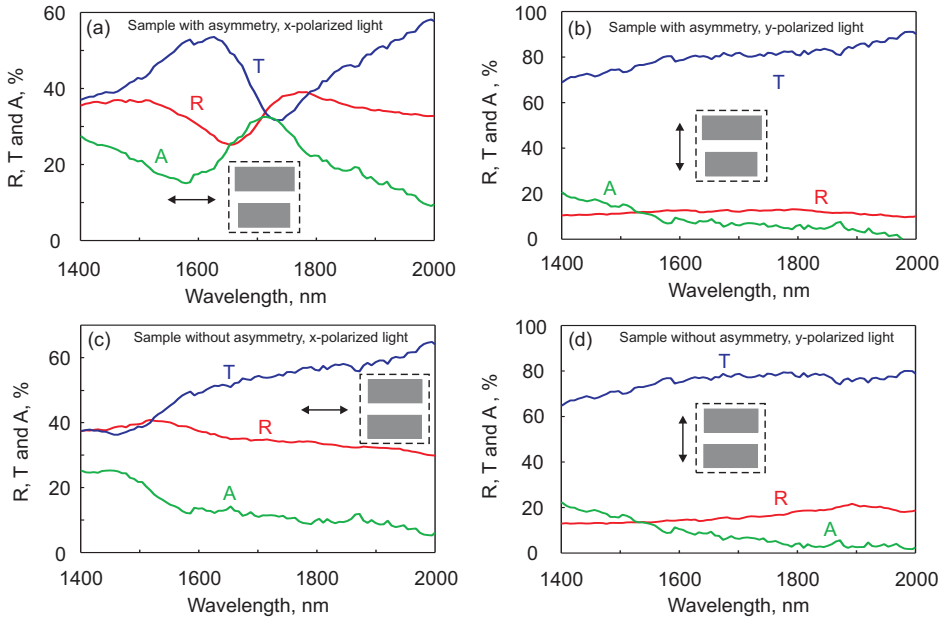

Figure 5.14: Near-IR magnetic resonance in an all dielectric metamaterial. (a) and (b) show reflection, transmission and absorption spectra for the structure,from microspectrophotometry measurements, for the experimental silicon metamaterial structure shown in Fig. 5.13(b) under normally-incident illumination polarized parallel (a) and perpendicular (b) to the long axes of the Si nano-bars. (c) and (d) show spectra for a control sample in which there is no asymmetry between the two Si bars in each unit cell [i.e. they have identical dimensions] under x-polarized [electric field parallel to long nano-bar axis as in part (a)] (c) and y-polarized [electric field perpendicular to long nano-bar axis as in part (b)] (d) light.

Figs. 5.14(a) and (b) show measured, normal-incidence optical transmission, reflection and absorption spectra for the metamaterial sample shown in Fig. 5.13(b) for light polarized parallel and perpendicular respectively to the long (x) axes of the Si bars. There is a pronounced resonance at around $\lambda = 1700$ nm for incident light polarized

(i.e. with electric field) parallel to the long axes of the dielectric bars. For y-polarized light (i.e. with electric field perpendicular to the long axes of the dielectric bars), there is no resonance (Fig. 5.14(b)). For comparison, a 'symmetric' control sample was manufactured in which each unit cell contained two identical silicon 700 nm long silicon bars (160 nm height, 300 nm width and 900 nm array period as above). The spectra for this sample (Fig. 5.14(c) and (d)) show no resonance for normally incident light polarized either parallel or perpendicular to the long axes of the dielectric bars, thereby illustrating the essential nature of the unit cell asymmetry to the excitation of the trapped mode resonance seen in Fig. 5.14(a).

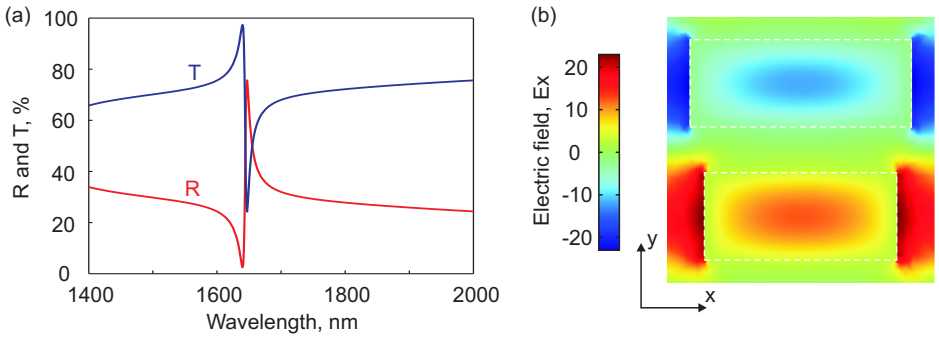

Figure 5.15: Numerical modeling of NIR dielectric metamaterials. (a) Simulated normal incidence transmission and reflection spectra for a rectilinear metamaterial geometry based on the experimental sample design parameters shown in Fig. 5.13(b). The two silicon bar are assumed to be 160 nm thick, 300 nm wide cuboids with lengths of 750 nm and 650 nm, respectively. Here silicon is assumed to be lossless with a refractive index n=3.5 and the refractive index of substrate is 1.46; (b) Magnitude of the x-component of electric field across an asymmetric Si nano-bar unit cell of the metamaterial structure at the resonance wavelength $\lambda = 1644\ nm$. Data are presented for the xy plane bisecting the nano-bars at a height of 80 nm above the substrate surface.

Further insight into the nature and origins of the resonance is provided by full-wave electromagnetic numerical simulations using COMSOL MultiPhysics (see Appendix A for details of COMSOL modeling). Fig. 5.15(a) presents simulated spectra for a model structure corresponding to the experimental sample design above for normally incident x-polarized light. The calculations assume a silicon refractive index n_{Si} of 3.5, a substrate index of 1.46, zero absorption in both cases, and ideal cuboid Si bar geometries. As such the resonance features in the simulated spectra are very sharp, but that aside the correlation with experimental data (Fig. 5.14(a)) is good. Fig. 5.13a illustrates that the zero-loss assumption is reasonable for the amorphous Si film in the wavelength range under consideration, and the glass substrate can also be considered lossless in this

range. The damping of spectral resonance features in experiment is therefore attributed to manufacturing imperfections, specifically in Si nano-bar shape (individual deviations from the cuboid geometry and variations across the array), surface roughness (which introduces scattering losses) and gallium contamination from the FIB milling process (introducing absorption).

Fig. 5.15(b) shows the electric field distribution for a nano-bar pair unit cell of the metamaterial structure at the resonance wavelength. The two bars are excited in anti-phase, with electric polarizations of almost equal amplitude, and thereby display a magnetic mode resonance through electric coupling [181]. (Similar resonances have been extensively studied in metallic planar metamaterials with a broken structural symmetry [40]) The electric dipole radiation of currents oscillating in the two dielectric bars is canceled within the unit cell while magnetic dipole radiation is suppressed among neighboring cells. As a result, scattered electromagnetic fields are very weak, which dramatically reduces coupling to free space and therefore radiation losses. Such resonances are designated 'trapped modes' as they provide an effective means of trapping electromagnetic energy in metamaterial structures.

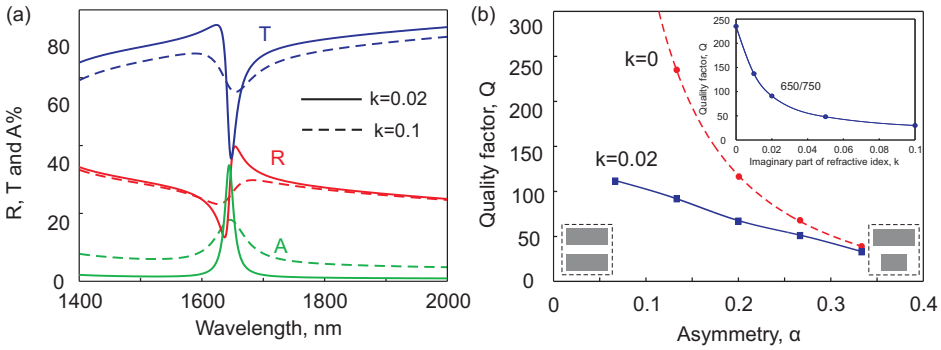

Figure 5.16: The impact of absorption and asymmetry on dielectric magnetic resonances. (a) Simulated transmission, reflection and absorption spectra for the same metamaterial geometry [and the same x-polarized normally-incident illumination conditions] employed in Fig. 3 with non-zero values of the silicon absorption coefficient: solid lines assume $n_{Si} = 3.5 + 0.02i$; dashed lines $n_{Si} = 3.5 + 0.1i$. (b) Magnetic resonance quality factor as a function of asymmetry α, defined as the relative difference of the bars' lengths. Dashed line assumes $n_{Si} = 3.5 + 0i$; solid line $n_{Si} = 3.5 + 0.02i$. The inset shows magnetic resonance quality factor as a function of silicon loss coefficient for asymmetry $\alpha = 0.133$ [curves labeled with two bar lengths]

As in metallic metamaterials composed of asymmetric split rings, the quality of trapped-mode resonances in dielectric metamaterials can be increased by reducing the asymmetry of the resonant elements [40] (Fig. 5.16(b)). However, as the radiation

losses are very low, absorption loss is the limiting quantity on achievable quality factor ($Q = \lambda_r/\Delta\lambda$ where λ_r is the resonance frequency and $\Delta\lambda$ is the half-maximum linewidth) in such metamaterials. In Fig. 5.15(a), the quality factor of the magnetic resonance is approximately 230. Fig. 5.16 illustrates how this value decreases with increasing absorption in the silicon (introduction and variation of a non-zero imaginary part in the assumed refractive index of silicon). Remarkably, for $n_{Si} = 3.5 + 0.02i$ the magnetic resonance retains a quality factor of ∼90 and even at $n_{Si} = 3.5 + 0.1i$ Q ∼30. Indeed, based on the measured parameters for PECVD films (Fig. 5.13c), a silicon metamaterial resonant at λ= 700 nm, where $n_{Si} = 3.87 + 0.006i$, may present magnetic resonances with Q values approaching 100. The experimental metamaterial sample presented here has a magnetic resonance quality factor of ∼15 but crucially this is limited not by the intrinsic properties of the material from which it is made (as is the case in metallic structures at visible and near-infrared wavelengths) but rather only by the shortcomings of the current manufacturing process (described above). Thus, with improvements in fabrication techniques, visible and near-IR resonances with quality factors much higher than those typically achieved in conventional metallic metamaterials or plasmonic systems [38] can be realized in dielectric structures, even in the presence of non-trivial losses.

5.7 Summary

In summary, photonic metamaterials, with the unprecedented ability of controlling electromagnetic field, provide an unique platform for studying, manipulating and harnessing optical forces. Optical forces in plasmonic as well as dielectric metamaterial structures have been studied via the Maxwell stress tensor integral with electric E and magnetic H field distributions obtained from fully three-dimensional finite element Maxwell solver simulations.

Firstly, the optical force between a nanostructured plasmonic metamaterial film and a dielectric or metal surface have been investigated . It has been demonstrated that, in addition to the radiation force, a near-field optical force emerges when a metamaterial is placed in close proximity to another object. This near-field force is related to Fano resonances of plasmonic metamaterials and is always attractive at resonance. The strength

of the optical force increases as the gap between a metamaterial and a dielectric/metal surface decreases. For a dielectric surface, the near-field optical force increases as the refractive index of the dielectric increase while even stronger resonant optical force can be realized between a plasmonic metamaterial and a metal surface. The near-field optical force can greatly exceed the associated radiation pressure and it is sufficient to overcome gravity at illumination intensities of just a few tens of $nW/\mu m^2$, providing a light-controlled mechanism mimicking 'gecko toe'. Optical 'gecko toe' present opportunities to extend/enhance the functionality of optical tweezers/taps and to design novel optomechanical devices.

Then optical forces in a planar dielectric metamaterial are studied. Dielectric metamaterials don't suffer from high losses of inherent absorption, thus supporting resonances with much higher quality factors. A type of dielectric metamaterials consisting of closely spaced, dissimilar dielectric nano-bars and showing sharp optical magnetic resonance akin to the well-known 'trapped mode' resonances of metallic asymmetric split ring are invastigated. Optical forces exerting on the dielectric elements of metamaterials drive them both perpendicular to the metamaterial plane (in the propagation direction of light) and within the dielectric plane (perpendicular to the propagation direction of light). It has been demonstrated that resonant optical forces both in and out of the dielectric metamaterial plane can be tens of times stronger than the radiation pressure with a gap of hundreds of nanometers between the resonant elements and could be one order higher than that in plasmonic metamaterials. Optical forces in dielectric metamaterials make a bridge between optical properties and mechanical properties and they could be exploited as a controlled mechanism for all optically tunable/reconfigurable optical metamaterials.

As an example of tremendous opportunities that could be realized by harnessing optical forces in metamaterials, the concept of 'optomechanical metamaterials' is proposed. An nonlinear dielectric optomechanical metamaterial consisting of subwavelength dielectric resonant elements supported by elastic nano-beams is designed. Under the illumination of optical radiation, resonant optical forces are generated on the dielectric resonant elements and bend the elastic nano-beams, leading to reconfiguration of the metamaterial and change of its optical properties. Therefore the mutual interactions of optical and mechanical responses provides a mechanism for strong nonlinear opti-

cal responses. The optomechanical metamaterial displays high contrast, near-infrared asymmetric transmission and optical bistability at optical intensity levels of only a few hundred $\mu W/\mu m^2$. Optomechanical metamaterials have potential for applications in optical isolators, self-adaptive photonic devices and tunable metamaterials.

Finally, planar dielectric metamaterials composed of asymmetric silicon nano-rods have been experimentally demonstrated, which exhibit sharp magnetic resonances in the VIS-NIR range. The resonance depends critically on the asymmetry between the pair of dielectric bars (samples with unit cells comprising two identical bars show no resonance) and simulations indicate that magnetic resonances with quality factors of several hundreds at visible and near-infrared wavelengths may be achieved in silicon metamaterials though manufacturing imperfections limit current experimental samples to Q values of 15. These structures offer a new route to the realization of low loss optical magnetism at such frequencies and provide opportunities in controlling the emission of quantum emitters [43, 182], and even in the development of lasing spasers [41]. Moreover, they provide a platform for developing optomechanical devices and their experimental demonstration makes an important step towards optomechanical metamaterials.

Chapter 6

Switchable metamaterials

6.1 Introduction

The capability to dynamically tune or reversely switch the properties of metamaterials is of great significance [3,183]. Metamaterials with tunable properties will greatly enhance their functionalities by operating at dynamic situations and broader frequency ranges. An invisibility cloak that can be switched 'on' and 'off' or a metamaterial lens [184,185] that can work at tunable focusing distances or different wavelengths will be very useful indeed. Moreover, metamaterials can significantly enhance the linear and nonlinear properties of natural materials and switchable metamaterials will enable dramatic modulation of electromagnetic signals on a deep subwavlength scale [15, 16]. The ability to tune and switch the electromagnetic properties of materials, especially at subwavelength dimensions, are something very rarely offered by nature. For example, THz technology promises many useful applications [186]. However, one major bottleneck at present for advancing this field is the lack of efficient devices to manipulate the THz electromagnetic waves. At optical frequencies, there are quite a lot of modulators and switches. But switching optical signals on the nanoscale is not a trivial problem: conventional modulators exploiting the Pockels or Kerr effects are based on interference over distances much longer than the wavelength, necessitating devices with dimensions of several centimeters in the propagation direction. Modulating a signal by controlling the absorption coefficient or refractive index of a medium also requires substantial propagation lengths over which amplitude/phase changes accumulate, or interferometric arrangements that are inherently longer than the wavelength. Such difficulties could

be overcome by switchable metamaterials where a relatively small change of electromagnetic properties of either materials consisting of metamaterials or surrounding media could be profoundly amplified by metamaterials resonances [38].

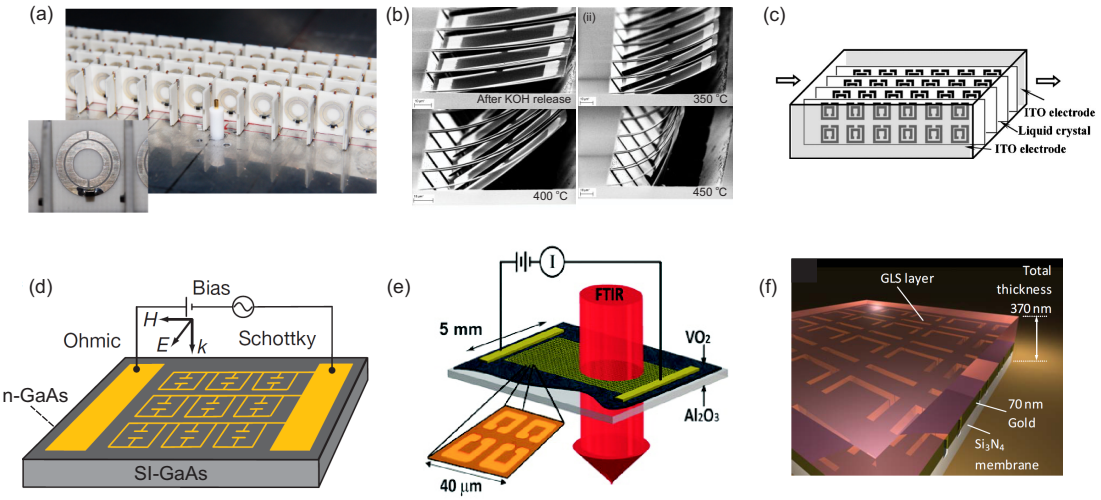

Figure 6.1: Active and switchable metamaterials. (a) A nonlinear tunable microwave metamaterial consisting of metallic split ring resonators loaded with variable capacitors [187]. (b) A mechanically reconfigurable terahertz metamaterial [188]. (c) A electrically tunable negative permeability metamaterial consisting of SRRs and infiltrated LC [189]. (d) An active terahertz metamaterial device consisting of an array of gold resonator elements fabricated on a semiconductor substrate [15]. (e) A THz memory metamaterial functionalized by hybridizing with the phase change material vanadium dioxide [78]. (f) A nanoscale switchable photonic metamaterial using gallium lanthanum sulphide (GLS) chalcogenide glass [16]. Figure reproduced with permission from: (a), ref. [187], ©2008 NPG; (b), ref. [188], ©2009 AIP; (c), ref. [189], ©2007 AIP; (d), ref. [15], ©2006 NPG; (e), ref. [78], ©2009 AAAS; (f), ref. [16], ©2010 AIP.

There have been lots of research efforts towards tunable metamaterials in the past few years (Fig. 6.1). Many early designs of tunable metamaterials focused on changing directly the distributed capacitance or distributed inductance of resonance cells by adding a tunable capacitor or inductance (Fig. 6.1(a)) [187, 190–192]. This method, though effective, is difficult to be implemented in optical metamaterials. Tuning the electromagnetic properties of metamaterial by structural reconfiguration has been demonstrated in microwave [193], THz [188, 194] and optical frequencies (Fig. 6.1(b)) [195]. However, the switch speed of mechanically reconfigurable metamaterials are limited by the mechanical responses, which have reached several MHz [17] but is still far away from GHz or higher frequencies. Alternative methods are tuning the properties of the constitutive materials themselves. The functions of metal are generally robust and difficult to be tuned by external stimulus. Luckily, the electromagnetic func-

tions of metamaterials are also very sensitive to the surrounding environment, which provides another dimension for active metamaterials. Incorporating materials with switchable electrical or optical properties allows control over the resonant response in metamaterials. The hybrid metamaterial approach has been proven to be effective in various tunable metamaterials and a variety of thermally, electrically, optically and magnetically tunable and switchable materials such as liquid crystals (Fig. 6.1(c)), doped semiconductors (Fig. 6.1(d)), phase change materials (Fig. 6.1(e,f)), yttrium iron garnet, as well as carbon nanotube and graphene, have been explored for active metamaterials [15, 42, 189, 196–198].

For practical nanophotonic applications, materials with fast switching speeds, good availability, and robust, reliable and high-performance properties should be utilized. Chalcogenide glasses promise to be an ideal choice as a reliable and robust switch material found at the heart of today's rewritable optical disk technologies and next generation non-volatile electronic memories [199]. Here we demonstrate a phase-change metamaterial employing Germanium Antimony Telluride (GST), a phase change chalcogenide glass most widely used in optical data storage media, such as DVDs and CDs [200]. GST is a semiconducting chalcogenide alloy with a crystallisation temperature of around 160^oC and a melting temperature of around 600^oC. It is ideal as an optical switching medium with a high transmission and reflection contrast between its crystalline and amorphous phases. And it has proven itself to be a robust non-volatile switching medium with the ability to switch back and forth reliably under industrial and commercial usage. However, experimental realization of switchable metamaterials using GST is not trivial. For data memory applications, it is generally desirable to make each memory unit (i.e. single switching area) as small as possible to increase the data density. On the contrary, a large-area (e.g. thousands of square microns for photonic metamaterials), uniform switching of GST by single pulse is required to effectively switch a metamaterial covering enough unit cells and tune its optical properties. In this chapter we show the first demonstration of large-area (more than 2000 μm^2), non-volatile, bi-directional, all-optical switching in plasmonic metamaterials functionalized with GST chalcogenide glass.

6.2 Numerical simulations and designs

Three-dimensional finite element Maxwell solver simulations (in Comsol MultiPhysics, see Appendix A for details of modeling) are employed for switchable metamaterial design. Again, we employ a set of planar structures consisting of asymmetric split rings belonging to a class of metamaterials that support trapped-mode plasmonic excitations [38, 40]. Weak coupling of the excitation mode to free-space radiation modes within these structures creates narrow reflection, transmission, and absorption resonances with asymmetric, Fano type dispersion. Through the combination of a nanoscale layer of phase change material with a planar plasmonic metamaterial one can exploit the fact that the position of sharp resonances in certain metamaterials are strongly dependent on the near-field dielectric environment; thus small changes in the refractive index of a chalcogenide nano-layer in the course of the switching between its amorphous and crystalline states in contact with such a metamaterial produces a massive change in its resonance frequency and as a result the transmission and reflection characteristics of the hybrid device.

We first simulate a hybrid metamaterial showing trapped mode resonances in the mid-infrared range. This is an important spectrum range with lots of research interests for applications in security, astronomy, biology as well as defense. Fig. 6.2(a) shows the schematic and dimensions of the metamaterial. The plasmonic metamaterial consists of asymmetric split rings by milling through a 50 nm thick gold film. The period of unit cell is $P = 750$ nm. We choose calcium fluoride (CaF2) as the substrate as it is transparent for wavelengths from around 150 nm to around 9 μm. 30 nm of ZnS:SiO2 are used as a buffer layer between the plasmonic metamaterial and chalcogenide layer while 100 nm of ZnS:SiO2 are used as a capping layer. Here both layers are for the benefit of heat management to efficiently switch the phase change layer and protection of the whole structure from degradation (melting of gold and oxidation of the chalcogenide layer) during the switching. The thickness of chacogenide layer is 40 nm. For the optical parameters, the refractive index of CaF2 substrate is assumed to be $n_{CaF2} = 1.4$ and the refractive index of ZnS:SiO2 buffer and capping layers is $n_{ZnS:SiO2} = 2.2$. The permittivity of gold in the mid-infrared spectral regime is described by the Drude model with plasma frequency $\omega_{pl} = 2\pi \times 2.175 \times 10^{15} s^{-1}$, and the damping constant

$\omega_\tau = 3 * 2\pi \times 6.5 \times 10^{12} s^{-1}$. Here the damping constant is three times larger than the bulk value considering the surface scattering of the gold film. We assume that grooves of gold metamaterials are filled with ZnS:SiO2, which is verified by our experiment.

Fig. 6.2(b,c,d) shows that resonance position in the optical spectrum redshifts about 400 nm at the range of 4 to 8 μm when the chalcogenide layer switches from amorphous to crytalline. As a result of the spectral shift, high switch contrasts are achieved around the Fano-resonance (Fig. 6.2(e)).

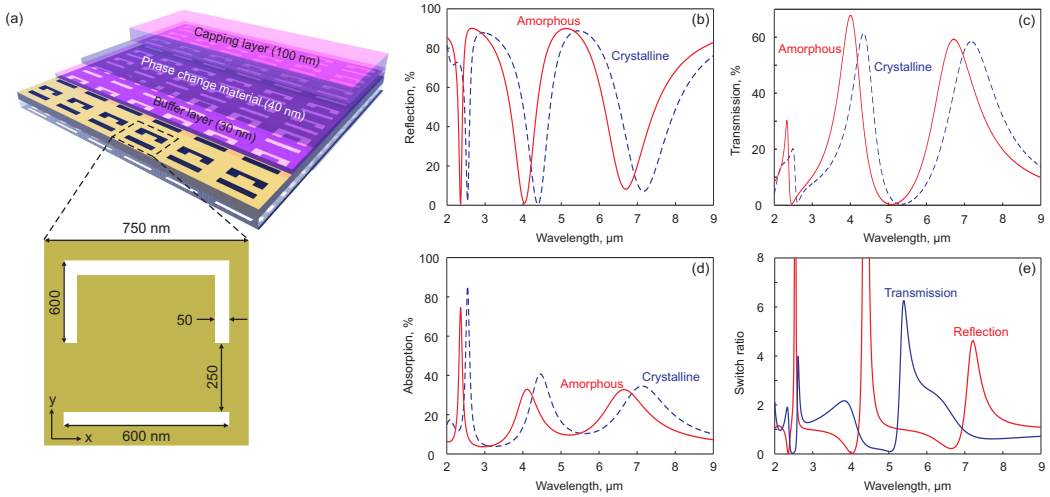

Figure 6.2: Simulated switch of a phase change metamaterial working in the mid-infrared range. (a) Schematic of the hybrid metamaterial design. A 40 nm thick phase change chalcogenide glass (i.e. GST) layer is hybridized with a plasmonic metamaterial for switching functionalities. The phase change layer is sandwiched by a thin buffer layer (30 nm) and a capping layer (100 nm), both of which are for the benefit of efficient switching as well as protection of the structure. The plasmonic metamaterial consists of periodical unit cells of asymmetric split ring design and the period is 750 nm. (b-d) show the shift of reflection, transmission and absorption spectra of the metamaterial as the phase of chalcogenide glass layer changes from one state to another. (e) shows the contrast ratio of transmission and reflection between amorphous and crystalline state. For simplification, we assume the chalcogenide glass layer to be lossless with a refractive index of $n_a = 4$ at amorphous state and $n_c = 6$ at crystalline state, respectively.

A metamaterial for telecom wavelength is also designed by scaling down the metamaterial unit cell size. As shown in Fig. 6.3, the period of unit cell is 400 nm. Instead of using CaF2 substrate, glass substrates are used here with a refractive index of 1.5. Again ZnS:SiO2 is used for buffer and capping layers with thickness of 10 nm and 100 nm, respectively. Here the thickness of buffer layer is thinner than that for mid-infrared design as the electromagnetic field is more localized near the plasmonic metamaterial so the active layer should be put nearer to ensure effective change of the

metamaterial's optical properties by switching. The thickness of the chalcogenide layer is 15 nm.

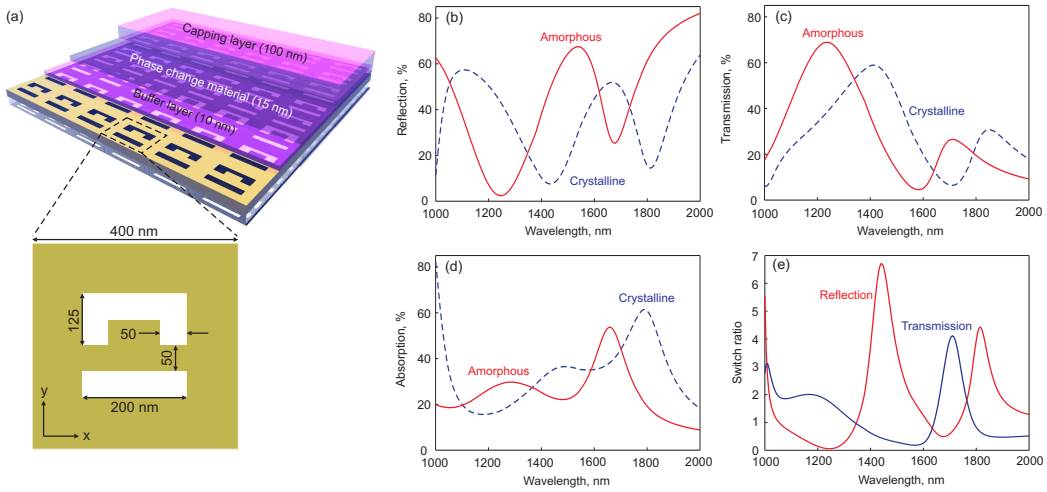

Figure 6.3: Simulated switch of a phase change metamaterial working in the near-infrared range. (a) Schematic of the hybrid metamaterial design. A 15 nm thick phase change chalcogenide glass (i.e. GST) layer is hybridized with a plasmonic metamaterial for switching functionalities. The phase change layer is sandwiched by a thin buffer layer (10 nm) and a capping layer (100 nm). The plasmonic metamaterial consists of periodical unit cells of asymmetric split ring design and the period is 400 nm. (b-d) show the shift of reflection, transmission and absorption spectra of the metamaterial as the phase of chalcogenide glass layer changes from one state to another. (e) shows the contrast ratio of transmission and reflection between amorphous and crystalline state. For simplification, we assume the chalcogenide glass layer to be lossless with a refractive index of $n_a = 4$ at amorphous state and $n_c = 6$ at crystalline state, respectively.

Similar to the mid-IR metamaterials, optical switching with high contrast ratio can also be achieved at telecom wavelength in the near-IR metamaterial. Fig. 6.3(b,c,d) shows that optical spectra redshift about 200 nm at the range of 1 to 2 μm when the chalcogenide layer switch from amorphous to crytalline, leading to a maximum switch contrast ratio of about 7 for reflection and about 4 for transmission.

6.3 Experimental demonstrations of bi-directional, all-optical switching in a phase-change metamaterial

Through collaboration with the Novel Glass Group of Optoelectronics Research Centre at the University of Southampton, bi-directional, all-optical switching in a phase-change metamaterial has been demonstrated for the first time. The metamaterial array structure was fabricated by milling through a 50 nm thick gold film evaporated either on a

1mm thick calcium fluoride (for mid infrared switches) or 150 μm thick fused quartz (for near infrared switches) substrates. A gold film with surface roughness of 2-3 nm was obtained using low pressure 2×10^{-6} mbar thermal evaporation. 50×50 μm^2 metamaterial arrays with a square unit cell size of either 400 nm (near infrared switches) or 750 nm (mid-infrared switches) were manufactured using focused ion beam milling. A functional 15 - 40 nm film of chalcogenide glass (GST sputtered under argon) is then deposited on the patterned gold film; this comprises also of an inert sputtered ZnS/SiO2 or SiO2 buffer and capping layers either side of the chalcogenide nanolayer to prevent metal diffusion into the glass and degradation in air at elevated phase transition temperatures, respectively. (In this collaboration project, designing, numerical modeling and optimization of phase change metamaterials, most of the fabrication of near-IR samples and characterization of optical spectra, were conducted by Jianfa Zhang. Most of the fabrication of mid-IR plasmonic metamaterials, deposition of phase change glasses and optical switching experiment, were done by Behrad Gholipour.)

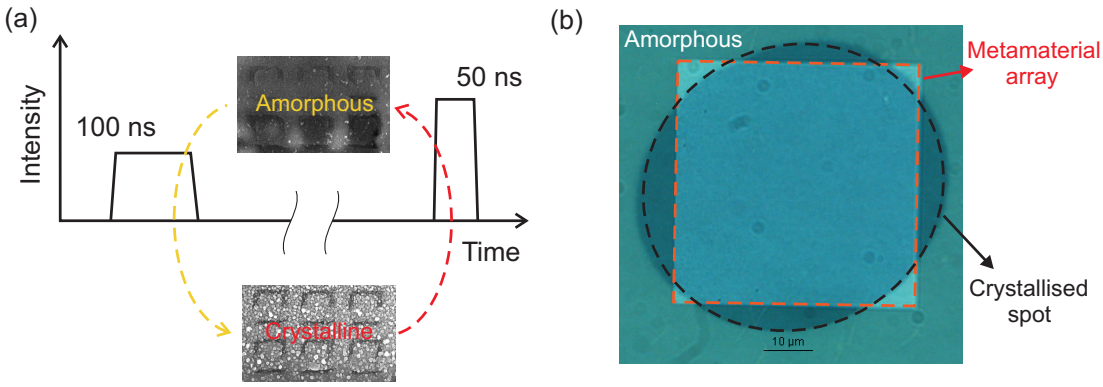

Figure 6.4: Switching chalcogenide phase change metamaterials. (a) Schematic of bi-directional optical switching of phase change metamaterials using laser pulses. Switching from amorphous to crystalline can be realized by 'long' (100 ns) pulse with 'low' (0.1 $mW/\mu m^2$) peak power intensity while reversed switching can be obtained by a 'short' (50 ns) pulse with 'high' (0.25 $mW/\mu m^2$) peak power intensity. (b) Optical microscope image of a phase change metamaterial switched by a single pulse. The metamaterial array (about 50×50 μm) was originally covered by an amorphous layer of GST. Phase transition was initiated uniformly across a large area ((about 2000 μm^2) of the GST film by single-pulse laser excitation, as shown by the clear change of colour under optical microscope.

GST can be switched between amorphous and crystalline states with different pulses. By heating amorphous GST to a temperature above its crystallization point (about 160^oC), but below the melting point (about 600^oC), and holding it for some time, it will transform into a crystalline state. When GST is heated to a high tempera-

ture above its melting point, and cooled quickly, it is frozen into an amorphous glass-like state. Phase transitions were initiated uniformly across large (about 2000 μm^2) areas of the GST film by single-pulse laser excitation, using a laser pulse of 660 nm wavelength with pulse energy and duration optimized separately for the forward (amorphous-crystalline) (down to 100 ns) and reverse (crystalline-amorphous) (down to 50 ns) transition directions. The pulses were shaped using an Agilent 8110A pulse generator. The optical change in the GST layer was monitored in real time allowing the identification and optimization of the amorphous to crystalline transition point.

As shown in Fig. 6.4, this reversible transition mechanism which occurs as a result of localised heating from the laser pulse, was used to switch the entire region on top of the nanostructured metamaterial array achieving a uniform switched area. As set out, to switch back the device, shorter higher powered pulses are used to switch the now crystalline GST layer cladding the metamaterial array back to an amorphous state. This brings about the melting and rapid quenching of the nanoscale chalcogenide layer allowing its transition back to a glassy state.

The transmission, reflection and absorption characteristics of the optical switch were quantified using a FTIR based microspectrophotometer. This reversible large area optical transition brings about a dramatic change in the spectral position of the trapped mode resonance, bringing a red shift of 500 nm in the spectral range 4 to 8 μm for the mid-IR metamaterial sample (see Fig. 6.5(b-d)). The transmission and reflection modulation contrast associated with the reversible chalcogenide phase switching can be seen in Fig. 6.5(e). It can be observed that the transmission changes by as much as a factor of four from approximately 25 percent to 7 percent at around 6.5 μm. The reflectivity changes resulting from phase switching are also substantial, reaching almost 3.3:1 at around 5 μm in the near-IR switches.

For near-infrared metamaterial sample, similar results are obtained as shown in Fig. 6.6. The transmission, reflection and absorption characteristics of the optical switch were quantified using a microspectrophotometer by CRAIC technology. In the spectral range 1 to 2 μm, measured optical transmission, reflection and absorption show clear resonances. Phase transition of GST layer from amorphous to crystalline state leads to a red shift of 200 nm in the spectrum. High modulation contrasts are realized for both reflection (up to a factor of 4.3 at around 1.5 μm) and transmission (about 2.5

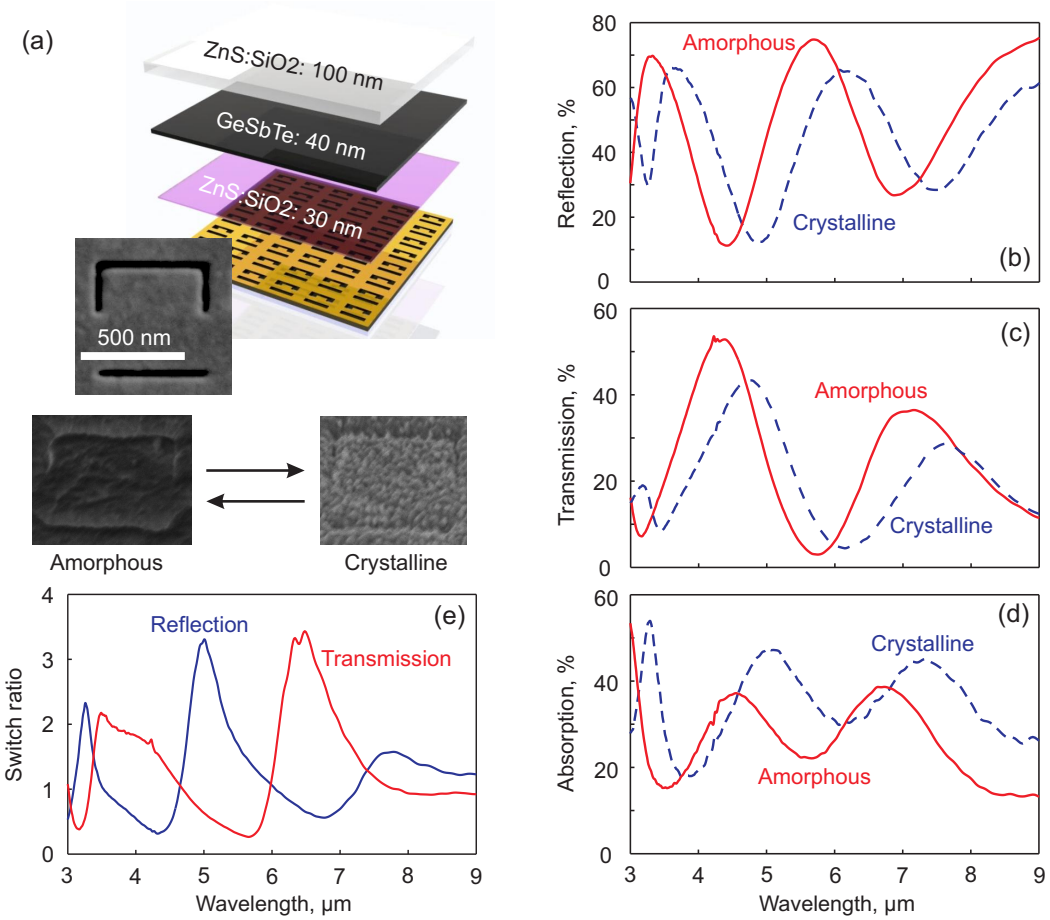

Figure 6.5: Experimental demonstration of optical switch of a phase change metamaterial working in the mid-infrared range. (a) Schematic of the fabricated hybrid metamaterial for mid-infrared. A buffer layer (30 nm), GST layer (40 nm) and a capping layer (100 nm) is deposited on top of a plasmonic metamatateriral by sputtering. An electron microscope image with a scale bar is shown for a unit cell of the bare plasmonic metamaterial before function layer deposition. At the bottom are two electron microscope images for the phase change metamaterial as it switches from amorphous state to crystalline state, which confirms the physical change of the active layer during swithing. (b-d) show the measured reflection, transmission and absorption spectra of the metamaterial as the GST switches between amorphous and crystalline. (e) shows the contrast ratio of transmission and reflection between amorphous and crystalline state.

at around 1.2 μm). Experimental results for both mid- and near- infrared metamaterials agree very well with simulations though the resonances in measured spectra of near-infrared samples are relatively less sharper compared to simulation results. This may be attributed to the increased difficulty of fabricating the near-infrared sample for its small pattern sizes (i.e. the geometry and size of fabricated sample are not exactly the same as simulated), the loss of gold film in the near infrared due to boundary effects and surface roughness that might not be correctly considered in simulations, as well as

the higher losses of GST at shorter wavelength which is not considered in simulations.

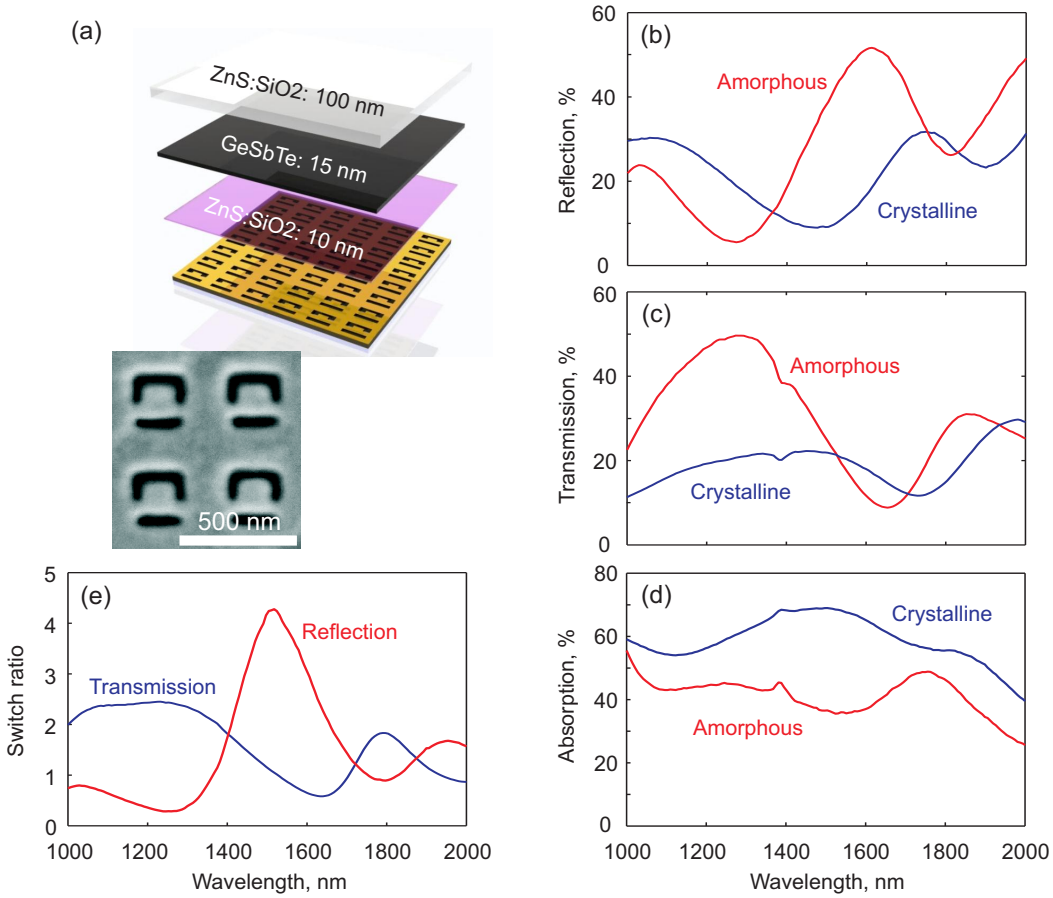

Figure 6.6: Experimental demonstration of optical switch of a phase change metamaterial working in the near-infrared range. (a) Schematic of the fabricated hybrid metamaterial for near-infrared. A buffer layer (10 nm), GST layer (15 nm) and a capping layer (100 nm) is deposited on top of a plasmonic metamatatarial by sputtering. An electron microscope image with a scale bar is shown for a unit cell of the bare plasmonic metamaterial before function layer deposition. (b-d) show the measured reflection, transmission and absorption spectra of the metamaterial as the GST switches between amorphous and crystalline. (e) shows the contrast ratio of transmission and reflection between amorphous and crystalline state.

The reversibility of the optical switching was further reaffirmed by repeated switching of the device between the two states in the order of 50 times and consequent scanning electron microscopy images of the surface of the devices (see Fig. 6.5(a)) confirmed our understanding that reversible phase transitions in the dielectric medium from crystalline to amorphous and vice versa were responsible for the switching capability of the device.

6.4 Summary

In the past few years, hybridization of photonic metamaterials with active media has been proved to be a very effective route for realizing tunable/switchable metamaterials. However, non-volatile switchable metamaterials based on materials with fast switching speeds, good availability, robust, reliable and high-performance properties have yet to be demonstrated for practical nanophotonic applications. Here the phase change medium widely used for optical data storage and next generation electronic memories has been utilized as the non-volatile optically switchable medium in combination with planar photonic metamaterials to achieve an ultra-fast, high contrast all optical reversible metamaterial switch.

Firstly, full wave three-dimension finite element electromagnetic simulations have been used to model the performance and optimize the design of switchable metamaterials. Planar plasmonic metamaterials showing sharp Fano resonances have been employed. Two groups of switchable metamaterials have been designed with one working in the mid-infrared wavelength range and the other at the telecom wavelength range. By covering the plasmonic metamaterials with tens of nm thick phase change chalcogenide glass as well as buffer layers and capping layers, simulations show that the optical spectra for both the mid-infrared and near infrared metamaterials can be shifted by hundreds of nm as the chalcogneide glass switches from amorphous state to crystalline state and vice versa. This leads to a dramatic switch contrast ratio for both reflection and transmission signals that ranges from several to more than 10.

In collaboration with the Novel Glass Group of the Optoelectronics Research Centre at the University of Southampton, large area bi-directional all-optical switching in plasmonic metamaterials functionalized with phase-change chalcogenide glass has been experimentally demonstrated for the first time. Phase transitions were initiated uniformly across large (about 2000 μm^2) areas of the GST film by single-pulse laser excitation. For the mid-IR metamaterial, measured optical spectra show very good resonances from 4 to 8 μm and redshift about 500 nm as the GST layer transits from amorphous phase to crystalline phase due to the higher refractive index of the later. As such, modulation contrast of transmission (T_a/T_c) reaches about 4 at 6.5 μm and modulation contrast of reflection (R_a/R_c) gets its maximum of 3.3 around 5 μm. Ex-

perimental results agree very well with simulations. For the near-IR metamaterial, measured spectra show resonances from 1 to 2 μm and also redshift about 200 nm along with the phase transition of the GST layer from amorphous to crystalline. Even though resonances in measured spectra are not as sharp as those in simulations due to increased fabrication difficulty for the smaller pattern size of metamaterial as well as higher losses of GST layer at shorter wavelength, high-contrast modulations of transmission and reflectivity (up to a factor of 4.3 at around 1.5 μm) are realized in the infrared range. Repeated switching of up to 50 times was demonstrated before the sample broke down due to diffusion of gold. And the switching is achieved at optical excitation levels below 0.25 $mW/\mu m^2$ in device structures only $\frac{1}{30}$ (mid-IR) to $\frac{1}{8}$ (near-IR) of a wavelength thick.

Chalcogenide phase-change metamaterials can be switched electronically and thermally as well as optically to produce high-contrast intensity and phase modulation, and may be engineered through metamaterial design to function at any visible to mid-infrared wavelength within the chalcogenide's transparency range. As such these hybrid materials offer a platform for the development of an entire new generation of nanophotonic switches, memory and spatial light modulation devices.

Chapter 7

Conclusions and outlook

Photonics technology is widely regarded as a key enabling technology for the 21st century and the ability to control light is in the key of photonics. Photonic metamaterials exhibit unprecedented capabilities of controlling light and provide tremendous opportunities for studying exciting physics as well as developing novel optical devices. This thesis has been dedicated to several efforts towards controlling light with photonic metamaterials for desired functionalities during my PhD study.

7.1 Intaglio and bas-relief metamaterials

Chapter 3 introduces a new class of continuously metallic metamaterials formed of a indented or raised subwavelength pattern in an optically thick plasmonic metal film are introduced and coined as 'intaglio' and 'bas-relief' metamaterials. Intaglio/bas-relief photonic metamaterials offer a robust and flexible paradigm for engineering the spectral response of metals in the visible and near-infrared domains without changing their chemical or electrical properties.

Trapping of electromagnetic energy and strong enhancement of electromagnetic field are realized in intaglio/bas-relief metamaterials via excitation of localized plasmonic resonances, which can be explored for enhancing linear and nonlinear optical effects. The resonance intensities are stronger than those in conventional metamaterials/metasurfaces or metallic nanoparticles as the transmission channel is blocked in intaglio/bas-relief metamaterials. And the capability of modification of reflection intensity as well as phase of optical incidence radiation provides intaglio/bas-relief meta-

materials functionalities ranging from perfect absorbers to optical magnetic mirrors. Moreover, the dependence of optical responses on polarization, the resonance frequencies as well as the absorption/reflection intensities of intaglio/bas-relief metamaterials are widely tunable by structural design such as depth/width of grooves, geometry of pattern and refractive index of covering media. This wide tunability provides opportunities for applications such as controlling the colour of metals, as demonstrated experimentally in this thesis. As an extension of intaglio/bas-relief photonic metamaterials, the concept of dielectric loaded metamaterials is introduced and demonstrated. Dielectric loaded metamaterials give a complementary way of modifying the optical responses of continually metallic surfaces in the visible and near-infrared domains and may provide additional abilities for controlling the optical responses optically or thermally by employing active dielectric media such as doped semiconductors.

In contrast to conventional (discrete meta-molecule) metamaterial forms demonstrated for absorption control in infrared sensing/imaging applications [68,69]; to metallic films structured via micro-sphere lithography for broadband omnidirectional near-infrared absorption [71]; and to surfaces laser-roughened to suppress reflection below a monotonically tunable cut-off wavelength [201], continuously metallic intaglio and bas-relief designs offer a highly controllable mechanism for engineering and manipulating diffraction-free, angle-invariant absorption resonances. Potential applications of intaglio/bas-relief photonic metamaterials range from aesthetic (e.g. jewelry) to optical sensing and security (e.g. in banknote/document anti-forgery features that must be difficult to imitate without substantial up-front investment in design and fabrication technology). New applications and technology advancements are emerging. For example, it has been recently demonstrated that structured gold surfaces similar to intaglio metamaterials could act as broadband perfect absorbers in the visible range, which is called 'black gold' [202]. Another interesting topic is incorporating intaglio/bas-relief metamaterials with active media such as quantum dots to engineer their emission properties.

For wide-spread applications, low cost fabrication technology for large area intaglio/bas-relief metamaterials is critical. Even though the proof-of-principle demonstrations reported in this thesis rely on focused ion beam milling and electron beam lithography, intaglio/bas-relief photonic metamaterials may ultimately be implemented using sim-

ple, low-cost scalable fabrication techniques such as nano-imprint or template stripping techniques, even on non-planar surfaces.

7.2 Controlling light-with-light without nonlinearity

In Chapter 4, it is demonstrated for the first time that a plasmonic metamaterial - a single layer of nanostructured metal much thinner than the wavelength of light - can be used to modulate light with light without nonlinerity. Regimes of near-total absorbtion and near-total suppression of plasmonic losses have been experimentally observed. The phenomenon relies on the coherent interaction of light beams on the metamaterial and provides functionality that can be implemented freely across a broad visible to infrared range by varying the structural design. The modulation could be achieved at arbitrarily low optical power intensity and the modulation frequency bandwidth can reach several THz.

Controlling light with light using metamaterials opens a new door for manipulating electromagnetic fields via conherent interactions in the nanoscale. Besides applications in coherent detectors or sensors, potential applications in optical data communication and processing such as 'coherence filtering' and 'pulse restoration' have been particularly proposed and discussed. Future work in this topic includes using optical pulses instead of continuous beams for manipulating light with light in a metamaterial and integrating our experiment in a fibre system, which could be a significant step towards signal processing applications. Similar concepts can also be extended to plasmonic and semiconductor waveguides for on-chip signal processing, or to mid-IR and other spectrum range where a metamaterial film could be integrated with thin absorbing layer (e.g. semiconductors) for detectors or other applications.

Particularly, metamaterial coherent perfect absorption could be regarded as the time-reversed process of lasing spaser [41] and it find applications in subwavelength imaging [203]. It may also be interesting to think about the quantum applications of coherent metamaterial absorber e.g. generation of entangled photon pairs with planar plasmonic metamaterials.

7.3 Optomechanical forces in metamaterials

Chapter 5 introduces the concept of 'optical gecko toe' and the concept of 'optomechanical metamateials', showing the great potentials of utilizing photonic metamaterials as an unique platform for manipulating and harnessing optical forces on the nanoscale. In the past few decades, optical forces have been exploited for applications such as optical tweezers, laser cooling as well as optical binding. Recently, with the development of micro- and nano- photonics, optical forces have been increasingly studied and explored in nanophotonic systems,leading to the emerging research fields such as cavity optomechanics and actuation of nanophotonic devices by optical forces. Now, the unprecedented capabilities of controlling electromagnetic fields using metamaterials provide new opportunities for merging nanophotonics and nanomechanics via optical forces.

Firstly, trapping of electromagnetic energy and enhancement of electromagnetic fields by planar plasmonic metamaterials has been explored for realizing giant optical near field forces, leading to the concept of 'optical gecko toe'. Numerical simulations show that in addition to the conventional, well-understood force of radiation pressure a much stronger light-driven near-field force may be generated between an illuminated planar plasmonic metamaterial and a dielectric or metallic surface. This newly identified near-field force has a resonant nature linked to the excitation of the metamaterial's plasmonic mode and acts to close the gap between the metamaterial film and the surface. As such, optical gecko toe provides an optically controllable mechanism for generating adhesion forces between a metamaterial film and a surface. Similar optical forces may also be generated between a metamaterial film and micro- or nano- particles.

There are also both in plane and out of plane resonant optical forces within planar dielectric metamaterials as well as planar plasmonic metamaterials. The proposed dielectric metamaterials consist of closely spaced, dissimilar dielectric nano-bars and show sharp optical magnetic resonances akin to the well-known 'trapped mode' resonances of metallic asymmetric split ring. Dielectric metamaterials don't suffer from inherent Joule losses of metals and thus can achieve sharp resonances with quality factor not available in plasmonic structures. Furthermore, the less confined electromagnetic fields near resonant elements of dielectric metamaterials provide advantages

for harnessing the resonant optical forces (i.e. strong near field optical forces may be generated between dielectric elements separated by hundreds of nanometers), which leads to the idea of nonlinear optomechanical metamaterials. Optical bistability and high contrast asymmetric transmission at telecom wavelength have been numerically demonstrated in optomechanical metamaterials at optical intensity levels of only a few hundred $\mu W/\mu m^2$ through interactions of optical and mechanical responses while many other nonlinear and self-adptive behaviors may also be realized.

As a first step for demonstrating optomechanical metamaterials, dielectric metamaterials on both solid silica substrate and thin silicon nitride membrane have been fabricated and sharp magnetic resonances in dielectric metamaterials have been experimentally demonstrated. Following the theoretical and numerical studies, experiments on modulating light with light in metamaterials using optomechanical forces are being conducted. Though in the infancy, research of optomechanical forces in metamaterials are very promising with applications in optical manipulations, active optomechanical devices as well as quantum mechanics. More theoretical investigations as well as experimental progresses are expected to be seen in this emerging research field in the next few years.

7.4 Switchable metamaterials

Chapter 6 shows the first demonstration of non-volatile, bi-directional, all-optical switching in a phase-change metamaterial. This work was done in collaboration with the Novel Glass Group of Optoelectronics Research Centre at the University of Southampton. High-contrast transmission and reflection modulation at visible and infrared wavelengths has been obtained in device structures only less than 1/8 of a wavelength thick. Nanoscale all-optical modulation was realized based on the fact that the resonant optical properties of a plasmonic metamaterial strongly dependent on the near-field dielectric environment. Using Germanium Antimony Telluride (GST), a phase change chalcogenide glass most widely used in optical data storage media, is a significant achievement in this study as it represents an important step towards practical applications of switchable metamaterial devices.

Here phase transitions were initiated uniformly across large (2000 μm^2) areas of

the GST film by single-pulse laser excitation, which is an important advantage and achievement. However, switching of a small area (less than 1 μm^2, limited by diffraction limitation of focusing) is also possible, enabling all-optical switching from large area to single unit cell. This may be used for various applications such as spatial phase modulators and spatial optical filters.

In the 'proof of principle' demonstration, repeated switching of up to 50 times were demonstrated before the sample broke down due to diffusion of gold. For practical applications, the life time of switching needs to be improved. This can be achieved by further optimizing the structure, e.g. increasing the thickness of buffer layer, and optimizing the switching conditions, i.e., the width and intensity of switching laser pulses. In the mid-IR or far-IR, metals with high melting temperatures, such as titanium, tungsten and molybdenum, may be used as alternative of gold. These metals may not be suitable for plasmonic and metamaterial applications in the near infrared or visible due to their high losses, but they can be used as building blocks for metamaterials to achieve reasonably good resonances in mid- and far- infrared frequency ranges. Replacing gold with titanium, tungsten or molybdenum for phase change metamaterials in the infrared will not only improve their high temperature properties and switching life but also reduce the fabrication cost.

Finally, it should be noted that chalcogenide glass are a type of amazingly flexible materials. Besides their wide applications in rewriteable DVDs, GST and other phase change materials have also been proposed to achieve many other functionalities such as reconfigurable logic devices, and even cognitive devices [204]. Incorporating phase-change chalcogenide glass with metamaterials will bring together the extroordinary properties of both and may provide opportunities for developing a group of novel optical devices for reconfigurable logic applications and biology-inspired/neuromorphic applications.

In summary, new phenomena and novel physics are still emerging in the field of photonic metamaterials while there are increasing interests in developing functional metamaterials or metadevices [19] using their unprecedent capabilities of controlling light. Actually, this PhD project has generated three patents of applications besides the interesting concepts and properties that have been demonstrated (see Appendix D.2). Along with the parallel advances in the capabilities and availability of micro- and

nano-fabrication technologies, photonic metamaterials are expected to play a significant role for developing enabling and disruptive photonics technologies in the near future, leading to ground breaking solutions for telecom, energy and light generation, imaging, lithography, data storage, sensing, and security applications.

Appendix A

Comsol simulations

Full wave three dimension numerical simulations are conducted in this thesis to study the electromagnetic properties of photonic metamaterials. These simulations are performed using the commercial software COMSOL Multiphysics 3.5a. COMSOL Multiphysics is a finite element analysis, solver and simulation software package for various physics and engineering applications, especially coupled phenomena, or multiphysics. It offers an extensive interface to MATLAB and its toolboxes for a large variety of programming, preprocessing and postprocessing possibilities [205]. For electromagnetic simulations, its RF Module is employed. Here a brief introduction to modelling photonic metamaterials in COMSOL is given.

The first step to model a metamaterial in COMSOL is defining the structure. Metamaterials studied in this thesis are generally comprised of a planar array of periodical unit cells, so only a unit cell with periodical boundary conditions in the plane needs to be modelled. Fig. A.1 shows the geometry of a unit cell in COMSOL for a plasmonic metamaterial design, whose optical spectra has been show in Fig. 2.5. This geometry consists of a 50 'nm' thick structured thin film surrounded by 2 adjacent rectangular blocks on each side, each 300×300 'nm' in cross-section.

The next step is to define the domain material properties (permittivity and permeability) and boundary conditions. In most cases studied in this thesis, established experimental values of the complex dielectric parameters for metals from Ref. [60] are employed. Here periodical boundary conditions are applied for both x- and y- boundaries (for 'type of periodicity', 'continuity' is chose for radiation at normal incidence

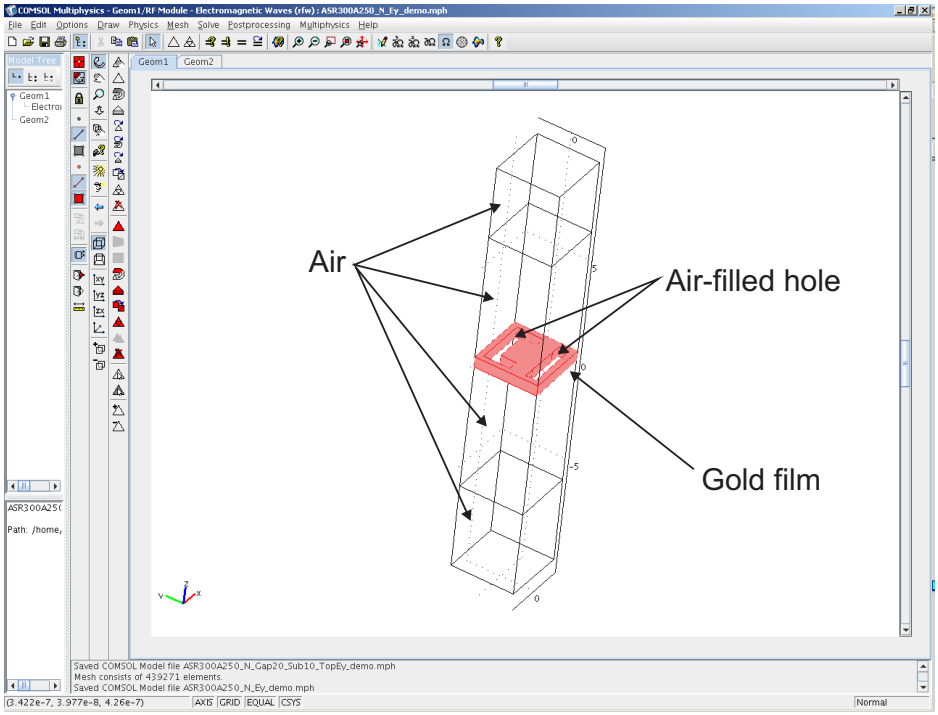

Figure A.1: Geometry of a metamaterial unit cell in COMSOL.

while 'Floquet periodicity' should be used if oblique incidence is to be studied). At z-direction, scattering boundary conditions are employed. Internal boundary conditions are 'continuity' as default. An incident plane wave can be apply by defining an incident field at the scattering boundary. In most situations, the scattering boundary condition is good enough to minimize the scattering at the boundary. However, an PML layer could be added at the top and bottom boundaries in z-direction to further reduce the scattering if necessary.

For mesh parameters, maximum element size in each domain should be one tenth of wavelength or smaller (this means mesh in domains with high refractive index should be finer than in the air) for linear-Vector element. For metallic areas, a maximum mesh element size of 20 nm is generally used and areas with fine features should also be meshed with small element size accordingly. To get reliable simulations results, the element size of mesh may be limited by the capability of simulation platforms (COMSOL simulations in this thesis are performed with a 16 processor, 64 bit, 128 GB linux workstation) but it should be as small as possible until stable results are reached (e.g. reflection and transmission change less than 1% when number of mesh elements increases by a factor of two). For periodical boundary conditions, it must ensure that

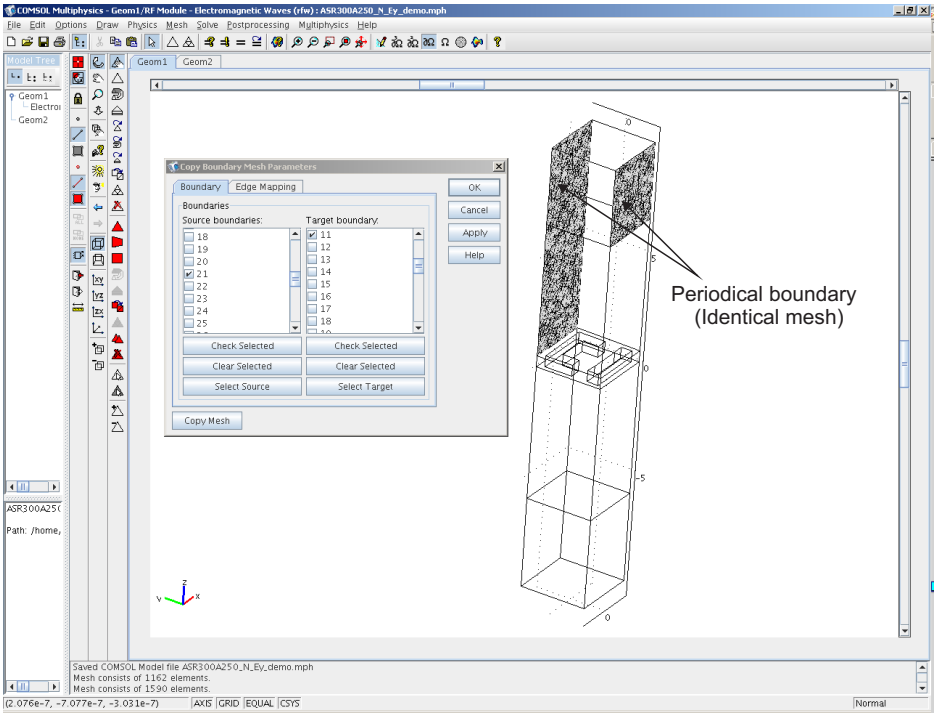

Figure A.2: Identical mesh for periodical boundaries.

mesh nodes on each pair of periodical boundaries are identical, which can be done by meshing one boundary first and then copying the mesh to the other (see Fig. A.2).

Once the simulation wavelength/frequency is set, all the materials properties in domains and boundary conditions are defined, and mesh have completed, one only needs to set suitable solver parameters and starts running the simulation. When the modelling completes, field distributions can be obtained directly by postprocessing while transmission, reflection and absorption data can be calculated via data of power flow at proper boundaries (see Fig. 2.5).

Appendix B

Optical constants of metals used in the thesis

Experimental values of the complex dielectric parameters for gold frequently used in the thesis for simulations. Below are the permittivities from 200 nm to 2000 nm ($\varepsilon_{gold} = \varepsilon' + i\varepsilon''$) [60]:

Wavelength (m)	ε'	ε''	Wavelength (m)	ε'	ε''
2E-7	0.56129	3.46641	5.6E-7	-7.91723	1.80405
2.1E-7	0.26782	3.81035	5.7E-7	-8.32053	1.67592
2.2E-7	0.09536	4.05361	5.8E-7	-8.50874	1.53976
2.3E-7	-0.07655	4.30804	5.9E-7	-8.69694	1.4036
2.4E-7	-0.27517	4.60406	6E-7	-8.88621	1.32818
2.5E-7	-0.54887	4.93642	6.1E-7	-9.07554	1.25579
2.6E-7	-0.7932	5.33626	6.2E-7	-9.26486	1.1834
2.7E-7	-0.7623	5.84351	6.3E-7	-9.45795	1.14123
2.8E-7	-0.694	6.28656	6.4E-7	-9.65104	1.09906
2.9E-7	-0.56337	6.66539	6.5E-7	-9.84413	1.0569
3E-7	-0.44421	6.90885	6.6E-7	-10.81341	1.08039
3.1E-7	-0.32216	7.01256	6.7E-7	-12.05991	1.12733
3.2E-7	-0.22988	6.96853	6.8E-7	-13.3064	1.17427
3.3E-7	-0.21114	6.78311	6.9E-7	-14.53727	1.22178
3.4E-7	-0.26762	6.62314	7E-7	-15.64312	1.2738
3.5E-7	-0.35154	6.48867	7.1E-7	-16.74896	1.32582
3.6E-7	-0.46147	6.40874	7.2E-7	-17.85481	1.37784
3.7E-7	-0.6345	6.4262	7.3E-7	-18.95617	1.43021
3.8E-7	-0.82485	6.47114	7.4E-7	-19.98576	1.48823
3.9E-7	-0.97205	6.4826	7.5E-7	-21.01535	1.54624
4E-7	-1.07697	6.4861	7.6E-7	-22.04494	1.60426
4.1E-7	-1.13719	6.42646	7.7E-7	-23.07453	1.66227
4.2E-7	-1.16361	6.30305	7.8E-7	-24.11456	1.72373
4.3E-7	-1.17313	6.14776	7.9E-7	-25.16503	1.78864
4.4E-7	-1.18265	5.99247	8E-7	-26.2155	1.85355
4.5E-7	-1.26762	5.65053	8.1E-7	-27.26597	1.91846
4.6E-7	-1.38719	5.2311	8.2E-7	-28.31644	1.98337
4.7E-7	-1.56202	4.7762	8.3E-7	-29.328	2.05165
4.8E-7	-1.82232	4.2854	8.4E-7	-30.26175	2.12666
4.9E-7	-2.27496	3.71382	8.5E-7	-31.1955	2.20168
5E-7	-2.852	3.2174	8.6E-7	-32.12924	2.2767
5.1E-7	-3.61564	2.83371	8.7E-7	-33.06299	2.35172
5.2E-7	-4.44603	2.49842	8.8E-7	-33.99673	2.42673
5.3E-7	-5.40992	2.25992	8.9E-7	-34.98791	2.50635
5.4E-7	-6.3578	2.03224	9E-7	-36.05568	2.5921
5.5E-7	-7.13751	1.91814			

Wavelength (m)	ε'	ε"	Wavelength (m)	ε'	ε"
9.1E-7	-37.12345	2.67785	1.46E-6	-112.25725	10.69216
9.2E-7	-38.19122	2.7636	1.47E-6	-114.44506	10.9097
9.3E-7	-39.25899	2.84936	1.48E-6	-116.63286	11.12724
9.4E-7	-40.32676	2.93511	1.49E-6	-118.82067	11.34477
9.5E-7	-41.39452	3.02086	1.5E-6	-121.00847	11.56231
9.6E-7	-42.43274	3.11517	1.51E-6	-123.19628	11.77985
9.7E-7	-43.45249	3.21484	1.521E-6	-125.60287	12.01914
9.8E-7	-44.47224	3.31451	1.53E-6	-127.57189	12.21492
9.9E-7	-45.492	3.41418	1.54E-6	-129.75969	12.43246
1E-6	-46.51175	3.51385	1.55E-6	-131.9475	12.65
1.01E-6	-47.5315	3.61352	1.56E-6	-133.48007	12.92462
1.02E-6	-48.55125	3.71319	1.57E-6	-135.01264	13.19923
1.03E-6	-49.571	3.81286	1.58E-6	-136.5452	13.47385
1.04E-6	-50.82474	3.9243	1.59E-6	-138.07777	13.74847
1.05E-6	-52.19548	4.04164	1.6E-6	-139.61034	14.02308
1.06E-6	-53.56622	4.15897	1.61E-6	-141.14291	14.2977
1.07E-6	-54.93696	4.27631	1.62E-6	-142.67547	14.57232
1.08E-6	-56.3077	4.39364	1.63E-6	-144.20804	14.84693
1.09E-6	-57.67844	4.51098	1.64E-6	-145.74061	15.12155
1.1E-6	-59.04918	4.62831	1.65E-6	-147.27318	15.39617
1.11E-6	-60.41992	4.74565	1.66E-6	-148.80574	15.67078
1.12E-6	-61.79065	4.86299	1.67E-6	-150.33831	15.9454
1.13E-6	-63.12595	4.98646	1.68E-6	-151.87088	16.22002
1.14E-6	-64.36673	5.12632	1.69E-6	-153.40345	16.49463
1.15E-6	-65.60751	5.26617	1.7E-6	-154.93601	16.76925
1.16E-6	-66.84829	5.40603	1.71E-6	-156.46858	17.04387
1.17E-6	-68.08907	5.54589	1.72E-6	-158.00115	17.31849
1.18E-6	-69.32984	5.68574	1.73E-6	-159.53372	17.5931
1.19E-6	-70.57062	5.8256	1.74E-6	-161.06628	17.86772
1.2E-6	-71.8114	5.96546	1.75E-6	-162.59885	18.14234
1.21E-6	-73.05218	6.10531	1.76E-6	-164.13142	18.41695
1.22E-6	-74.29296	6.24517	1.77E-6	-165.66399	18.69157
1.23E-6	-75.53374	6.38502	1.78E-6	-167.65896	19.04273
1.24E-6	-76.77452	6.52488	1.79E-6	-169.731	19.40666
1.25E-6	-78.04425	6.69752	1.8E-6	-171.80304	19.77058
1.26E-6	-79.31399	6.87017	1.81E-6	-173.87508	20.1345
1.27E-6	-80.58372	7.04281	1.82E-6	-175.94712	20.49843
1.28E-6	-81.85345	7.21545	1.83E-6	-178.01916	20.86235
1.29E-6	-83.12319	7.3881	1.84E-6	-180.09119	21.22627
1.3E-6	-84.39292	7.56074	1.85E-6	-182.16323	21.5902
1.31E-6	-85.66266	7.73338	1.86E-6	-184.23527	21.95412
1.32E-6	-86.93239	7.90603	1.87E-6	-186.30731	22.31804
1.33E-6	-88.20213	8.07867	1.88E-6	-188.37935	22.68197
1.34E-6	-89.47186	8.25131	1.89E-6	-190.45139	23.04589
1.35E-6	-90.7416	8.42396	1.9E-6	-192.52343	23.40981
1.36E-6	-92.01133	8.5966	1.91E-6	-194.59547	23.77374
1.37E-6	-93.28106	8.76924	1.92E-6	-196.66751	24.13766
1.38E-6	-94.75481	8.95186	1.93E-6	-198.73955	24.50158
1.39E-6	-96.94262	9.1694	1.94E-6	-200.81159	24.86551
1.4E-6	-99.13042	9.38694	1.95E-6	-202.88363	25.22943
1.41E-6	-101.31823	9.60447	1.96E-6	-204.95567	25.59335
1.42E-6	-103.50603	9.82201	1.97E-6	-207.02771	25.95728
1.43E-6	-105.69384	10.03955	1.98E-6	-209.09975	26.3212
1.44E-6	-107.88164	10.25709	1.99E-6	-211.17179	26.68512
1.45E-6	-110.06945	10.47462	2E-6	-213.24383	27.04905

Experimental values of the complex dielectric parameters for aluminum ($n_{aluminum} = n' + ik$) [60]:

Wavelength (m)	n'	k	Wavelength (m)	n'	k
2.917E-07	0.261	3.51	6.526E-07	1.63	7.49
3E-07	0.276	3.61	6.702E-07	1.78	7.66
3.1E-07	0.294	3.74	6.888E-07	1.94	7.83
3.179E-07	0.31	3.84	7.085E-07	2.13	8
3.263E-07	0.326	3.95	7.293E-07	2.34	8.15
3.351E-07	0.344	4.06	7.514E-07	2.57	8.25
3.444E-07	0.364	4.17	7.749E-07	2.87	8.23
3.5E-07	0.375	4.24	7.999E-07	3.04	8.08
3.542E-07	0.385	4.3	8.266E-07	2.94	7.76
3.647E-07	0.407	4.43	8.551E-07	2.53	7.61
3.757E-07	0.432	4.56	8.856E-07	2.14	7.75
3.875E-07	0.46	4.71	9.184E-07	1.82	8.14
4E-07	0.49	4.86	9.537E-07	1.58	8.69
4.133E-07	0.523	5.02	9.919E-07	1.41	9.19
4.275E-07	0.558	5.2	1.033E-06	1.32	9.73
4.428E-07	0.598	5.38	1.078E-06	1.25	10.3
4.5E-07	0.618	5.47	1.127E-06	1.23	10.9
4.592E-07	0.644	5.58	1.181E-06	1.22	11.6
4.769E-07	0.695	5.8	1.24E-06	1.25	12.2
4.959E-07	0.779	5.84	1.305E-06	1.3	12.9
5.061E-07	0.818	5.93	1.378E-06	1.35	13.7
5.166E-07	0.852	6.1	1.459E-06	1.43	14.5
5.276E-07	0.891	6.23	1.55E-06	1.5	15.5
5.391E-07	0.944	6.36	1.653E-06	1.59	16.5
5.51E-07	1	6.52	1.771E-06	1.75	17.8
5.636E-07	1.07	6.64	2E-06	2.15	20.7
5.767E-07	1.15	6.77	2.065E-06	2.27	21.4
5.904E-07	1.22	6.93	2.254E-06	2.62	23.3
6.048E-07	1.31	7.09	2.48E-06	3.07	25.6
6.199E-07	1.4	7.21	2.755E-06	3.68	28.3
6.358E-07	1.51	7.37	3E-06	4.24	30.6

Appendix C

Calculation of chromaticity coordinates

In Chapter 3, perceived colour coordinates (x, y) are derived from reflection spectra using colour matching functions. The chromaticity coordinates are calculated in the CIE 1931 colourimetric system and weighted-ordinate method is used [206, 207] :

$$X = k \sum_{\lambda=\lambda_a}^{\lambda=\lambda_b} R(\lambda)S(\lambda)\overline{x}(\lambda)\Delta\lambda$$

$$Y = k \sum_{\lambda=\lambda_a}^{\lambda=\lambda_b} R(\lambda)S(\lambda)\overline{y}(\lambda)\Delta\lambda$$

$$Z = k \sum_{\lambda=\lambda_a}^{\lambda=\lambda_b} R(\lambda)S(\lambda)\overline{z}(\lambda)\Delta\lambda$$

$$x = \frac{X}{X+Y+Z}$$

$$y = \frac{Y}{X+Y+Z}$$

where k is the normalizing factor. $R(\lambda)$ is the reflection. $\overline{x}$, $\overline{y}$, $\overline{z}$ are the CIE colour matching fuctions. We use Judd-Vos-modified CIE 2-deg colour matching functions (1978) [84] from the Colour Vision Research laboratory (CVRL) database of University College London [86] (The data can aslo be found in Ref. [207]), which is shown in Fig. C.1. $S(\lambda)$ is the relative radiant power, which is assumed to have a spectrum

radiant power distribution of 6500K blackbody radiator following Plank's radiation law:

$$S(\lambda) = \frac{2h\nu^3}{c^2} \frac{1}{e^{\frac{h\nu}{kT}} - 1}$$

Where h is the Planck constant; c is the speed of light in a vaccum; k is the Boltzmann constant; $\nu = \frac{c}{\lambda}$ is the frequency of the electromagnetic radiation; and T=6500K is the temperature of the body in kelvins.

In summation, $\Delta\lambda = 5$ nm is used and $R(\lambda)$ and $S(\lambda)$ is assumed constant with the value at the centre wavelength for all wavelength with the wavelength interval. Summation is done from 400 nm to 780 nm.

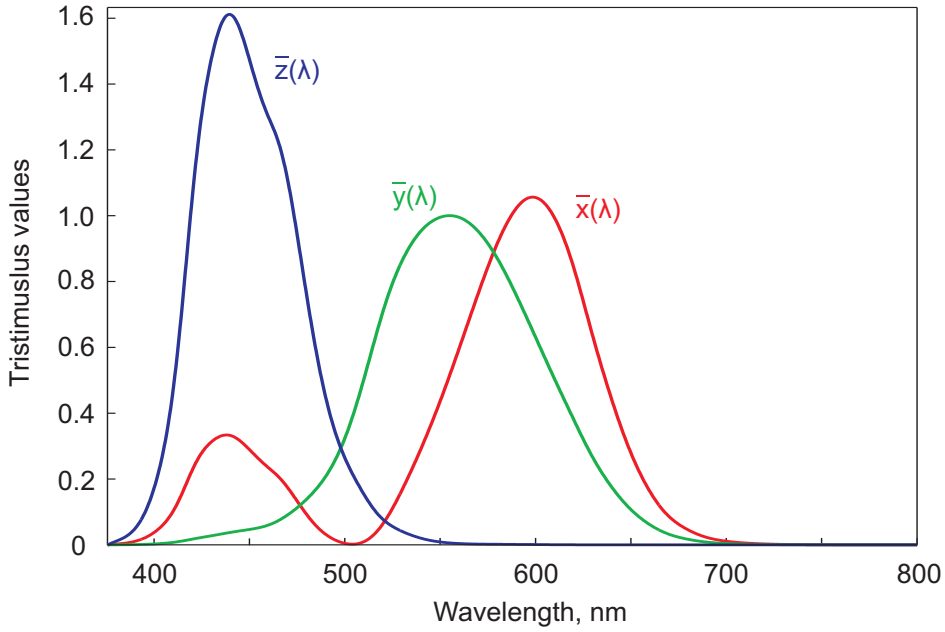

Figure C.1: Colouring matching functions.. Judd-Vos-modified CIE 2-deg colour matching functions (1978) [84] are used to calculate CIE tristimulus values and chromaticity coordinates [86].

Appendix D

Publications

D.1 Journal publications

D.1.1 Published

- B. Gholipour, J. Zhang, K. F. MacDonald, D. W. Hewak and N. I. Zheludev "All-optical, Non-volatile, Bi-directional, Phase-change Meta-switch". *Advanced Materials*, in press.

- J. Y. Ou, E. Plum, J. Zhang, and N. I. Zheludev. "An electromechanically reconfigurable plasmonic metamaterial operating in the near-IR". *Nature Nanotechnology*, in press.

- J. Zhang, K. F. MacDonald, and N. I. Zheludev. "Controlling light-with-light without nonlinearity". *Light: Science and Applications,*, 1(7):e18, 2012.

- J. Zhang, J. Y. Ou, K. F. MacDonald, and N. I. Zheludev. "Optical response of plasmonic relief meta-surfaces". *Journal of Optics-IOP Publishing*, 14(11):114002, 2012.

- J. Zhang, K. F. MacDonald, and N. I. Zheludev. "Optical gecko toe: Optically controlled attractive near-field forces between plasmonic metamaterials and dielectric or metal surfaces". *Physical Review B*, 85(20):205123, 2012.

- M. Ren, B. Jia, J. Y. Ou, E. Plum, J. Zhang, K. F. MacDonald, A. E. Nikolaenko, J. Xu, M. Gu, and N. I. Zheludev. "Nanostructured Plasmonic Medium for

Terahertz Bandwidth All-Optical Switching". *Advanced Materials*, 23:5540-5544, 2011.

- J. Zhang, J. Y. Ou, N. Papasimakis, Y. Chen, K. F. MacDonald, and N. I. Zheludev. "Continuous metal plasmonic frequency selective surfaces". *Opt. Express*, 19(23):23279-23285, 2011.

D.1.2 In preparation or under review

- J. Zhang, K. F. MacDonald, and N. I. Zheludev. "Nonlinear dielectric optomechanical metamaterials". *Light: Science and Applications*, under review
- J. Zhang, J. Y. Ou, K. F. MacDonald, and N. I. Zheludev. "Sharp Magnetic Resonances in All-dielectric Metamaterials at Near Infrared Wavelengths". to be submitted
- J. Zhang, J. Y. Ou, K. F. MacDonald, and N. I. Zheludev. "Dielectric-loaded metamaterials". in preparation
- J. Zhang, K. F. MacDonald, and N. I. Zheludev. "Giant optical forces in dielectric metamaterials". in preparation

D.1.3 Non-peer reviewed publications

- J. Zhang, J. Y. Ou, N. Papasimakis, Y. Chen, K. F. MacDonald, and N. I. Zheludev. "Control of metal color using surface relief metamaterial nanostructuring". *SPIE Newsroom*, 2012. DOI: 10.1117/2.1201201.004119.

D.2 Patents

- N. I. Zheludev, K. F. MacDonald, J. Zhang, D. J. Richardson, "Optical Devices, Systems and Methods". publication pending
- N. I. Zheludev, E. Plum, J-Y. Ou, K. F. MacDonald, A. Nikolaenko, J. Zhang, M. Ren, B. Jia, "Nonlinear materials and related devices (Nanometa)". US Application 13/473,038 (16/05/2012); GB Application 1108139.5 (21/11/2012).

- N. I. Zheludev, K. F. MacDonald, N. Papasimakis, J. Zhang, J. Y. Ou, "Method And Device For Controlling The Color Of Metals". US Application 13/182,084 (13/070/2011); GB Application 1011720.8 (13/07/2010).

D.3 Conference Contributions

- (Poster) J. Zhang, K. F. MacDonald and N. I. Zheludev. "Nonlinear dielectric optomechanical metamaterials". *NANOMETA 2013*, Seefeld, Austria, 3 - 6 Jan 2013

- (oral) J. Zhang, J-Y. Ou, R. Chen, M. D. Charlton, K. F. MacDonald and N. I. Zheludev. "Optical magnetic response in All-Dielectric Metamaterials". *NANOMETA 2013*, Seefeld, Austria, 3 - 6 Jan 2013

- (Poster) H. Yasuda, J. Zhang, G. Adamo, K. F. MacDonald, and N. I. Zheludev. "Fishing for carbon nanotubes with a photonic metamaterial net". *NANOMETA 2013*, Seefeld, Austria, 3 - 6 Jan 2013

- (invited) E. Plum, J. Y. Ou, J. Valente, J. Zhang, and N. I. Zheludev. "Reconfiguring photonic metamaterials with electromagnetic forces". *NANOMETA 2013*, Seefeld, Austria, 3 - 6 Jan 2013

- (invited) E. Plum, J. Y. Ou, J. Valente, J. Zhang, and N. I. Zheludev. "Reconfiguring Photonic Metamaterials". *UK-China Physics Workshop*, Beijing, China, 7 - 8 Dec 2012

- (invited) N. I. Zheludev, J. Zhang, K. F. MacDonald. "Controlling light". *Metamaterials 2012*, St Petersburg, Russia 17-22 Sep 2012

- (Oral) J. Zhang, K. F. MacDonald, and N. I. Zheludev. "Perfect plasmonic absorption and transparency: The anti-lasing spaser ". *Photon12*,Durham, UK, 3 - 6 Sep 2012

- (Oral) B.Gholipour, J. Zhang, K. F. MacDonald, D. W. Hewak, N. I. Zheludev. "Chalcogenide metamaterial phase change all-optical switch of nanoscale thickness ". *EPCOS 2012* , Tampere Finland 8-10 July 2012

- (oral) J. Zhang, K. F. MacDonald, and N. I. Zheludev. "Metamaterial Coherent Perfect Absorber: The Anti-Lasing-Spaser". *6th International Conference on Nanophotonics (ICNP'2012)*, Beijing, China, 27 - 30 May 2012

- (Oral) B. Gholipour, J. Zhang, F. Al-Saab, K. F. MacDonald, K. F. MacDonald, B. Hayden, D. Hewak, N. I. Zheludev. "Chalcogenide Glass Photonics: Non-volatile, Bi-directional, All-optical Switching in Phase-change Metamaterials". *CLEO:2012*, San Jose, United States, 06 - 11 May 2012

- (Oral) J. Zhang, H. Yasuda, K. F. MacDonald, and N. I. Zheludev. "Metamaterial 'Gecko Toe': Optically-Controlled Adhesion to Any Surface". *CLEO:2012*, San Jose, United States, 06 - 11 May 2012

- (oral) J. Zhang, K. F. MacDonald, and N. I. Zheludev. "Metamaterial Coherent Light Absorption: The Time-reversed Analogue of the Lasing Spaser". *CLEO:2012*, San Jose, United States, 06 - 11 May 2012

- (poster) J. Zhang, K. F. MacDonald, N. I. Zheludev. "Optical 'gecko toe': Near-field force sticks a metamaterial to any surface". *SPIE Photonics Europe*, Brussels, Belgium, 16 - 19 Apr 2012

- (poster) J. Zhang, K. F. MacDonald, N. I. Zheludev. "Light absorption by interference of radiation in a metamaterial - an anti-LASER". *SPIE Photonics Europe*, Brussels, Belgium, 16 - 19 Apr 2012

- (poster) B. Gholipour, J. Zhang, K. F. MacDonald, D. W. Hewak, N. I. Zheludev. "Non-volatile bi-directional all-optical switching in chalcogenide glass metamaterials". *SPIE Photonics Europe*, Brussels, Belgium, 16 - 19 Apr 2012

- (Poster) J. Zhang, J. Y. Ou, T. Uchino, K. F. MacDonald, N. I. Zheludev. "Frequency selective reflectors, magnetic walls and perfect optical absorbers based on new classes of metal and dielectric-loaded relief metamaterials". *Metamaterials 2011*, Barcelona, Spain 10-15 Oct 2011

- (Invited) M. Ren, J. Y. Ou, B. Jia, E. Plum, J. Zhang, L. Jiang, A. Nikolaenko, J. J. Xu, M. Gu, K. F. MacDonald, N. I. Zheludev. "Functional photonic metamaterials". *IEEE Photonics 2011*,Arlington, USA 9-13 Oct 2011

- (Invited) J. Y. Ou, J. Zhang, T. S. Kao, E. Plum, K. F. MacDonald, N. I. Zheludev. "Manipulating light with photonic metamaterials". *SPIE Optics & Photonics (Plasmonics: Metallic Nanostructures and Their Optical Properties IX)* , San Diego, USA 21-25 Aug 2011

- (Invited) K. F. MacDonald, M. Ren, J. Zhang, B. Gholipour, N. Papasimakis, A. E. Nikolaenko, Z. X. Shen, D. Hewak, N. I. Zheludev. "Advances in nonlinear and switchable photonic metamaterials". *SPP5*, Busan, S. Korea 15-20 May 2011

- (oral) J. Zhang, J. Y. Ou, N. Papasimakis, K. F. MacDonald, N. I. Zheludev. "Intaglio and bas-relief metamaterials: Controlling the colour of metals". *Nanometa 2011* , Seefeld, Austria 3-6 Jan 2011

- (oral) Z. L. Samson, B. Gholipour, F. De Angelis, S. Li, K. J. Knight, J. Zhang, T. Uchino, C. C. Huang, K. F. MacDonald, P. Ashburn, E. Di Fabrizio, D. W. Hewak, N. I. Zheludev. "Active photonic metamaterials". *8th Electro-Optics and infrared Conference*, Shrivenham, UK 7-9 Jul 2010

- (oral) Z. L. Samson, J. Zhang, G. Adamo, T. Uchino, B. Gholipour, K. Knight, C. C. Huang, F. De Angelis, K. F. MacDonald, P. Ashburn, E. Di Fabrizio, D. W. Hewak, N. I. Zheludev. "Chalcogenide plasmonic metamaterial switches". *SPIE Optics & Photonics 2010*, San Diego, USA 1-5 Aug 2010

Appendix E

Media coverage of my research work

E.1 Press release coverage summary: Controlling the colour of metals

The work on controlling the colour of metals has attracted lots of attentions. After a press release by EPSRC, many national and international public media as well as specialist science media reported this work. Below is only an incomplete summary of press release coverage on this topic:

E.1.1 Press release sources

- EPSRC press release: http://www.epsrc.ac.uk/newsevents/news/2012/Pages/ midastouch.aspx
- ORC: http://www.orc.soton.ac.uk/midastouch.html
- FPAS: http://www.fpas.soton.ac.uk/news?id=4082
- UoS: http://www.southampton.ac.uk/mediacentre/news/2012/oct/12 _188.shtml

E.1.2 Local and national news

- Alpha Galileo: http://www.alphagalileo.org/ViewItem.aspx?ItemId= 125234CultureCode=en

- BBC online: http://www.bbc.co.uk/news/uk-england-hampshire-20067736
- Bognor Regis Observer: http://www.bognor.co.uk/news/regional/experts- change-the-colour-of-gold-1-4401883
- Chichester Observer: http://www.chichester.co.uk/news/regional/experts -change-the-colour-of-gold-1-4401883
- Daily Echo: http://www.dailyecho.co.uk/news/10003860.Scientists _ change _the _co/
- Eastbourne Herald: http://www.eastbourneherald.co.uk/news/regiona l-news/experts-change-the-colour-of-gold-1-4401883
- Hastings Observer: http://www.hastingsobserver.co.uk/news/regional -news/experts-change-the-colour-of-gold-1-4401883
- Hayling Islander: http://www.haylingtoday.co.uk/news/regional/experts- change-the-colour-of-gold-1-4401883
- Heart South Coast: http://www.heart.co.uk/southcoast/news/local/experts -change-colour-gold/
- Littlehampston Gazette: http://www.littlehamptongazette.co.uk/news/ regional/experts-change-the-colour-of-gold-1-4401883
- London Evening Standard: http://www.standard.co.uk/news/techandgadgets/any-colour-you-like-as-long-as-its-gold–scientists-create-red-and-green-metals- 8224069.html
- Mid-Sussex Times: http://www.midsussextimes.co.uk/news/regional/experts- change-the-colour-of-gold-1-4401883
- Petersfield Post: http://www.petersfieldpost.co.uk/news/regional/experts- change-the-colour-of-gold-1-4401883
- Winchester News Online: http://www.winol.co.uk/

E.1.3 International news

- China Daily: http://bbs.chinadaily.com.cn/thread-801605-1-1.html
- Chinese Today: http://www.corriere.it/scienze _e _tecnologie/12 _ottobre _ 30/oro-colorato _18074542-21db-11e2-867a-35e5030cc1c9.shtml
- Corriere della Sera: http://www.deccanherald.com/content/287670/ scientists-change-colour-gold.html
- Financial Express.com: http://m.financialexpress.com/news/scientist- change-the-colour-of-gold/1021831/
- Hindustan Times (e-paper): http://paper.hindustantimes.com/epaper/viewer.aspx
- I4U News: http://www.i4u.com/2012/10/chantelle-houghton/gold-colour- experts-change
- in.gr: http://news.in.gr/science-technology/article/?aid=1231219146
- Indian Express: http://www.indianexpress.com/comments/scientists-change- the-colour-of-gold/1021831/
- Irish Independent: http://www.independent.ie/and-finally/experts-change- the-colour-of-gold-3270851.html
- LS:N Global: https://www.lsnglobal.com/search/southampton
- MSN: http://news.uk.msn.com/odd-news/experts-change-the-colour-of-gold
- News24online.com (India Middle East): http://www.news24online.com/ scientists-first-time-find-way-to-change-colour-of-gold _LatestNews24 _4728.aspx
- NewsPoint Africa: http://newspoint.co.za/story/412/2722-changing -color-different-metals-no-coating-no-chemicals
- RedOrbit: http://www.redorbit.com/news/science/1112719712/changing-the- color-of-gold/
- SBS World News (Australia): http://www.sbs.com.au/news/article/1704581/ Experts-change-colour-of-gold

- Talktalk: http://www.talktalk.co.uk/news/odd/article/experts-change- the-colour-of-gold/65899/
- The Belfast Telegraph: http://www.belfasttelegraph.co.uk/breaking-news/ offbeat/experts-change -the-colour-of-gold-16228677.html
- The Economic Times (India): http://articles.economictimes.indiatimes.com/ 2012-10-25/news/34729716 _1 _colour-red-light-ion-beam
- The Hindu Business Line: http://www.thehindubusinessline.com/news/science/scientists-successful-in-changing-the-colour-of-gold/article4031104.ece
- The Press Association (UKPA): http://www.google.com/hostednews/ukpress/article/ALeqM5ijeBLn8IncEVCiSzyb0CR8RE4gig?docId=N02868813509989613 64A
- Times of India: http://articles.timesofindia.indiatimes.com/ 2012-10-26/science/34749571 _1 _colour-scientists-change
- United Daily News: http://udn.com/NEWS/BREAKINGNEWS/BREAKINGNEWS9/7456350.shtml
- UPI.com (United Press International): http://www.upi.com/Science _News/2012/10/24/Nanotechnology-can-change-color-of-gold/UPI-11191351124728/
- Yahoo Taiwan: http://tw.news.yahoo.com/80-
- Yahoo UK: http://uk.news.yahoo.com/experts-change-colour-gold -230406521.html

E.1.4 Specialist science media

- Above top secret (website): http://www.abovetopsecret.com/forum/ thread893097/pg1
- Azonano.com (A to Z of Nano): http://www.azonano.com/news.aspx? newsID=25809
- DViCE (Syfy online): http://dvice.com/archives/2012/10/gold-is -now-ava.php
- E! Science News: http://esciencenews.com/sources/science.daily/2012/10/24/a.new.take.midas.touch.changing.color.gold
- EU Science News: http://www.science-news.eu/nano-physics-news/ cluster195552/

- Gizmag: http://www.gizmag.com/color-changing-gold/24698/
- Hall of Wendigo: http://hallofthewendigo.informe.com/forum/viewtopic.php?f=111t=4846
- Ingeniren: http://ing.dk/artikel/134212-nanosandblaest-moenster-kan- skifte-farve-paa-metaller
- iScience.ru: http://iscience.ru/2012/10/26/nanotexnologii-pomogut- izmenit-cvet-metallov/
- ITOP: http://itop-portal.net/news/779/show
- Knovel: http://why.knovel.com/all-engineering-news/1992-changing-the-color-of-gold-optical-illusion-could-be-a-security-feature.html?utm _source=dlvr.itutm _medium=twitter-create-red-and-green-metals-8224069.html
- Laboratory Equipment: http://www.laboratoryequipment.com/news/2012/ 10/tiny-patterns-change-color-gold
- Materials Today: http://www.materialstoday.com/view/29020/a-new-take- on-the-midas-touch/
- MessageToEagle: http://www.messagetoeagle.com/ changecolorofgold.php.UJE7BoYsIUM
- Metamorphose: http://www.metamorphose-vi.org/
- Nanotechnology Now.com: http://www.nanotech-now.com/ news.cgi?story _id=46225
- NanoWerk: http://www.nanowerk.com/news2/newsid=27078.php
- PhysOrg: http://phys.org/news/2012-10-midas-colour-gold.html
- RDmag.com: http://www.realclearscience.com/2012/10/25/how _to _change _the _ color _of _gold _249704.html
- Rediff.com: http://www.rediff.com/business/report/scientists-change-the- colour-of-gold/20121025.htm
- Science & Technology (Aarhus University): http://scitech.au.dk/en/current-affairs/news/show/artikel/guld-kan-skifte-farve/

- ScienceDaily: http://www.smartplanet.com/blog/bulletin/coming-to-a- jeweler-near-you-blue-gold/3749
- Smartplanet.com: http://www.sci-news.com/physics/article00675.html
- spectroscopyNOW: http://www.theengineer.co.uk/news/team-changes-colour- of-gold-by-altering-surface-structure/1014356.article
- Ubergizmo: http://www.ubergizmo.com/2012/10/scientists-have-changed- the-color-of-gold/?utm _source=mainrss
- Unexplained Mysteries: http://www.unexplained-mysteries.com/forum/index.php?showtopic=236514
- Wired.co.uk: http://www.wired.co.uk/news/archive/2012-10/16/thin-metal- colour-change-art
- ZME Science: http://www.zmescience.com/research/technology/nanotech- changed-colour-of-gold-and-metals-041343/

E.1.5 Specialist industry media (jewellery)

- Annai-Illan: http://dhileep-annai-illam.blogspot.co.uk/2012/10/experts- change-colour-of-gold.html
- Ecouterre - Wearable Technology: http://www.ecouterre.com/u-k-scientists- change-the-color-of-gold-without-chemical-treatments/
- Gems and Jewlry: http://gemandjewelrydoctor.com/2012/10/25/science-has- found-a-new-way-to-change-the-colour-of-gold/
- jckonline: http://www.jckonline.com/2012/10/25/scientists-discover-way- to-turn-gold-and-silver-different-colors
- Jewelryne.ws: http://www.jewelryne.ws/a-new-take-on-the-midas-touch -changing-the-colour-of-gold/
- Samchar.com: http://www.samachar.com/Scientists-change-the-colour-of- gold-mkzmTMhejcj.html

E.1.6 Miscellaneous

- Comedy Central: http://www.comedycentral.co.uk/news/physicists-change-the-colour-of-gold-fbbf7e60/
- Market Management Psychology: http://multibaggerstockcalls.blogspot.co.uk/2012/10/scientists-successful-in-changing.html
- tvHayka: http://www.facebook.com/tvnauka/posts/121294624691306
- Apocalypse news: http://apocalypsenews.ru/NOVOSTI/SKORO-POYAVITSYA-KRASNOE-I-ZELENOE-ZOLOTO/

E.1.7 Print and Radio coverage

- (Print) Science and Technology Daily (China)
- (Print) Deccan Chronicle (Hyderabad)
- (Print) Deccan Herald (Bangalore)
- (Print) Hindustan Times (Patna, Chandigarh)
- (Print) Ingeniren
- (Print) The Times
- (Print) The Times of India (Patna, Panaji, Chennai, Bangalore, Bhopal)
- (Radio) Jack FM Radio Interview

E.2 Media coverage summary: Optical 'gecko toe'

Another work that has made headlines is about optical 'gecko toe':Optically controlled attractive near-field forces between plasmonic metamaterials and dielectric or metal surfaces. Below is an incomplete summary of media coverage on this work:

- Physicsworld.com: http://physicsworld.com/cws/article/news/48394
- Phys.org: http://phys.org/news/2012-01-british-team-metamaterials-gecko-toe.html

- Wissenschaft-online: http://www.wissenschaft-online.de/artikel/1140042
- MIT Technology Review: http://www.technologyreview.com/blog/arxiv/27501/;
- Nextbigfuture.com: http://nextbigfuture.com/2012/01/metamaterial-for -gecko-toes-for.html;
- Techeye.net: http://news.techeye.net/science/spiderman-copycats-get -a-boost-with-gecko -toe-discovery;
- Engadget.com: http://www.engadget.com/2012/01/18/the-amazing-gecko -man-a-superhero-future-made-possible-by-proba/
- Nanotechweb.org: http://nanotechweb.org/cws/article/tech/48457

References

[1] National Research Council (US). Committee on Optical Science, National Research Council (US). Board on Physics, National Research Council (US). National Materials Advisory Board, National Research Council (US). Commission on Engineering, and Technical Systems. *Harnessing light: optical science and engineering for the 21st century*. National Academies Press, 1998.

[2] Committee on Harnessing Light: Capitalizing on Optical Science Trends, Challenges for Future Research; National Materials, Manufacturing Board; Division on Engineering, and Physical Sciences; National Research Council. *Optics and Photonics: Essential Technologies for Our Nation*. 2012.

[3] N.I. Zheludev. "The road ahead for metamaterials". *Science*, 328(5978):582, 2010.

[4] Sir John Pendry. "Metamaterials and the control of electromagnetic fields". In *Conference on Coherence and Quantum Optics*. Optical Society of America, 2007.

[5] RA Shelby, DR Smith, and S. Schultz. "Experimental verification of a negative index of refraction". *Science*, 292(5514):77, 2001.

[6] T.J. Yen, WJ Padilla, N. Fang, DC Vier, DR Smith, JB Pendry, DN Basov, and X. Zhang. "Terahertz magnetic response from artificial materials". *Science*, 303(5663):1494–1496, 2004.

[7] S. Linden, C. Enkrich, M. Wegener, J. Zhou, T. Koschny, and C.M. Soukoulis. "Magnetic response of metamaterials at 100 terahertz". *Science*, 306(5700):1351–1353, 2004.

[8] C.M. Soukoulis and M. Wegener. "Past achievements and future challenges in the development of three-dimensional photonic metamaterials". *Nature Photonics*, 5(9):523–530, 2011.

[9] J.B. Pendry. "Negative refraction makes a perfect lens". *Physical Review Letters*, 85(18):3966–3969, 2000.

[10] N. Fang, H. Lee, C. Sun, and X. Zhang. "Sub–diffraction-limited optical imaging with a silver superlens". *Science*, 308(5721):534, 2005.

[11] V.M. Shalaev. "Optical negative-index metamaterials". *Nature photonics*, 1(1):41–48, 2007.

[12] J. Yao, Z. Liu, Y. Liu, Y. Wang, C. Sun, G. Bartal, A.M. Stacy, and X. Zhang. "Optical negative refraction in bulk metamaterials of nanowires". *Science*, 321(5891):930–930, 2008.

[13] J.B. Pendry, D. Schurig, and D.R. Smith. "Controlling electromagnetic fields". *Science*, 312(5781):1780–1782, 2006.

[14] U. Leonhardt. "Optical conformal mapping". *Science*, 312(5781):1777–1780, 2006.

[15] H.T. Chen, W.J. Padilla, J.M.O. Zide, A.C. Gossard, A.J. Taylor, and R.D. Averitt. "Active terahertz metamaterial devices". *Nature*, 444(7119):597–600, 2006.

[16] ZL Sámson, KF MacDonald, F. De Angelis, B. Gholipour, K. Knight, CC Huang, E. Di Fabrizio, DW Hewak, and NI Zheludev. "Metamaterial electro-optic switch of nanoscale thickness". *Applied Physics Letters*, 96:143105, 2010.

[17] J.Y. Ou, E. Plum, J. Zhang, and N.I. Zheludev. "Reconfigurable photonic metamaterial exploiting nanoscale electrostatic forces". *submitted to Nature Nanotechnology*, 2012.

[18] J.K. Gansel, M. Thiel, M.S. Rill, M. Decker, K. Bade, V. Saile, G. von Freymann, S. Linden, and M. Wegener. "Gold helix photonic metamaterial as broadband circular polarizer". *Science*, 325(5947):1513–1515, 2009.

[19] N.I. Zheludev and Y.S. Kivshar. "From metamaterials to metadevices". *Nature Materials*, 11(11):917–924, 2012.

[20] D. Schurig, JJ Mock, BJ Justice, S.A. Cummer, JB Pendry, AF Starr, and DR Smith. "Metamaterial electromagnetic cloak at microwave frequencies". *Science*, 314(5801):977–980, 2006.

[21] W. Cai and V. Shalaev. "Optical metamaterials: fundamentals and applications". 2009.

[22] S.A. Maier. *Plasmonics: fundamentals and applications*. Springer, 2007.

[23] W.L. Barnes, A. Dereux, and T.W. Ebbesen. "Surface plasmon subwavelength optics". *Nature*, 424(6950):824–830, 2003.

[24] H. Kuwata, H. Tamaru, K. Esumi, and K. Miyano. "Resonant light scattering from metal nanoparticles: Practical analysis beyond Rayleigh approximation". *Applied physics letters*, 83(22):4625–4627, 2003.

[25] E. Hao and G.C. Schatz. "Electromagnetic fields around silver nanoparticles and dimers". *The Journal of chemical physics*, 120:357, 2004.

[26] S.A. Maier and H.A. Atwater. "Plasmonics: Localization and guiding of electromagnetic energy in metal/dielectric structures". *Journal of Applied Physics*, 98:011101, 2005.

[27] H. Raether. *Surface plasmons on smooth and rough surfaces and on gratings*. Springer, 1988.

[28] A. Campion and P. Kambhampati. "Surface-enhanced Raman scattering". *Chem. Soc. Rev.*, 27(4):241–250, 1998.

[29] T.W. Ebbesen, HJ Lezec, HF Ghaemi, T. Thio, and PA Wolff. "Extraordinary optical transmission through sub-wavelength hole arrays". *Nature*, 391(6668):667–669, 1998.

[30] J. B. Pendry, L. Martn-Moreno, and F. J. Garcia-Vidal. "Mimicking Surface Plasmons with Structured Surfaces". *Science*, 305(5685):847–848, 2004.

[31] E. Hutter and J.H. Fendler. "Exploitation of localized surface plasmon resonance". *Advanced Materials*, 16(19):1685–1706, 2004.

[32] J.A. Schuller, E.S. Barnard, W. Cai, Y.C. Jun, J.S. White, and M.L. Brongersma. "Plasmonics for extreme light concentration and manipulation". *Nature Materials*, 9(3):193–204, 2010.

[33] H.A. Atwater and A. Polman. "Plasmonics for improved photovoltaic devices". *Nature materials*, 9(3):205–213, 2010.

[34] A.J. Haes and R.P. Van Duyne. "A nanoscale optical biosensor: sensitivity and selectivity of an approach based on the localized surface plasmon resonance spectroscopy of triangular silver nanoparticles". *Journal of the American Chemical Society*, 124(35):10596–10604, 2002.

[35] GA Wurtz, R. Pollard, W. Hendren, GP Wiederrecht, DJ Gosztola, VA Podolskiy, and AV Zayats. "Designed ultrafast optical nonlinearity in a plasmonic nanorod metamaterial enhanced by nonlocality". *Nature nanotechnology*, 6(2):107–111, 2011.

[36] C. Rockstuhl, F. Lederer, C. Etrich, T. Zentgraf, J.Ř. Kuhl, and H. Giessen. "On the reinterpretation of resonances in split-ring-resonators at normal incidence". *Optics express*, 14(19):8827–8836, 2006.

[37] C.Y. Chen, S.C. Wu, and T.J. Yen. "Experimental verification of standing-wave plasmonic resonances in split-ring resonators". *Applied Physics Letters*, 93(3):034110–034110, 2008.

[38] B. Luk'yanchuk, N.I. Zheludev, S.A. Maier, N.J. Halas, P. Nordlander, H. Giessen, and C.T. Chong. "The Fano resonance in plasmonic nanostructures and metamaterials". *Nature materials*, 9(9):707–715, 2010.

[39] S. Prosvirnin and S. Zouhdi. "Resonances of closed modes in thin arrays of complex particles". *Advances in electromagnetics of complex media and metamaterials*, pages 281–290, 2003.

[40] VA Fedotov, M. Rose, SL Prosvirnin, N. Papasimakis, and NI Zheludev. "Sharp trapped-mode resonances in planar metamaterials with a broken structural symmetry". *Physical review letters*, 99(14):147401, 2007.

[41] N. I. Zheludev, S. L. Prosvirnin, N. Papasimakis, and V. A. Fedotov. "Lasing spaser". *Nat. Photon.*, 2:351–354, 2008.

[42] A. Nikolaenko, F. De Angelis, S. A. Boden, N. Papasimakis, P. Ashburn, E. Di Fabrizio, and N. I. Zheludev. "Carbon Nanotubes in a Photonic Metamaterial". *Physical Review Letters*, 104:153902, 2010.

[43] K. Tanaka, E. Plum, JY Ou, T. Uchino, and NI Zheludev. "Multifold enhancement of quantum dot luminescence in plasmonic metamaterials". *Physical review letters*, 105(22):227403, 2010.

[44] C. Rockstuhl, T. Zentgraf, T.P. Meyrath, H. Giessen, and F. Lederer. "Resonances in complementary metamaterials and nanoapertures". *Optics Express*, 16(3):2080–2090, 2008.

[45] Eric Plum, Kenji Tanaka, Wei T Chen, Vassili A Fedotov, Din P Tsai, and NI Zheludev. "A combinatorial approach to metamaterials discovery". *Journal of Optics*, 13(5):055102, 2011.

[46] N. Papasimakis and N.I. Zheludev. "Metamaterial-induced transparency: Sharp Fano resonances and slow light". *Optics and Photonics News*, 20(10):22–27, 2009.

[47] A.E. Nikolaenko, N. Papasimakis, E. Atmatzakis, Z. Luo, Z.X. Shen, F. De Angelis, S.A. Boden, E. Di Fabrizio, and N.I. Zheludev. "Nonlinear graphene metamaterial". *Applied Physics Letters*, 100(18):181109–181109, 2012.

[48] M. Ren, B. Jia, J.Y. Ou, E. Plum, J. Zhang, K.F. MacDonald, A.E. Nikolaenko, J. Xu, M. Gu, and N.I. Zheludev. "Nanostructured Plasmonic Medium for Terahertz Bandwidth All-Optical Switching". *Advanced Materials*, 2011.

[49] C.M. Soukoulis, S. Linden, and M. Wegener. "Negative refractive index at optical wavelengths". *Science*, 315(5808):47–49, 2007.

[50] DR Smith, JB Pendry, and MCK Wiltshire. "Metamaterials and negative refractive index". *Science*, 305(5685):788–792, 2004.

[51] J. Zhang, J.Y. Ou, N. Papasimakis, Y. Chen, K.F. MacDonald, and N.I. Zheludev. "Continuous metal plasmonic frequency selective surfaces". *Opt. Express*, 19(23):23279–23285, 2011.

[52] B. Hooberman. "Everything you ever wanted to know about frequency-selective surface filters but were afraid to ask". *http://calvin. phys. columbia. edu/group$_w$eb/filter$_d$evelopment/download/filter.pdf*, 2005.

[53] D. Sievenpiper, L. Zhang, R.F.J. Broas, N.G. Alexopolous, and E. Yablonovitch. "High-impedance electromagnetic surfaces with a forbidden frequency band". *Microwave Theory and Techniques, IEEE Transactions on*, 47(11):2059–2074, 1999.

[54] J.C. Vardaxoglou. *Frequency selective surfaces: analysis and design*. Research Studies Press, 1997.

[55] A.P. Feresidis, G. Goussetis, S. Wang, and J.C. Vardaxoglou. "Artificial magnetic conductor surfaces and their application to low-profile high-gain planar antennas". *Antennas and Propagation, IEEE Transactions on*, 53(1):209–215, 2005.

[56] J. Zhang, JY Ou, KF MacDonald, and NI Zheludev. "Optical response of plasmonic relief meta-surfaces". *Journal of Optics-IOP Publishing*, 14(11):114002, 2012.

[57] S.I. Bozhevolnyi, V.S. Volkov, E. Devaux, and T.W. Ebbesen. "Channel plasmon-polariton guiding by subwavelength metal grooves". *Physical review letters*, 95(4):46802, 2005.

[58] E. Moreno, S.G. Rodrigo, S.I. Bozhevolnyi, L. Martin-Moreno, and FJ Garcia-Vidal. "Guiding and focusing of electromagnetic fields with wedge plasmon polaritons". *Physical review letters*, 100(2):23901, 2008.

[59] R. De Waele, S.P. Burgos, A. Polman, and H.A. Atwater. "Plasmon dispersion in coaxial waveguides from single-cavity optical transmission measurements". *Nano letters*, 9(8):2832–2837, 2009.

[60] E.D. Palik, editor. *Handbook of Optical Constants of Solids*. Academic Press, Orlando, 1984.

[61] MB Sobnack, WC Tan, NP Wanstall, TW Preist, and JR Sambles. "Stationary surface plasmons on a zero-order metal grating". *Physical review letters*, 80(25):5667–5670, 1998.

[62] J. Le Perchec, P. Quemerais, A. Barbara, and T. Lopez-Rios. "Why metallic surfaces with grooves a few nanometers deep and wide may strongly absorb visible light". *Physical review letters*, 100(6):66408, 2008.

[63] M. Bora, B.J. Fasenfest, E.M. Behymer, A.S.P. Chang, H.T. Nguyen, J.A. Britten, C.C. Larson, J.W. Chan, R.R. Miles, and T.C. Bond. "Plasmon resonant cavities in vertical nanowire arrays". *Nano letters*, 10(8):2832, 2010.

[64] A.S. Schwanecke, VA Fedotov, VV Khardikov, SL Prosvirnin, Y. Chen, and NI Zheludev. "Optical magnetic mirrors". *Journal of Optics A: Pure and Applied Optics*, 9:L1, 2007.

[65] K.Y. Bliokh, Y.P. Bliokh, V. Freilikher, S. Savelev, and F. Nori. "Colloquium: Unusual resonators: Plasmonics, metamaterials, and random media". *Reviews of Modern Physics*, 80(4):1201, 2008.

[66] J.J. Greffet, R. Carminati, K. Joulain, J.P. Mulet, S. Mainguy, and Y. Chen. "Coherent emission of light by thermal sources". *Nature*, 416(6876):61–64, 2002.

[67] NI Landy, S. Sajuyigbe, JJ Mock, DR Smith, and WJ Padilla. "Perfect metamaterial absorber". *Physical review letters*, 100(20):207402, 2008.

[68] N. Liu, M. Mesch, T. Weiss, M. Hentschel, and H. Giessen. "Infrared perfect absorber and its application as plasmonic sensor". *Nano letters*, 10:2342–2348, 2010.

[69] X. Liu, T. Starr, A.F. Starr, and W.J. Padilla. "Infrared spatial and frequency selective metamaterial with near-unity absorbance". *Physical review letters*, 104(20):207403, 2010.

[70] J. Hao, L. Zhou, and M. Qiu. "Nearly total absorption of light and heat generation by plasmonic metamaterials". *Physical Review B*, 83(16):165107, 2011.

[71] TV Teperik, F.J.G. De Abajo, AG Borisov, M. Abdelsalam, PN Bartlett, Y. Sugawara, and JJ Baumberg. "Omnidirectional absorption in nanostructured metal surfaces". *Nature Photonics*, 2(5):299–301, 2008.

[72] VG Kravets, F. Schedin, and AN Grigorenko. "Plasmonic blackbody: Almost complete absorption of light in nanostructured metallic coatings". *Physical Review B*, 78(20):205405, 2008.

[73] S.I. Bozhevolnyi and T. Søndergaard. "General properties of slow-plasmon resonant nanostructures: nano-antennas and resonators". *Optics Express*, 15(17):10869–10877, 2007.

[74] E.J.R. Vesseur, F.J. Garcia de Abajo, and A. Polman. "Modal Decomposition of Surface- Plasmon Whispering Gallery Resonators". *Nano letters*, 9(9):3147–3150, 2009.

[75] I. Sersic, M. Frimmer, E. Verhagen, and A.F. Koenderink. "Electric and magnetic dipole coupling in near-infrared split-ring metamaterial arrays". *Physical review letters*, 103(21):213902, 2009.

[76] R. Singh, C. Rockstuhl, and W. Zhang. "Strong influence of packing density in terahertz metamaterials". *Applied Physics Letters*, 97(24):241108–241108, 2010.

[77] M. J. Dicken, K. Aydin, I. M. Pryce, L. A. Sweatlock, E. M. Boyd, S. Walavalkar, J. Ma, and H. A. Atwater. "Frequency tunable near-infrared metamaterials based on VO2 phase transition". *Optics Express*, 17(20):18330–18339, 2009.

[78] T. Driscoll, H.-T. Kim, B.-G. Chae, B.-J. Kim, Y.-W. Lee, N. M. Jokerst, S. Palit, D. R. Smith, M. Di Ventra, and D. N. Basov. "Memory Metamaterials". *Science*, 325:1518–1521, 2009.

[79] B. Kang, J. H. Woo, E. Choi, H. H. Lee, E. S. Kim, J. Kim, T. J. Hwang, Y. S. Park, D. H. Kim, and J. W. Wu. "Optical switching of near infrared light transmission in metamaterial-liquid crystal cell structure". *Opt. Express*, 18(16):16492–16498, 2010.

[80] A.R. Parker. "515 million years of structural colour". *Journal of Optics A: Pure and Applied Optics*, 2:R15, 2000.

[81] A.R. Parker and H.E. Townley. "Biomimetics of photonic nanostructures". *Nature Nanotechnology*, 2(6):347–353, 2007.

[82] M. Kolle, P.M. Salgard-Cunha, M.R.J. Scherer, F. Huang, P. Vukusic, S. Mahajan, J.J. Baumberg, and U. Steiner. "Mimicking the colourful wing scale structure of the Papilio blumei butterfly". *Nature Nanotechnology*, 5(7):511–515, 2010.

[83] J. Huang, X. Wang, and Z.L. Wang. "Controlled replication of butterfly wings for achieving tunable photonic properties". *Nano letters*, 6(10):2325–2331, 2006.

[84] J.J. Vos. "Colorimetric and photometric properties of a 2 fundamental observer". *Color Research & Application*, 3(3):125–128, 1978.

[85] G. Wyszecki and W.S Stiles. *Color science: Concepts and methods, quantitative data and formulae*. Wiley (New York), 1982.

[86] "Colour & Vision Research Laboratory Database". *(University College London), http://www.cvrl.org.*

[87] T. Holmgaard and S.I. Bozhevolnyi. "Theoretical analysis of dielectric-loaded surface plasmon-polariton waveguides". *Physical Review B*, 75(24):245405, 2007.

[88] Mewes R. Huygens C, Lommel E. *Abhandlung U ber Das Licht: Worin Die Ursachen Der Vorgange Bei Seiner Zuru ckwerfung Und Brechung Und Besonders Bei Der Eigenthumlichen Brechung Des Islandischn Spathes Dargelegt Sind.* 2010 [reprint].

[89] J.D. Jackson. *Classical Electrodynamics*. John Wiley & Sons, Inc, 1998.

[90] H.M. Gibbs. *Optical bistability: controlling light with light*. Academic Press, Inc., Orlando, FL, 1985.

[91] V.R. Almeida, C.A. Barrios, R.R. Panepucci, and M. Lipson. "All-optical control of light on a silicon chip". *Nature*, 431(7012):1081–1084, 2004.

[92] M. Soljačić and JD Joannopoulos. "Enhancement of nonlinear effects using photonic crystals". *Nature materials*, 3(4):211–219, 2004.

[93] T.F. Krauss. "Slow light in photonic crystal waveguides". *Journal of Physics D: Applied Physics*, 40(9):2666, 2007.

[94] T.S. Kao, SD Jenkins, J. Ruostekoski, and NI Zheludev. "Coherent control of nanoscale light localization in metamaterial: Creating and positioning isolated subwavelength energy hot spots". *Physical Review Letters*, 106(8):085501, 2011.

[95] S. Longhi. "Backward lasing yields a perfect absorber". *Physics*, 3:61, 2010.

[96] K.F. Braun. "Electrical oscillations and wireless telegraphy". *Nobel Lecture, December*, 11(1909):226–245, 1909.

[97] R.J. Mailloux. *Phased array antenna handbook*. Artech House Boston, 2005.

[98] S.E. Harris. "Electromagnetically induced transparency". *Physics Today*, 50:36, 1997.

[99] M. Fleischhauer, A. Imamoglu, and J.P. Marangos. "Electromagnetically induced transparency: Optics in coherent media". *Reviews of Modern Physics*, 77(2):633, 2005.

[100] R.W. Boyd and D.J. Gauthier. "Controlling the velocity of light pulses". *Science*, 326(5956):1074–1077, 2009.

[101] H.J. Kimble. "The quantum internet". *Nature*, 453(7198):1023–1030, 2008.

[102] Q. Xu, S. Sandhu, M.L. Povinelli, J. Shakya, S. Fan, and M. Lipson. "Experimental realization of an on-chip all-optical analogue to electromagnetically induced transparency". *Physical review letters*, 96(12):123901, 2006.

[103] J. Pan, Y. Huo, S. Sandhu, N. Stuhrmann, M.L. Povinelli, J.S. Harris, MM Fejer, and S. Fan. "Tuning the coherent interaction in an on-chip photonic-crystal waveguide-resonator system". *Applied Physics Letters*, 97(10):101102–101102, 2010.

[104] N. Papasimakis, V.A. Fedotov, NI Zheludev, and SL Prosvirnin. "Metamaterial analog of electromagnetically induced transparency". *Physical Review Letters*, 101(25):253903, 2008.

[105] S. Zhang, D.A. Genov, Y. Wang, M. Liu, and X. Zhang. "Plasmon-induced transparency in metamaterials". *Physical Review Letters*, 101(4):47401, 2008.

[106] N. Liu, L. Langguth, T. Weiss, J. Kästel, M. Fleischhauer, T. Pfau, and H. Giessen. "Plasmonic analogue of electromagnetically induced transparency at the Drude damping limit". *Nature materials*, 8(9):758–762, 2009.

[107] S. Weis, R. Rivière, S. Deléglise, E. Gavartin, O. Arcizet, A. Schliesser, and T.J. Kippenberg. "Optomechanically induced transparency". *Science*, 330(6010):1520–1523, 2010.

[108] A.H. Safavi-Naeini, T.P.M. Alegre, J. Chan, M. Eichenfield, M. Winger, Q. Lin, J.T. Hill, DE Chang, and O. Painter. "Electromagnetically induced transparency and slow light with optomechanics". *Nature*, 472(7341):69–73, 2011.

[109] M. Durach, A. Rusina, M.I. Stockman, and K. Nelson. "Toward full spatiotemporal control on the nanoscale". *Nano letters*, 7(10):3145–3149, 2007.

[110] M.I. Stockman, S.V. Faleev, and D.J. Bergman. "Coherent control of femtosecond energy localization in nanosystems". *Physical review letters*, 88(6):67402, 2002.

[111] G. Volpe, G. Molina-Terriza, and R. Quidant. "Deterministic subwavelength control of light confinement in nanostructures". *Physical review letters*, 105(21):216802, 2010.

[112] B. Gjonaj, J. Aulbach, P.M. Johnson, A.P. Mosk, L. Kuipers, and A. Lagendijk. "Active spatial control of plasmonic fields". *Nature Photonics*, 5(6):360–363, 2011.

[113] YD Chong, L. Ge, H. Cao, and A.D. Stone. "Coherent perfect absorbers: Time-reversed lasers". *Physical review letters*, 105(5):53901, 2010.

[114] W. Wan, Y. Chong, L. Ge, H. Noh, A.D. Stone, and H. Cao. "Time-reversed lasing and interferometric control of absorption". *Science*, 331(6019):889, 2011.

[115] S. Dutta-Gupta, O.J.F. Martin, S. Dutta Gupta, and GS Agarwal. "Controllable coherent perfect absorption in a composite film". *Optics Express*, 20(2):1330–1336, 2012.

[116] M. Pu, Q. Feng, M. Wang, C. Hu, C. Huang, X. Ma, Z. Zhao, C. Wang, and X. Luo. "Ultrathin broadband nearly perfect absorber with symmetrical coherent illumination". *Optics Express*, 20(3):2246–2254, 2012.

[117] H. Noh, Y. Chong, A.D. Stone, and H. Cao. "Perfect coupling of light to surface plasmons by coherent absorption". *Physical Review Letters*, 108(18):186805, 2012.

[118] S. Feng and K. Halterman. "Coherent perfect absorption in epsilon-near-zero metamaterials". *Physical Review B*, 86(16):165103, 2012.

[119] V. Klimov, S. Sun, and G.Y. Guo. "Coherent perfect nanoabsorbers based on negative refraction". *arXiv preprint arXiv:1202.1749*, 2012.

[120] J. Zhang, K.F. MacDonald, and N.I. Zheludev. "Controlling light-with-light without nonlinearity". *Light: Science & Applications*, 1(7):e18, 2012.

[121] C. Hagglund, S.P. Apell, and B. Kasemo. "Maximized optical absorption in ultrathin films and its application to plasmon-based two-dimensional photovoltaics". *Nano letters*, 2010.

[122] S. Thongrattanasiri, F.H.L. Koppens, and F.J. García de Abajo. "Complete Optical Absorption in Periodically Patterned Graphene". *Physical Review Letters*, 108(4):47401, 2012.

[123] J. Hao, J. Wang, X. Liu, W.J. Padilla, L. Zhou, and M. Qiu. "High performance optical absorber based on a plasmonic metamaterial". *Applied Physics Letters*, 96(25):251104–251104, 2010.

[124] K. Aydin, V.E. Ferry, R.M. Briggs, and H.A. Atwater. "Broadband polarization-independent resonant light absorption using ultrathin plasmonic super absorbers". *Nature Communications*, 2:517, 2011.

[125] C.H. Gan, G. Gbur, and T.D. Visser. "Surface plasmons modulate the spatial coherence of light in Youngs interference experiment". *Physical review letters*, 98(4):43908, 2007.

[126] P. Lebedew. "Untersuchungen über die Druckkräfte des Lichtes". *Annalen der Physik*, 311(11):433–458, 1901.

[127] EF Nichols and GF Hull. "The pressure due to radiation.(Second paper.)". *Physical Review (Series I)*, 17(1):26, 1903.

[128] K. Dholakia and T. Čižmár. "Shaping the future of manipulation". *Nature Photonics*, 5(6):335–342, 2011.

[129] M. Padgett and R. Bowman. "Tweezers with a twist". *Nature Photonics*, 5(6):343–348, 2011.

[130] K. Dholakia and P. Zemánek. "Colloquium: Gripped by light: Optical binding". *Reviews of Modern Physics*, 82(2):1767, 2010.

[131] J. Chen, J. Ng, Z. Lin, and CT Chan. "Optical pulling force". *Nature Photonics*, 5(9):531–534, 2011.

[132] T.J. Kippenberg and K.J. Vahala. "Cavity optomechanics: Back-action at the mesoscale". *Science*, 321(5893):1172–1176, 2008.

[133] M. Li, WHP Pernice, C. Xiong, T. Baehr-Jones, M. Hochberg, and HX Tang. "Harnessing optical forces in integrated photonic circuits". *Nature*, 456(7221):480–484, 2008.

[134] J. Ma and M.L. Povinelli. "Mechanical Kerr nonlinearities due to bipolar optical forces between deformable silicon waveguides". *Optics Express*, 19(11):10102–10110, 2011.

[135] J. Roels, I. De Vlaminck, L. Lagae, B. Maes, D. Van Thourhout, and R. Baets. "Tunable optical forces between nanophotonic waveguides". *Nature nanotechnology*, 4(8):510–513, 2009.

[136] G.S. Wiederhecker, L. Chen, A. Gondarenko, and M. Lipson. "Controlling photonic structures using optical forces". *Nature*, 462(7273):633–636, 2009.

[137] H. Taniyama, M. Notomi, E. Kuramochi, T. Yamamoto, Y. Yoshikawa, Y. Torii, and T. Kuga. "Strong radiation force induced in two-dimensional photonic crystal slab cavities". *Physical Review B Condensed Matter And Materials Physics*, 78(16):165129, 2008.

[138] V. Liu, M. Povinelli, and S. Fan. "Resonance-enhanced optical forces between coupled photonic crystal slabs". *Optics Express*, 17(24):21897–21909, 2009.

[139] D. Van Thourhout and J. Roels. "Optomechanical device actuation through the optical gradient force". *Nature Photonics*, 4(4):211–217, 2010.

[140] V.G. Veselago et al. "The electrodynamics of substances with simultaneously negative values of ε and μ". *Physics-Uspekhi*, 10(4):509–514, 1968.

[141] A. Agarwal H. J. Lezec and K. Chau. In *NanoMeta 2011, Seefeld-in-Tirol, Austria*, 2011.

[142] H. Chen, CT Chan, and P. Sheng. "Transformation optics and metamaterials". *Nature Materials*, 9(5):387–396, 2010.

[143] M. Lapine, I.V. Shadrivov, D.A. Powell, and Y.S. Kivshar. "Magnetoelastic metamaterials". *Nature Materials*, 11:30–33, 2011.

[144] S.K. Lamoreaux. "The Casimir force: background, experiments, and applications". *Reports on progress in Physics*, 68(1):201, 2004.

[145] R. Zhao, P. Tassin, T. Koschny, and C.M. Soukoulis. "Optical forces in nanowire pairs and metamaterials". *Arxiv preprint arXiv:1011.2566*, 2010.

[146] M. Liu, T. Zentgraf, Y. Liu, G. Bartal, and X. Zhang. "Light-driven nanoscale plasmonic motors". *Nature nanotechnology*, 5(8):570–573, 2010.

[147] SB Wang, J. Ng, H. Liu, HH Zheng, ZH Hang, and CT Chan. "Sizable electromagnetic forces in parallel-plate metallic cavity". *Physical Review B*, 84(7):075114, 2011.

[148] H. Liu, J. Ng, SB Wang, ZF Lin, ZH Hang, CT Chan, and SN Zhu. "Strong Light-Induced Negative Optical Pressure Arising from Kinetic Energy of Conduction

Electrons in Plasmon-Type Cavities". *Physical Review Letters*, 106(8):087401, 2011.

[149] M.L. Juan, M. Righini, and R. Quidant. "Plasmon nano-optical tweezers". *Nature Photonics*, 5(6):349–356, 2011.

[150] K. Autumn, M. Sitti, Y.A. Liang, A.M. Peattie, W.R. Hansen, S. Sponberg, T.W. Kenny, R. Fearing, J.N. Israelachvili, et al. "Evidence for van der Waals adhesion in gecko setae". *Proceedings of the National Academy of Sciences*, 99(19):12252, 2002.

[151] J. Zhang, KF MacDonald, and NI Zheludev. "Optical gecko toe: Optically controlled attractive near-field forces between plasmonic metamaterials and dielectric or metal surfaces". *Physical Review B*, 85(20):205123, 2012.

[152] B. C. Trrissen. *[http://en.wikipedia.org/wiki/File:Gecko$_f$oot$_o$n$_g$lass.JPG](CCBY-SA*3.0).

[153] A.W. Rodriguez, A.P. McCauley, P.C. Hui, D. Woolf, E. Iwase, F. Capasso, M. Loncar, and S.G. Johnson. "Bonding, antibonding and tunable optical forces in asymmetric membranes". *Optics Express*, 19(3):2225–2241, 2011.

[154] C. Hu, Z. Zhao, X. Chen, and X. Luo. "Realizing near-perfect absorption at visible frequencies". *Optics express*, 17(13):11039–11044, 2009.

[155] VB Svetovoy, PJ Van Zwol, G. Palasantzas, and J.T.M. De Hosson. "Optical properties of gold films and the Casimir force". *Physical Review B*, 77(3):035439, 2008.

[156] A.W. Rodriguez, F. Capasso, and S.G. Johnson. "The Casimir effect in microstructured geometries". *Nature Photonics*, 5(4):211–221, 2011.

[157] M. Lisanti, D. Iannuzzi, and F. Capasso. "Observation of the skin-depth effect on the Casimir force between metallic surfaces". *Proceedings of the National Academy of Sciences of the United States of America*, 102(34):11989, 2005.

[158] Q. Zhao, J. Zhou, F. Zhang, and D. Lippens. "Mie resonance-based dielectric metamaterials". *Materials Today*, 12(12):60–69, 2009.

[159] A.I. Kuznetsov, A.E. Miroshnichenko, Y.H. Fu, J.B. Zhang, and B. Lukyanchuk. "Magnetic light". *Scientific Reports*, 2(492), 2012.

[160] J.C. Ginn, I. Brener, D.W. Peters, J.R. Wendt, J.O. Stevens, P.F. Hines, L.I. Basilio, L.K. Warne, J.F. Ihlefeld, P.G. Clem, et al. "Realizing Optical Magnetism from Dielectric Metamaterials". *Physical Review Letters*, 108(9):97402, 2012.

[161] V.V. Khardikov, E.O. Iarko, and S.L. Prosvirnin. "A giant red shift and enhancement of the light confinement in a planar array of dielectric bars". *Journal of Optics*, 14:035103, 2012.

[162] M. Bagheri, M. Poot, M. Li, W.P.H. Pernice, and H.X. Tang. "Dynamic manipulation of nanomechanical resonators in the high-amplitude regime and non-volatile mechanical memory operation". *Nature Nanotechnology*, 2011.

[163] P.B. Deotare, I. Bulu, I.W. Frank, Q. Quan, Y. Zhang, R. Ilic, and M. Loncar. "All optical reconfiguration of optomechanical filters". *Nature Communications*, 3:846, 2012.

[164] P.T. Rakich, M.A. Popović, M. Soljačić, and E.P. Ippen. "Trapping, corralling and spectral bonding of optical resonances through optically induced potentials". *Nature Photonics*, 1(11):658–665, 2007.

[165] S. Manipatruni, J.T. Robinson, and M. Lipson. "Optical Nonreciprocity in Optomechanical Structures". *Physical review letters*, 102(21), 2009.

[166] B. Bhusan. *Nanotribology and Nanomechanics: Measurement Techniques and Nanomechanics*, volume 1. Springer, 2011.

[167] C. Liu, V.B. Mungurwadi, and A.V. Nandi. *Foundations of MEMS*. Prentice Hall, 2006.

[168] C. Enkrich, M. Wegener, S. Linden, S. Burger, L. Zschiedrich, F. Schmidt, JF Zhou, T. Koschny, and CM Soukoulis. "Magnetic metamaterials at telecommunication and visible frequencies". *Physical review letters*, 95(20):203901, 2005.

[169] E. Plum, VA Fedotov, P. Kuo, DP Tsai, and NI Zheludev. "Towards the lasing spaser: controlling metamaterial optical response with semiconductor quantum dots". *Optics Express*, 17(10):8548–8551, 2009.

[170] Z.G. Dong, H. Liu, T. Li, Z.H. Zhu, S.M. Wang, J.X. Cao, S.N. Zhu, and X. Zhang. "Optical loss compensation in a bulk left-handed metamaterial by the gain in quantum dots". *Applied Physics Letters*, 96(4):044104–044104, 2010.

[171] S. Xiao, V.P. Drachev, A.V. Kildishev, X. Ni, U.K. Chettiar, H.K. Yuan, and V.M. Shalaev. "Loss-free and active optical negative-index metamaterials". *Nature*, 466(7307):735–738, 2010.

[172] A. Boltasseva and H.A. Atwater. "Low-loss plasmonic metamaterials". *Science*, 331(6015):290–291, 2011.

[173] J.A. Schuller, R. Zia, T. Taubner, and M.L. Brongersma. "Dielectric metamaterials based on electric and magnetic resonances of silicon carbide particles". *Physical review letters*, 99(10):107401, 2007.

[174] K. Vynck, D. Felbacq, E. Centeno, AI Căbuz, D. Cassagne, and B. Guizal. "All-dielectric rod-type metamaterials at optical frequencies". *Physical review letters*, 102(13):133901, 2009.

[175] A. García-Etxarri, R. Gómez-Medina, L.S. Froufe-Pérez, C. López, L. Chantada, F. Scheffold, J. Aizpurua, M. Nieto-Vesperinas, and JJ Sáenz. "Strong magnetic response of submicron silicon particles in the infrared". *Optics express*, 19(6):4815–4826, 2011.

[176] Lei Shi, T. Umut Tuzer, Roberto Fenollosa, and Francisco Meseguer. "A New Dielectric Metamaterial Building Block with a Strong Magnetic Response in the Sub-1.5-Micrometer Region: Silicon Colloid Nanocavities". *Advanced Materials*, pages n/a–n/a, 2012.

[177] A.B. Evlyukhin, S.M. Novikov, U. Zywietz, R.L. Eriksen, C. Reinhardt, S.I. Bozhevolnyi, and B.N. Chichkov. "Demonstration of magnetic dipole resonances of dielectric nanospheres in the visible region". *Nano letters*, 12(7):3749–3755, 2012.

[178] L. Peng, L. Ran, H. Chen, H. Zhang, J.A. Kong, and T.M. Grzegorczyk. "Experimental observation of left-handed behavior in an array of standard dielectric resonators". *Physical review letters*, 98(15):157403, 2007.

[179] B.I. Popa and S.A. Cummer. "Compact dielectric particles as a building block for low-loss magnetic metamaterials". *Physical review letters*, 100(20):207401, 2008.

[180] Q. Zhao, L. Kang, B. Du, H. Zhao, Q. Xie, X. Huang, B. Li, J. Zhou, and L. Li. "Experimental demonstration of isotropic negative permeability in a three-dimensional dielectric composite". *Physical review letters*, 101(2):27402, 2008.

[181] N. Katsarakis, T. Koschny, M. Kafesaki, EN Economou, and CM Soukoulis. "Electric coupling to the magnetic resonance of split ring resonators". *Applied physics letters*, 84(15):2943–2945, 2004.

[182] K. Hennessy, A. Badolato, M. Winger, D. Gerace, M. Atatüre, S. Gulde, S. Fält, A.I. EL Hu, et al. "Quantum nature of a strongly coupled single quantum dot–cavity system". *Nature*, 445(7130):896–899, 2007.

[183] A.D. Boardman, V.V. Grimalsky, Y.S. Kivshar, S.V. Koshevaya, M. Lapine, N.M. Litchinitser, V.N. Malnev, M. Noginov, Y.G. Rapoport, and V.M. Shalaev. "Active and tunable metamaterials". *Laser & Photonics Reviews*, 5(2):287–307, 2011.

[184] N. Kundtz and D.R. Smith. "Extreme-angle broadband metamaterial lens". *Nature materials*, 9(2):129–132, 2009.

[185] F. Aieta, P. Genevet, M.A. Kats, N. Yu, R. Blanchard, Z. Gaburro, and F. Capasso. "Aberration-free ultra-thin flat lenses and axicons at telecom wavelengths based on plasmonic metasurfaces". *Nano Letters*, 2012.

[186] M. Tonouchi. "Cutting-edge terahertz technology". *Nature photonics*, 1(2):97–105, 2007.

[187] I.V. Shadrivov, A.B. Kozyrev, D.W. Van Der Weide, and Y.S. Kivshar. "Tunable transmission and harmonic generation in nonlinear metamaterials". *Applied Physics Letters*, 93(16):161903–161903, 2008.

[188] H. Tao, AC Strikwerda, K. Fan, WJ Padilla, X. Zhang, and RD Averitt. "Reconfigurable terahertz metamaterials". *Physical review letters*, 103(14):147401, 2009.

[189] Q. Zhao, L. Kang, B. Du, B. Li, J. Zhou, H. Tang, X. Liang, and B. Zhang. "Electrically tunable negative permeability metamaterials based on nematic liquid crystals". *Applied physics letters*, 90(1):011112–011112, 2007.

[190] S. Lim, C. Caloz, and T. Itoh. "Metamaterial-based electronically controlled transmission-line structure as a novel leaky-wave antenna with tunable radiation angle and beamwidth". *Microwave Theory and Techniques, IEEE Transactions on*, 52(12):2678–2690, 2004.

[191] O. Reynet and O. Acher. "Voltage controlled metamaterial". *Applied physics letters*, 84(7):1198–1200, 2004.

[192] I. Gil, J. Bonache, J. Garcia-Garcia, and F. Martin. "Tunable metamaterial transmission lines based on varactor-loaded split-ring resonators". *Microwave Theory and Techniques, IEEE Transactions on*, 54(6):2665–2674, 2006.

[193] M. Lapine, D. Powell, M. Gorkunov, I. Shadrivov, R. Marqués, and Y. Kivshar. "Structural tunability in metamaterials". *Applied Physics Letters*, 95(8):084105–084105, 2009.

[194] W.M. Zhu, A.Q. Liu, X.M. Zhang, D.P. Tsai, T. Bourouina, J.H. Teng, X.H. Zhang, H.C. Guo, H. Tanoto, T. Mei, et al. "Switchable magnetic metamaterials using micromachining processes". *Advanced Materials*, 23(15):1792–1796, 2011.

[195] J.Y. Ou, E. Plum, L. Jiang, and N.I. Zheludev. "Reconfigurable photonic metamaterials". *Nano letters*, 11(5):2142, 2011.

[196] H. Zhao, J. Zhou, Q. Zhao, B. Li, L. Kang, and Y. Bai. "Magnetotunable left-handed material consisting of yttrium iron garnet slab and metallic wires". *Applied Physics Letters*, 91(13):131107–131107, 2007.

[197] K.M. Dani, Z. Ku, P.C. Upadhya, R.P. Prasankumar, SRJ Brueck, and A.J. Taylor. "Subpicosecond optical switching with a negative index metamaterial". *Nano letters*, 9(10):3565, 2009.

[198] L. Ju, B. Geng, J. Horng, C. Girit, M. Martin, Z. Hao, H.A. Bechtel, X. Liang, A. Zettl, Y.R. Shen, et al. "Graphene plasmonics for tunable terahertz metamaterials". *Nature nanotechnology*, 6(10):630–634, 2011.

[199] M. Wuttig and N. Yamada. "Phase-change materials for rewriteable data storage". *Nature materials*, 6(11):824–832, 2007.

[200] A.V. Kolobov, P. Fons, A.I. Frenkel, A.L. Ankudinov, J. Tominaga, and T. Uruga. "Understanding the phase-change mechanism of rewritable optical media". *Nature materials*, 3(10):703–708, 2004.

[201] A.Y. Vorobyev and C. Guo. "Colorizing metals with femtosecond laser pulses". *Applied Physics Letters*, 92:041914, 2008.

[202] T. Søndergaard, S.M. Novikov, T. Holmgaard, R.L. Eriksen, J. Beermann, Z. Han, K. Pedersen, and S.I. Bozhevolnyi. "Plasmonic black gold by adiabatic nanofocusing and absorption of light in ultra-sharp convex grooves". *Nature Communications*, 3:969, 2012.

[203] A.P. Mosk, A. Lagendijk, G. Lerosey, and M. Fink. "Controlling waves in space and time for imaging and focusing in complex media". *Nature Photonics*, 6(5):283–292, 2012.

[204] S. Raoux and M. Wuttig. *Phase Change Materials: Science and Applications*. Springer, 2008.

[205] C. Multiphysics. "Users Guide, version 3.5 a". *COMSOL AB*, 2008.

[206] *CIE. (1932). Commission Internationale de lclairage Proceedings, 1931.* Cambridge: Cambridge University Press.

[207] G. Wyszecki and W.S. Stiles. *Color science*. Wiley New York, 1982.